Soil moisture dynamics and soil moisture controlled runoff processes at different spatial scales: From observation to modelling

Dissertation submitted to the Faculty of Mathematics and Natural Sciences at the

University of Potsdam, Germany

for the degree of Doctor of Natural Sciences (Dr. rer. nat.) in Hydrology

Thomas Gräff

Published online at the
Institutional Repository of the University of Potsdam:
URL http://opus.kobv.de/ubp/volltexte/2011/5447/
URN urn:nbn:de:kobv:517-opus-54470
http://nbn-resolving.de/urn:nbn:de:kobv:517-opus-54470

Contents:

Abstract:

Soil moisture is a key state variable that controls runoff formation, infiltration and partitioning of radiation into latent and sensible heat. However, the experimental characterisation of near surface soil moisture patterns and their controls on runoff formation remains a challenge. This subject was one aspect of the BMBF-funded OPAQUE project (operational discharge and flooding predictions in head catchments). As part of that project the focus of this dissertation is on: (1) testing the methodology and feasibility of the Spatial TDR technology in producing soil moisture profiles along TDR probes, including an inversion technique of the recorded signal in heterogeneous field soils, (2) the analysis of spatial variability and temporal dynamics of soil moisture at the field scale including field experiments and hydrological modelling, (3) the application of models of different complexity for understanding soil moisture dynamics and its importance for runoff generation as well as for improving the prediction of runoff volumes.

To fulfil objective 1, several laboratory experiments were conducted to understand the influence of probe rod geometry and heterogeneities in the sampling volume under different wetness conditions. This includes a detailed analysis on how these error sources affect retrieval of soil moisture profiles in soils.
Concerning objective 2 a sampling strategy of two TDR clusters installed in the head water of the Wilde Weißeritz catchment (Eastern Ore Mountains, Germany) was used to investigate how well "the catchment state" can be characterised by means of distributed soil moisture data observed at the field scale. A grassland site and a forested site both located on gentle slopes were instrumented with two Spatial TDR clusters that consist of up to 39 TDR probes.
Process understanding was gained by modelling the interaction of evapotranspiration and soil moisture with the hydrological process model CATFLOW. A field scale irrigation experiment was carried out to investigate near subsurface processes at the hillslope scale. The interactions of soil moisture and runoff formation were analysed using discharge data from three nested catchments: the Becherbach with a size of 2 km², the Rehefeld catchment (17 km²) and the superordinate Ammelsdorf catchment (49 km²).
Statistical analyses including observations of pre-event runoff, soil moisture and different rainfall characteristics were employed to predict stream flow volume. On the different scales a strong correlation between the average soil moisture and the runoff coefficients of rainfall-runoff events could be found, which almost explains equivalent variability as the pre-event runoff.
Furthermore, there was a strong correlation between surface soil moisture and subsurface wetness with a hysteretic behaviour between runoff soil moisture.
To fulfil objective 3 these findings were used in a generalised linear model (GLM) analysis which combines state variables describing the catchments antecedent wetness and variables describing the meteorological forcing in order to predict event runoff coefficients. GLM results were compared to simulations with the catchment model WaSiM ETH. Hereby were the model results of the GLMs always better than the simulations with WaSiM ETH. The GLM analysis indicated that the proposed sampling strategy of clustering TDR probes in typical functional units is a promising technique to explore soil moisture controls on runoff generation and can be an important link between the scales. Long term monitoring of such sites could yield valuable

information for flood warning and forecasting by identifying critical soil moisture conditions for the former and providing a better representation of the initial moisture conditions for the latter.

Zusammenfassung

Abflussentwicklung, Infiltration und die Umverteilung von Strahlung in latenten und sensiblen Wärmestrom werden massgeblich durch die Bodenfeuchte der vadosen Zone gesteuert. Trotz allem, gibt s wenig Arbeiten die sich mit der experimentellen Charakterisierung der Bodenfeuchteverteilung und ihre Auswirkung auf die Abflussbildung beschäftigen. Dieses Thema war ein Bestandteil des BMBF geförderten Projektes OPAQUE (Operationelle Abfluss- und Hochwasservorhersage in Quellgebieten). Als Teil dieses Projektes war der Fokus dieser Dissertation darauf ausgerichtet: (1) die Methode des Spatial TDR und deren Anwendbarkeit einschließlich der Inversion des TDR Signals in heterogenen Böden zu prüfen, (2) die Analyse der räumlichen und zeitlichen Dynamik der Bodenfeuchte auf der Feldskala einschließlich Feldexperimenten und hydrologischer Modellierung, (3) der Aufbau verschiedener Modellanwendungen unterschiedlicher Komplexität um die Bodenfeuchtedynamiken und die Abflussentwicklung zu verstehen und die Vorhersage des Abflussvolumens zu verbessern.

Um die Zielsetzung 1 zu erreichen, wurden verschiedene Laborversuche durchgeführt. Hierbei wurde der Einfluss der Sondenstabgeometrie und versciedener Heterogenitäten im Messvolumen bei verschiedenen Feuchtegehalten untersucht. Dies beinhaltete eine detaillierte Analyse wie diese Fehlerquellen die Inversion des Bodenfeuchteprofils beeinflussen.
Betreffend der Zielsetzung 2, wurden 2 TDR-Cluster in den Quellgebieten der Wilden Weißeritz installiert (Osterzgebirge) und untersucht, wie gut der Gebietszustand mit räumlich hochaufgelösten Bodenfeuchtedaten der Feldskala charakterisiert werden kann. Ein Gras- und einem Forststandort, beides Hangstandorte mit leichter Neigung wurden mit bis zu 39 TDR Sonden ausgestattet.
Um die Interaktion zwischen Evapotranspiration und Bodenfeuchte zu untersuchen wurde das hydrologische Prozessmodell CATFLOW angewendet. Ein Beregnungsversuch wurde durchgeführt um die Zwischenabflussprozesse auf der Hangskala zu verstehen. Die Interaktion zwischen Bodenfeuchte und Abflussentwicklung wurde anhand von drei einander zugeordnetten Einzugsgebieten analysiert: dem Becherbach (2 km²), der Weißeritz bis zum Pegel Rehefeld (16 km²) und dem Pegel Ammelsdorf (49 km²).
Statistische Analysen unter Berücksichtigung von Basisabfluss, Bodenvorfeuchte und verschiedenen Niederschlagscharakteristika wurden verwendet, um auf das Abflussvolumen zu schließen. Auf den verschiedenen Skalen konnte eine hohe Korrelation zwischen der mittleren Bodenfeuchte und dem Abflussbeiwert der Einzelereignisse festgestellt werden. Hierbei konnte die Bodenfeuchte genausoviel Variabilität erklären wie der Basisabfluss.
Außerdem wurde eine hohe Korrelation zwischen Bodenfeuchte und Tiefenfeuchte festgestellt mit einer hysterestischen Reaktion zwischen Abfluss und Bodenfeuchte.
Im Hinblick auf Zielsetzung 3 wurden "Generalised liner models" (GLM) genutzt. Dabei wurden Prädiktorvariablen die den Gebietszustand beschreiben und solche die die Meteorologische Randbedingungen beschreiben genutzt um den Abflussbeiwert zu schätzen. Die Ergebnisse der GLMs wurden mit Simulationsergebnissen des hydrologischen Gebietsmodells WaSiM ETH verglichen. Hierbei haben die GLMs eindeutig bessere Ergebnisse geliefert gegenüber den WaSiM Simulationen. Die GLM Analysen haben aufgezeigt, dass die verwendete Messstrategie mehrerer TDR-Cluster in typischen funktionalen Einheiten eine vielversprechende Methode ist,

um den Einfluss der Bodenfeuchte auf die Abflussentwicklung zu verstehen und ein Bindeglied zwischen den Skalen darstellen zu können. Langzeitbeobachtungen solcher Standorte sind in der Lage wichtige Zusatzinformationen bei der Hochwasserwarnung und -vorhersage zu liefern durch die Identifizierung kritischer Gebietszustände für erstere und eine bessere Repräsentation der Vorfeuchte für letztere.

CHAPTER 1 INTRODUCTION

1.1 Motivation

1.1.1 Why soil moisture is important?

Only a minute amount of global water is stored as soil moisture: with an estimated volume of about 16,500 km³, soil moisture represents 0.0012 % and 0.05 % of total and fresh water, respectively (Dingman, 1994). And yet, this tiny hydrological component exerts crucial control over interactions between the atmosphere, land surface and groundwater since soil moisture determines the partitioning of net radiation energy into latent and sensible heat flux and supply of water for the terrestrial biomass. Vegetation relies on the availability of water for photosynthesis, and adjusts stomatal resistance to water transfer according to the availability of soil moisture (Schulze et al., 2005; Teuling et al., 2006; Carminati et al., 2010)). It also exerts a strong control on soil physical properties and biogeochemical cycling of nitrogen and carbon (Robinson et al., 2008; Koehler et al., 2010). Soil moisture influences, furthermore, plot scale generation of Hortonian and saturated excess overland flow (Zehe et al., 2007; Chaves et al., 2008), the switch between hydrophilic and hydrophobic conditions (Dekker et al., 2005; Blume et al., 2009), infiltration processes (Bronstert and Bárdossy, 1999) and plant dynamics (Porporato et al., 2004; Holsten et al., 2009; Carminati et al., 2010), as well as hillslope and catchment scale runoff response to extreme precipitation (e.g. Merz and Bárdossy, 1998; Bronstert and Bárdossy, 1999; Jayawardena and Zhou, 2000; Montgomery and Dietrich, 2002; Meyles et al., 2003; Chirico et al., 2003; Deeks et al., 2004; Zehe and Blöschl, 2004; Zehe et al., 2005; Blöschl and Zehe, 2005).

At the regional and continental scale, soil moisture controls water distribution through land surface atmosphere feedback mechanisms (Koster et al., 2004; Gerten et al, 2007). The spatiotemporal variation in soil moisture indicates the presence of "active" or "contributing" areas or periods (Ambroise, 2004; James and Roulet, 2007; Spence et al., 2009; Ali and Roy, 2010). This relates to hydrologic connectivity and to threshold processes with drastically different runoff responses (Zehe et al., 2007). Antecedent conditions are the major control on flood response: while these conditions are often estimated by pre-event runoff or groundwater levels (Peters et al., 2003; Vivoni et al., 2007; Latron and Gallart, 2008;), soil moisture is often described as another state variable which has major control on catchment response (e.g. Grayson et al., 1997; Gutknecht et al., 2002; Meyles et al., 2003; Borga et al., 2007; Detty and McGuire, 2010; Steinbrech and Weiler, 2010; Zehe et al., 2010). Therefore, determination of soil moisture values, with reasonable temporal and spatial resolution, is required to improve ecological, agricultural, hydrological understanding and modelling.

1.1.2 Problems in assessment –observe at the point scale, interested in catchment scale

If soil moisture is choosen as a descriptor of antecedent conditions that control flood response, the problem of how to assess and represent this state variable for the catchment of interestwill be appeare. Soil moisture is traditionally described by point measurements that either need to be made at representative locations or need to be interpolated to provide a measure for the overall

catchment state. However, both of these possibilities are error prone and difficult to evaluate in their representativeness. Therefore most studies concerned with flood response and its dependence on antecedent conditions rely to a large degree on modelling (see Chapter 4). Experimental studies that relate observations of spatiotemporal soil moisture dynamics at the field or headwater scale to observed flows, either at the surface or in the stream (Burt and Butcher, 1985; Grayson et al., 1997; Starr and Timlin, 2004; McNamara et al., 2005; Lin, 2006; Frisbee et al., 2007; James and Roulet, 2007; Ali and Roy, 2010; Penna et al., 2010), are challenging due to the fact that soil moisture at the headwater scale exhibits huge spatial variability and single or even snapshots of distributed soil moisture measurements yield non-representative data as they do not account for the temporal dynamics (Bronstert et al., 2011).

In recent years a number of experimental techniques and equipment have been developed that allow either for a large number of data points in space while at the same time providing high resolution time series of either soil moisture or a close proxy. These include:

- wireless sensor networks (Bogena et al., 2007, 2009; Trubilowicz et al., 2009) or
- estimation of soil moisture dynamics with thermal infrared imagery (Katra et al., 2006, 2007)
- distributed temperature sensing along a fibre optic cable (Steele-Dunne, 2010; Sayde et al., 2010)
- heat fluxes by scintillometry (Timmermans et al. 2009),
- cosmic ray neutron probes (Zreda et al., 2008; Rivera Villarreyes et al., 2011),
- GPS data sets (Larson et al., 2008, 2010) or
- gravity dynamics (Creutzfeldt et al., 2010, a, b) or
- sapflow data (Tromp-van Meerveld and McDonnell, 2006b; Kume et al., 2007, 2008; Zeppel et al., 2008).

Geophysical methods are also capable of investigating near surface patterns of soil moisture. Possible techniques include:

- ground-penetrating radar (GPR),
- electrical resistivity tomography (ERT) and
- electromagnetic induction surveying (EMI) (Butler, 2005).

In addition, there are several remote sensing methodologies available to observe surface soil moisture at the watershed scale (Wagner et al.; 2007a and Tang et al.; 2010). More details on the different techniques are given below, listed according to their spatial support/extent.

o Point measurements: Time and Frequency Domain Reflectometry

Time Domain Reflectometry (TDR) is based on the travel time analysis of a defined pulse along a wave guide (Robinson et al., 2003). The travel time is related to electrical permittivity which is a function of soil moisture. Frequency Domain Reflectometry (FDR) determines the electrical permittivity by measuring the frequency changes induced by a changing value of the soil permeated by the fringing fields of the capacitor sensor (Baumhardt et al., 2000). The methods are less invasive and investigate at the point scale. The accuracy depends on the calibration of the

probe to the specific soil (Lesmes and Freedman, 2005). Besides soil moisture, electrical conductivity can be measured. Because of the large difference between electrical permittivity of water and ice, the frost depth can be observed (Baker et al., 1982; Boike and Roth, 1997). It is also possible to obtain the soil moisture profile along the wave guide with inversion algorithms (Heimovaara et al., 2004; Schlaeger, 2005; Greco, 2006).

There are two common approaches to observe soil moisture in the field. One approach is to use a set of fixed TDR sensors to monitor temporal soil moisture dynamics at selected points, as for instance suggested by Bárdossy and Lehmann (1998) for the Weiherbach, Germany, Anctil et al. (2008) for the Orgeval watershed, France, Blume et al. (2009, 2008 a, b) for the Malalcahuello catchment in Chile, and Penna et al. (2009, 2010) for an alpine headwater in Italy. In recent years a number of experimental techniques and equipment has been developed that allow for the acquisition of a large number of data points in space while at the same time providing high resolution time series, e.g. wireless sensor networks (Bogena et al. 2007, 2009; Trubilowicz et al. 2009). The advantage of using fixed stations is that they allow a high temporal resolution, which permits either comparison of observed point soil moisture dynamics with event scale discharge response and piezometer response as suggested by Blume et al. (2008a), or to use this information to improve discharge predictions, as recently shown by Anctil et al. (2008).

The drawback of this approach is that it cannot be achieved a high spatial resolution, simply because of the high costs. Other authors thus prefer spatially highly resolved soil moisture sampling by means of mobile or portable TDR sensors, as for instance Grayson et al. (1997) or Grayson and Western (1998) for several catchments in Australia or Brocca et al. (2007, 2009b, 2010) for three field sites in the upper Tiber valley, Italy. Spatially distributed sampling allows identification of temporal changes in correlation structure and spatial variability depending on the average near- surface wetness. Albertson and Montaldo (2003) and Western et al. (2004) found analogy in a reduction in variance and an increasing correlation length with increasing wetness of a field sites in Australia. Similarly, Brocca et al. (2007) report that soil moisture variance reduced during wet conditions at their rather homogeneous site and soil moisture was normally distributed in the flat valleys areas. Brocca et al. (2007) and Grayson and Western (1998) defined representative sites where soil moisture values are always close to the overall average. Brocca et al. (2009a) found further that the ranks of their distributed measurements in the univariate soil moisture distribution at a fixed time did not change much between different observation times. This temporal stability of the ranks suggests that the moisture pattern reflects the pattern of stationary soil properties, at least at the seasonal scale. Blume et al. 2008 (a, b), however, found partly contradicting results at a much more heterogeneous forested site. The main drawback of measurement campaigns is the limited temporal resolution which is too coarse for relating observed soil moisture dynamics to systems behaviour under rainfall driven conditions.

o Geophysical methods

Geophysical methods offer the opportunity to rapidly collect subsurface information in a non- or minimally invasive manner. These techniques are sensitive to the different physical attributes of subsurface materials such as their magnetic and electrical properties. Much of the related work and progress made in this field within the past decade is documented in different works (Rubin and Hubbard, 2005; Vereecken et al., 2006; Kirsch, 2007). Promising technologies to assess spatially distributed three-dimensional soil moisture proxies at the field scale are ground

penetrating radar (GPR) (Binley et al., 2002; Huisman et al., 2003; Roth et al., 2004), electromagnetic induction (EMI) (Sheets and Hendrichx, 1995; Brevik et al., 2006) or electric resistivity tomography (ERT) (Kemna et al., 2002; Wenninger et al., 2008; Cassiani et al., 2009). The first method yields the subsurface pattern of the dielectric permittivity, the latter two the subsurface pattern of the apparent specific resistivity. GPR and EMI are non-invasive, while ERT is less invasive. GPR observes the upper subsurface layers, depending on soil moisture, to a depth of 0.08 m-0.12 m (Galagedara et al., 2005). The physical principle of GPR is the same as of TDR measurement. The main difference is that TDR uses a guided electromagnetic wave whereas the GPR technique is based on an unguided wave. To investigate near surface processes the signal of the direct ground wave is used (Wollny, 1999), which is the electromagnetic wave that directly propagates below the soil surface from the transmitter to the receiver. Compared to the TDR-method, the direct ground-wave method enables the non-invasive and rapid collection of data over a larger area. The penetration depth of EMI depends on the facility. Brevik et al. (2006) documented a maximum depth of 0.9 m. ERT penetration depth depends on the distance between the electrodes. The difficulty for the methods is that there are no general petrophysical relationships available to transform the observed variables into soil moisture. The relationships between geophysical and hydrological target variables are usually complex, non-unique and site-specific (Schön, 1998). Furthermore, geophysical parameters typically show complex dependencies on a variety of subsurface properties. For example, the electrical resistivity of subsurface materials depends on porosity, soil moisture, salinity of the pore fluid, mineral composition of the media, temperature, etc. (Schön, 1998). Therefore it is difficult to find a universal petrophysical relationship for the unsaturated zone (Paasche et al., 2006) Furthermore, reliable direct translations are impossible without detailed background information from for instance geology or soil science, which can be used to calibrate the petrophysical relationship for a specific site or landscape. In this context, flexible approaches to quantitatively integrate disparate data are needed (Holliger et al., 2008).

- Dynamics in gravity anomalies

Gravimetric observations have the ability to investigate the complete water storage of the surrounding surface and subsurface (up to a radius of 50 m to 150 m around the device) to characterise the hydrological system as a whole with high temporal resolution (Creutzfeldt et al., 2010a, b). Nevertheless, practical aspects limit the application of gravimeters for hydrology and they are expensive in acquisition and operation. In general, they need a good infrastructure and are operated at a fixed location. The exact sampling volume is difficult to define because the radius of influence changes over time, and it is problematic to unambiguously identify the signal source (Creutzfeldt et al., 2010b). Additional observations (e.g. alternative measurements of soil moisture, groundwater, runoff, snow cover) have to be available to identify the exact source of the gravity signal. The signal has to be inverted with a hydrological model (Creutzfeldt, 2010a). The new superconducting gravimeter generation – the iGravTM SG – will improve the applicability in terms of portability, low drift and usability (GWR, 2009) as documented by Jacob et al. (2008, 2009) for hydrological applications.

- Fibre optics and their feasibility for soil moisture monitoring

Distributed temperature sensing using fibre optic cables (DTS) has the potential to monitor soil moisture at temporal resolutions well under one hour and at high spatial resolution (≤1 m). The method could monitor soil moisture along cables exceeding 10,000 m in extent (Sayde et al., 2010; Steele-Dunne et al., 2010). The disadvantages are: strongly invasive installation and the difficulty to achieve an exact and uniform depth for the complete cable and the contact of the device with the medium.

o Global Positioning System (GPS)

Larson et al. (2008, 2010) have shown that with continuously operating Global Positioning System (GPS) receivers the soil moisture of the 2 cm to 5 cm above the subsurface can be easily observed with a spatial extent of 50 m radius around the device on a vegetation sparse area. GPS receivers gather energy from ground reflections in addition to the direct signal that travels between the GPS satellite and receiving antenna. The characteristics of the reflected signal change as soil moisture, and therefore the dielectric constant of the ground, varies.
For this reason denser vegetation patterns would have an effect on the measurement. After precipitation events the apparent soil moisture will overestimate the actual soil moisture, because only in the case of nearly saturated soils will the signal penetrate the soil (e.g. Larson et al., 2008, 2010).

o Cosmic ray

Zreda et al. (2008) and Rivera Villarreyes et al. (2011) showed that cosmic-ray neutrons could be used to estimate soil moisture for a spatial-scale of 300 m radius around the measurement device, averaged over a depth of several decimetres. Contrary to GPS and TDR techniques, under wet conditions the measurement depth decreases, from 80 cm in dry soils to 10 cm in wet soils. Water bodies (lakes, storage ponds) and dense vegetation influence the signal.

o Remote sensing

Remote sensing has the capability to observe patterns, dynamic signatures and exchange processes at the land surface across multiple spatial and temporal scales. For that reason these techniques are of great interest for large scale hydrological applications. Patterns of land surface characteristics and their dynamics are retrieved by measuring electromagnetic emission and reflection using the several sensors available to detect these signals. These comprise optical multi- and hyperspectral imaging in the visible and near infrared spectral region, thermal infrared emissivity or passive and active microwave remote sensing. An overview of remote sensing applications to hydrology is provided by Schmugge et al. (2002), Wagner et al. (2007a) and Tang et al. (2010).
Satellites with optical sensors provide remote sensing data on the extent of catchments which allow for identifying spatial surface structures of land use at spatial resolutions between 20 m and 250 m (Dixon and Candade, 2008). Also, sensors operating in the visible and infrared parts of the electromagnetic spectrum have been used to infer soil moisture indirectly through monitoring of surface temperature and other surface state variables (Hausbrock et al., 2008).
Microwave remote sensing can be used to determine the dielectric permittivity which is related to soil moisture of the soil surface (Kustas et al., 1998; Wagner et al., 2007b). Active systems (e.g. ENVISAT)operating in the C-band (wave length 3.8 cm - 7.5 cm) can observe soil moisture with

spatial resolution up to 3 m - 100 m. Multi-frequency passive systems (AMSR-E and SMOS) operate in the C- and L-Band (wave length 15 cm - 30 cm) with a resolution between 5 km and 70 km. Both active and passive microwave techniques are sensitive to the dielectric properties of the land surface and therefore to soil moisture in the upper few centimetres of the soil, but scattered and emitted radiation also depends on surface roughness, the distribution of soil moisture over depth, soil temperature and strongly on vegetation (Schneeberger et al., 2004; Wilker et al., 2006; Fernandez-Galvez, 2008; Hajnsek et al., 2009; Koyama et al., 2010).
The resolution in time is restricted to a few snapshots per day or even coarser. Aircraft or drone-mounted thermal, hyperspectral and/or microwave systems can be used to achieve higher temporal resolutions. The application of aircraft mounted systems is because of the high costs restricted to airborne campaigns (e.g. Famiglietti et al.; 2008, Hajnsek et al., 2009; Bronstert et al., 2011). The robustness and usefulness of less cost-intensive systems such as thermal cameras and/or multiple digital cameras using specific optical filters mounted on drones are currently under investigation. However, there are still limitations, such as the need for parallel ground truth measurements for validation aspects, uncertainties in polarimetric decomposition techniques (Polarimetric-SAR), the influence of vegetation coverage and surface roughness on the measurement, low penetration depth, and the non-availability of continuous measurements.
The studies presented by Albergel et al. (2009) and Brocca et al. (2010) show that with an exponential filter as the data preparation method, ASCAT (Advanced Scatterometer) data sets could be able to reproduce measurements at depths up to 40 cm, which would be important for assimilation of remote sensed data into hydrological models.
The GRACE (Gravity Recovery and Climate Experiment) mission provides monthly water storage changes in a coarse resolution of a few thousand kilometres. Using GPS and a microwave ranging system, GRACE infers Earth's gravity field through highly accurate measurements of the distance between a pair of satellites (Tang et al., 2010).

1.1.3 How is soil moisture represented in hydrological models (conceptual, large scale vs. hillslope scale)?

In hydrology two main types of model concepts can be characterised: conceptual and physically based models. Engineering practice has traditionally been either concerned with predictions of water driven hazards such as floods or with water resources management. This allows focus on successful prediction of catchment response, using conceptual hydrological models that represent the process patterns and redistribution of water inside the catchment with simplified concepts such as LARSIM (Bremicker, 1998), HBV (Lindstrom et al. 1997; Hundecha and Bárdossy, 2004), TOPMODEL (Beven and Kirkby, 1978; Buytaert and Beven, 2009), IHACRES (Croke and Jakeman, 2004), SWAT (Arnold et al., 1998) or SWIM (Krysanova, 1998). It implies a) a certain catchment size so that errors due to simplified process conceptualisations may average out (Dooge, 1986), and b) stationarity of climate conditions and of the hydrological system itself (Sivapalan et al., 2003). The soil storage is described as a linear storage or as a cascade of several of them, which can not be directly compared to observed soil moisture.
Conceptual hydrological models describe the processes inside the catchment and the underlying controls with a high degree of abstraction and by means of effective states, effective parameters and effective fluxes. Though these models often operate with very good results in upper meso-

scale catchments (>200 km² - 10^4 km²), they are a virtue made out of necessity. The charm of conceptual models is that they are parsimonious and still allow reproduction and prediction of hydrological responses – mainly stream flow at the mesoscale (Uhlenbrook and Leibundgut, 2002).

However, conceptual model predictions are subject to considerable uncertainty (Beven, 2002; Wagener and Gupta, 2005; Bárdossy, 2007). Several sets of model parameters allow an acceptable reproduction of discharge observations at a catchment of interest.

The major drawback of conceptual models is, however, that their ability to reproduce the runoff response at the catchment outlet does not necessarily mean that simulated dynamics inside the model domain can be expected to be consistent with the "true" distributed process dynamics within the catchment (Zehe and Sivapalan, 2009).

Conceptual models cannot be directly updated either, since which combination of local processes and redistribution mechanisms caused the observed response at the catchment outlet, or which internal structures and states control the space-time organisation of flow and transport is unknown. It is therefore rather difficult a) to predict how changes of the system will translate into altered hydrological functioning (Sivapalan et al., 2003; Zehe and Sivapalan, 2009), b) to expand these models for spatially distributed predictions of water driven processes such as erosion or tracer transport and c) to use such conceptual models for operational forecasts at the lower mesoscale, even under current conditions.

Physically based hydrological models describe soil water flow using the Darcy-Richards' approach (including different approaches for preferential flow), solute transport using the convection dispersion approach and overland flow by 1D- or 2D hydraulic approaches. Well known examples are, for instance, CATFLOW (Zehe et al., 2001), HILLFLOW (Bronstert and Plate, 1997), HillVi (Weiler and McDonnell, 2004), HYDRUS (Šimunek et al., 1999), InHM (VanderKwaak and Loague, 2001) and MIKE SHE (Refsgaard and Storm, 1995; Christiansen et al., 2004). The charm of these models is that they are able to integrate observed data sets and can reproduce the hydrological processes at the hillslope and the micro-catchment scales up to the order of 1 km². The models can be validated using distributed observations of soil moisture, runoff or evapotranspiration (ET) within the system. Hence, such models allow a much more reliable estimate of how local changes in system properties affect local process patterns and the redistribution of water into integral hillslope and catchment response. A direct comparison with state variables and therefore with soil moisture is possible. But they rely, however, on a vast amount of different parameters for soil, surface and vegetation. An adequate use of these models requires detailed high resolution data sets that capture the multivariate statistical and topological properties of subsurface parameters and flow paths. Except for a few microscale research catchments, this information will scarcely ever be available. However, application of physically based models at the lower mesoscale (10 km² - 200 km²) is not feasible, even if sufficiently resolved data were available. Achieving convergence, stability and accuracy of the numerical solution of a set of partial differential equations in a highly heterogeneous and very large model domain is a highly non-trivial issue of numerical mathematics. Thus, there is the obvious risk that too much effort has to be invested in implementing numerical solvers instead of working on the processes and process controls themselves. Increasing spatial resolution and moving to effective parameters while using the Richards' equation is unlikely to solve the problem either. There is considerable argument against the validity of the Richards' equation when used with grid sizes of

several 100 m (Vogel and Ippisch, 2008), on the validity/usefulness of large scale water retention curves (Zehe et al., 2006; Beven, 2006b; de Rooij, 2009; Baroni et al., 2010), or identifiability of useful effective parameters (Binley et al., 1989; Beven and Binley, 1992). Increasing the resolution and still using Richards' equation as in case of WaSiM ETH II (Schulla, 1997), MIKE SHE (Refsgaard and Storm, 1995), or DHDVM (Wigmosta and Lettenmaier, 1994) has the effect of losing the physical basis.

1.1.4 Can measured soil moisture data be used to improve hydrological models and how can that be implemented?

A profound knowledge of the catchment wetness conditions (average values, and possibly also the areal and vertical distribution) prior to a rainstorm is considered to be important information for an improved forecast performance for flood runoff (Dunne et al., 1975). In simulation of the hydrological system these state variables will be affected by the errors in estimated and measured meteorological forcing, which can result in wrong conditions and patterns of the catchment state and thus will have an impact on the runoff generation (Aubert, 2003). There is a variety of methods to improve the knowledge of the conditions and patterns of state variables. The most traditional methods are the use of the pre-event precipitation (antecedent precipitation index, API) or the pre-event runoff as an indicator for the subsurface storage (Fedora and Beschta, 1989; Pilgrim and Cordery, 1993; Berthet et al., 2009).

For the integration of state variables like soil moisture into conceptual hydrological models there exists a scale problem between the observed scale and the model scale and the problem of non commensurability between observed and simulated state variable. The scale of the observed state variable of a point measurement is the size of a few cubic centimetres, and because of their nonlinearity, these variables are not directly transferable into larger volumes (Blöschl and Sivapalan, 1995; Merz and Plate, 1997; Vogel and Roth, 2003).

Whichever measurement approach is employed (fixed set of sensors or measurement campaign) there is no simple method available to scale the information from the distributed set of point observations to the catchment scale because of non-linear process dynamics and strong sub-catchment heterogeneity of soils and vegetation. Geostatistical interpolation, including updating approaches, suffer from the fact that they either assume stationary relationships between drift parameters and soil moisture, or the sampling is not sufficient to obtain useful posterior probability distributions of soil moisture within different classes of available soft information. However, there are several developments available to integrate observed soil moisture into model applications. The methods range from ground based measurements to remotely sensed data sets and combinations of both. That includes the initialisation of soil moisture by field measurements (Goodrich et al., 1994; Jacobs et al., 2003; Zehe et al., 2005; Brocca at al., 2009a; Noto et al., 2008) and the updating by assimilation techniques (Aubert et al., 2003; Francois et al., 2003; Crow et al., 2005). An increase in model performance is observed but with minimal effect, according to Crow and Ryu (2009).

Despite the above criticism, further research is required to explore the limits and potentials of soil moisture assimilation in rainfall-runoff models. In this context, an important question is: How can soil moisture observations be related to the model's state variables? The answer to this

question is – on the one hand – subject to the modelling concept (e.g. lumped vs. distributed, event-based vs. continuous), and on the other hand the spatial scale and variability at that scale.

1.2 Key research questions and approach

1.2.1 Key questions:

* Can representative soil moisture measurements at the plot scale help to understand flood generation in headwater catchments?

Hydrologic systems often respond highly non-linear to rainfall events. Non-linear behaviour can have many reasons (Zehe et al., 2007). The system can be controlled by threshold processes which switch between system states and result in drastically different runoff response. This type of relationship can be found between runoff and driving forces such as precipitation (e.g. Tani, 2007; Detty and McGuire 2010; Graham et al. 2010), state variables such as soil moisture (e.g. Western et al. 1998; Weiler and McDonell, 2007; Zehe et al., 2007; Detty and McGuire 2010; Penna et al. 2010), or groundwater levels (McGlynn et al. 1999; Detty and McGuire 2010). In this context, soil moisture can be seen as a key state variable that controls hydrological dynamics at various spatial scales. There is experimental evidence that the onset of point scale threshold processes such as fast preferential flow in soils (Zehe and Flühler, 2001a; Blume et al., 2009), Hortonian overland flow initiation (Zehe et al., 2007), or the switch between hydrophilic and hydrophobic conditions (Dekker et al., 2005) are strongly controlled by antecedent soil moisture conditions. As mentioned above, soil moisture is highly variable in space and time which make its observation difficult. The clustering of several TDR probes within one field site seems a promising strategy to observe and describe the spatiotemporal variability of soil moisture and to understand its role in runoff generation. These detailed measurements of soil moisture, given that they are located at representative study sites, will indicate whether different conditions in this state variable affect the system response, namely runoff, and thus provide a means to gain insight into the underlying processes.

* Can representative soil moisture measurements at typical landscape elements help us to predict floods at the catchment scale?

Various studies suggest that the antecedent soil moisture state exerts crucial control on rainfall-runoff response at the field and headwater scale (Bronstert and Bárdossy, 1999; Gurtz et al., 1999; Jayawardena and Zhou, 2000; Montgomery and Dietrich, 2002; Meyles et al., 2003; Chirico et al., 2003; Zehe and Blöschl, 2004; Zehe et al., 2005, Blöschl and Zehe, 2005). Brocca et al. (2009a) presented the importance of covering the variance in soil moisture to give a reasonable estimate of state. A profound knowledge of soil moisture with a spatial extent which covers the variance will provide the possibility for an indicator of the catchment state. The importance of soil moisture in the forecast will be tested with a statistical generalised linear model technique and will prove that knowledge of observed soil moisture can be used to update catchment state in the conceptual model WaSiM ETH.

* How can additional information be used to observe near surface processes? What is the potential of Spatial TDR? What is the potential of clustering TDR sensors at representative locations?
There are different methods available to use the additional information gained from the reflection estimated with the TDR technique to observe near surface processes (e.g. Feng et al., 1999; Oswald et al., 2003; Schlaeger, 2005; Greco, 2006). To quantify the spatial distribution of the soil moisture along the wave guide, an inverse signal analyzing technology called "Spatial TDR" has been introduced by Becker (2004), Schlaeger (2005), and Scheuermann et al. (2009). The method promises to monitor moisture dynamics in a three dimensional way.
Exploring the capabilities and limitations of Spatial TDR is of great importance for assessment at plot, field, and small catchment scale.

1.3 Experimental approach and data analysis

These three key questions are investigated in this work by experimental approaches and data analysis, moving from the lab scale to the catchment scale.
The experimental approaches aim at testing the feasibility of the Spatial TDR systems under different conditions. The experiments can be distinguished according to their types of forcing conditions and investigation scales:

- Controlled lab experiments with defined initial conditions and input volumes are conducted at the soil column scale to investigate the capabilities of Spatial TDR measurements.
- An irrigation experiment in the field with controlled input volumes to investigate the dominating runoff processes at the hillslope scale.
- Long-term observations under natural conditions are carried out at the field scale to observe spatiotemporal patterns.

Data analysis and process modelling are used to validate inversion results, gain understanding of runoff processes and test the importance of soil moisture in the observed processes, again moving from the lab to the catchment scale.

- The Spatial TDR inversion results are validated to identify the effects of structures and heterogeneous soil moisture distributions on the inversion results.
- The field data are statistically analysed to understand spatial and temporal dynamics of a) the entire time series and b) selected flood events.
- Physically based modelling at the hillslope scale is used to determine the importance of ET for soil moisture.

In a last step a conceptual models at the catchment scale and a purely data driven model are compared to investigate the importance of soil moisture observations for the estimation of runoff volumes during flood events.

1.4 Structure of this dissertation

This dissertation is part of the OPAQUE (operational discharge and flooding predictions in head catchments) project that aims on a better prediction of flood events in mountainous headwaters and has its main researche catchment in the Weißeritz. The project is funded by the German Ministry of Education and Research (BMBF) as part of RIMAX (Risikomanagement extremer Hochwasserereignisse). In the project the focus of the dissertation aims on the investigation of the influence and the impact of soil moisture the runoff formation.
It is structured into five major chapters, which are briefly outlined below:

Chapter 1 Introduction
A general overview of the importance of soil moisture and the different techniques used to measure it, noting here the spatial and temporal resolution and error sources. The importance of soil moisture for hydrological systems is presented and how soil moisture is represented in hydrological models is described. The key questions are postulated and the approaches to answer them are presented.

Chapter 2 Spatial TDR technology– methodology and feasibility for heterogeneous field soils
This study presents an application of the Spatial TDR technology with the underlying theory. It will be reported in detail how error sources affect retrieval of soil moisture profiles in soils. Soil column experiments in glass beads and disturbed real soil from the study area under different conditions are presented. It will be reported in detail how these error sources affect retrieval of soil moisture profiles in these soils.

Chapter 3 Soil moisture dynamics and runoff generation in headwater catchments: learning from field data
An overview of the research area is presented. Spatial and temporal analyses of time series of soil moisture and runoff are carried out. Process understanding is gained by modelling the interaction of evapotranspiration (ET) on the soil moisture with the hydrological process model CATFLOW. A field scale irrigation experiment is carried out to get a better understanding of the near subsurface processes at the hillslope scale. A statistical analysis sheds light on the influence of different state variables and variables of meteorological forcing on the flood volume. A closer look is taken on selected events to understand the different responses during dry and wet conditions and identify possible threshold processes.

Chapter 4 Soil moisture dynamics and runoff generation in headwater catchments: Learning from models of different complexity
Here it will be discussed how different modelling strategies can help to increase the knowledge about relevant runoff processes and to improve the prediction of runoff volumes. The conceptual hydrological model WaSiM ETH I is used to asses if this kind of model can be helpful and if it is possible to incorporate measured values of state variables. Generalised linear models are evaluated to see how well they can predict runoff volumes.

Chapter 5 Discussion, outlook and recommendations
Section 5 contains the overall discussion and summary.

CHAPTER 2 SPATIAL TDR TECHNOLOGY– METHODOLOGY AND FEASIBILITY FOR HETEROGENEOUS FIELD SOILS

2.1 Introduction

Spatially and temporally distributed Time Domain Reflectometry (TDR) and Frequency Domain Reflectometry (FDR) measurements are widely used to observe soil moisture dynamics at the plot to hillslope scale (e.g. Starr and Timlin, 2002). Conventional TDR measurements allow estimation of the mean soil moisture and the bulk electrical conductivity of the surrounding media based on the travel time of a reflected electromagnetic wave guided in a waveguide/TDR probe installed in the soil. Excellent reviews are given by Robinson et al. (2003) and Cassiani et al. (2006). Several authors have shown that the shape of the reflected TDR signal, the reflectogram, contains information about the dielectric permittivity (ε) and thus the soil moisture along the probe (Oswald et al., 2003; Schlaeger, 2005). The retrieval of this detailed information is achieved by inversion or by graphical interpretation of the signal (Moret et al., 2006). Inverse estimation of the soil moisture profile seems to work well for synthetic data sets (Oswald, 2000), homogeneous soils at the lab scale (Becker, 2004; Greco, 2006; Bänninger et al., 2008) or volcanic ash soils with low bulk densities of ~1.0g cm^{-3} (Greco and Guida, 2008).
The essential idea of Spatial TDR is to cluster several wave guides in a small area, operate them by a single sampling TDR and invert the reflectograms to elucidate the evolution of the soil moisture profile. Spatial TDR is originally proposed by Schlaeger (2005) and further tested by Scheuermann et al. (2009) to monitor moisture in sandy dams. The reflectogram of the TDR measurement is influenced by the probe geometry (Spittlehouse, 2000; Bänninger et al., 2008), solids in the sphere of influence (Knight et al., 1997), layered soils (Greco, 2008) or energy dissipation along the probe due to clay and salinity (Jones and Or, 2004; Chen et al., 2007; Kupfer et al., 2007). These different factors may hamper the application of Spatial TDR measurements in real world settings. The use of coated rods protects the TDR signal from energy dissipation (Ferré et al., 1998; Nichol et al., 2002), increasing the signal-to-noise ratio and thus allows the use of longer TDR rods compared to uncoated rods, which is essential for Spatial TDR applications (Dalton and Van Genuchten, 1986). The drawbacks of coated rods are that they are less sensitive to ε, that a coated material needs specific calibration (Ferré et al., 1996), and that the measurement of bulk electrical conductivity is restricted (Moret-Fernández et al., 2009). As the high clay content of the soils in the study area is around 16 %, the use of TDR probes is preferred with three coated rods. This allows the use of 0.60 m long probes, which is favourable for the observation of infiltration processes into the subsurface.
In general, it is assumed that the TDR rods are installed parallel, but this is difficult to actually achieve when installing probes in natural soils, especially in the presence of stones, layers, or soil bulk density differences. Figure 1 shows an extreme example with rods converging or diverging with increasing depth for a rather heterogeneous soil located in the Ore Mountains, Saxony, Germany (see Section 3).
The effect of the probe deformation on the reflectogram and the retrieved soil moisture has thus to be studied in detail, because it is essential for the Spatial TDR approach to use long TDR rods.

The influence of insulating solids in the sampling volume is theoretically described by Knight et al. (1997), but there is no study which studied the influence of solids on the reflectogram.
The overall objective of this chapter is to shed light on the applicability of Spatial TDR in strongly heterogeneous field soils. Therefore, the questions posed for this research are: 1) How do coated probes of 0.60 m length react in these soils (heterogeneous, electrical loss), and are these probes indeed better suited for these soils compared to uncoated probes? 2) How does the effect of a) different probe deformations, b) solids (insulators, conductors) in the integration volume and c) high clay content in combination with a bulk density gradient influence the ε profile, the inverted moisture profiles and the average soil moisture along the probe? Different laboratory experiments are performed to shed light on these topics.

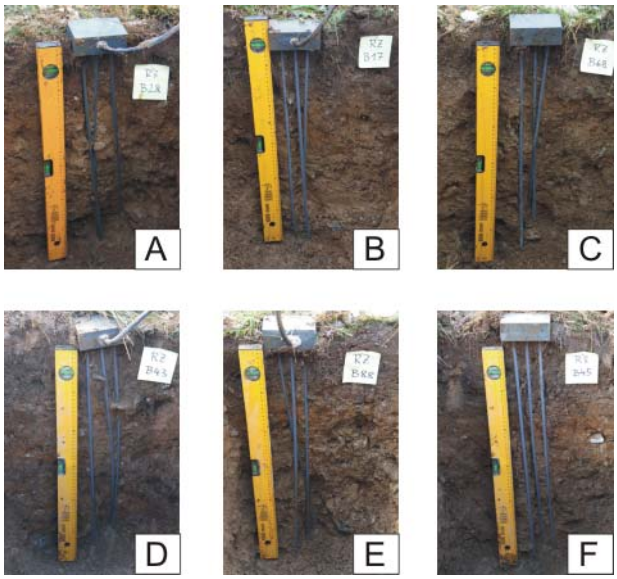

Figure 1: Typical soil profiles with different horizons and coarse gravel and possible deformations of the TDR wave guides when installed in the soil (A to F), by A. Bauer.

In Section 2.2 a review of different inversion techniques is given. Section 2.3 provides details on the technological components and discusses potential sources of errors observed in field applications. Section 2.4 introduces five different laboratory experiments. Section 2.5 discusses the step from applications in homogenous media or "the technical scale" to reliable applications in heterogeneous field soils, for instance when designing a site-specific calibration of transmission line properties. This step is crucial for hydrology because the relationship between soil moisture dynamics and runoff generation is not well understood yet; this is especially true for heterogeneous soils. These results are furthermore necessary to interpret soil moisture observations obtained with two Spatial TDR clusters installed in the Eastern Ore Mountains, presented in a closely related study by Section 3. That study will introduce the applicability of Spatial TDR in the field scale.

2.2 Theoretical background and Signal constrained inversion

2.2.1 TDR inversion approaches

In this section an introduction to the inversion methodology and an overview of the different inversion techniques is presented. Generally, it is necessary for the estimation of the soil moisture profiles along the TDR probe to simulate the propagation of the TDR signal in time domain by employing a numerical model (forward problem). This is achieved by simulating the forward and back propagation of the TDR signal along the wave guide and minimizing the differences between observed and simulated signals by using an optimization algorithm which updates the parameter profile along the transmission line. Full wave approaches solve Maxwell's equations within the forward step (Rejiba et al., 2005). The target parameter of the optimization is the profile of the ε along the wave guide. Other studies have proposed simplified approaches based on multi-section transmission lines (Heimovaara et al., 2004) or heterogeneous transmission lines (Greco, 2006); the Spatial TDR approach (Schlaeger; 2005) belongs to the latter category. The wave propagation along the TDR probe is approximated by the telegrapher's equation. The transmission line is conceptualized as a series of bulk electronic components such as resistors, inductors and capacitors. Hence, the target parameter of the optimization is the electrical capacitance profile (C). The Spatial TDR algorithm requires additional material laws that link C-ε-soil moisture and – in the case of TDR probes with coated rods – C and electrical conductance G of the transmission line (compare section 2.3).

2.2.2 STDR Signal inversion

The TDR signal $V_R^o(t,x_0)$ or reflectogram is a superposition of the input voltage $V_I^o(t,x_0)$, generated by the TDR device, and partial reflections of the input signal occurring at the junction of the probe and cable as well as at the end of the wave guide. The average ε along the transmission line is determined by the speed of the electromagnetic wave and can be calculated based on the travel time of the TDR signal. The average ε can be transformed into the average soil moisture content along the probe by appropriate calibration functions (see section 3.4). The form of the reflectogram between the first and second main reflection at the probe's beginning and end is a finger print of the dielectric profile along the wave guide.

The principle of the Spatial TDR inversion is to estimate the capacitance profile $C(x)$ along the wave guide by means of inverse modelling and transform it into a soil moisture profile $\theta(x)$. As explained above, the forward step of the Spatial TDR algorithm is based on the telegrapher's equation, which describes the propagation of a voltage pulse $V(x, t)$ along the transmission line:

Eq. 1

$$\left(L(x)C(x)\frac{\partial^2}{\partial t^2} + L(x)G(x)\frac{\partial}{\partial t} + \frac{\partial L(x)/\partial x}{L(x)}\frac{\partial}{\partial t} - \frac{\partial^2}{\partial x^2} \right) V(x,t) = 0 .$$

Here t is time and x the spatial coordinate along the wave guide. The capacitance $C(x)$ and electrical conductance $G(x)$ are both affected by the soil moisture profile $\theta(x)$ along the

transmission line. The inductance $L(x)$ is a function of the transmission-line only and piecewise constant for the coaxial cable and moisture probe, as long as the rods are parallel. The spatial derivative of L in Eq. (1) accounts for the difference between coaxial cable and probe. Compared to the general telegrapher's equation, it is assumed that resistive losses along the probe can be neglected and the electrical resistance $R = 0$. All parameter profiles will be given as specific values per unit length. Nichol et al. (2002) have shown that the true electric conductivity σ cannot be measured with coated probes. Therefore, G is not the real ionic conductance of the soil but an effective value of coating and soil conductivity.

Within the inverse procedure Eq. (1) is numerically solved with appropriate initial and boundary conditions to simulate $V_R^s(t,x_0 \mid C)$ for given parameter profiles $C(x)$ and $G(x)$. Based on the difference between the simulated $V_R^s(t,x_i \mid C)$ and observed signal $V_R^o(t,x_i)$ between the first (at $t = 0$) and the second main reflection (at $t = T$), the transmission line parameters $C(x)$ and $G(x)$ are updated by the conjugate gradient method until the objective function $J(C)$ in Eq. (2) is minimized.

Eq. 2

$$J(C) = \int_0^T \left(V_R^s(t, x_i \mid C) - V_R^o(t, x_i) \right)^2 dt$$

The high quality of the recorded signal of the TDR100 (Campbell Scientific Inc), which has a time to peak of roughly 200 pico seconds, allows inversion at a spatial resolution of 0.01 m (Oswald et al., 2003; Lin et al., 2005). The solution of Eq. (1) is a profile of $C(x)$ which has to be related to the permittivity profile of the porous medium $\varepsilon(x)$ and finally to the moisture profile $\theta(x)$ (compare next sections). Subsequently, it will be referred to the resulting soil moisture profile which is obtained after conversion as the inverted moisture profile. For more details see Schlaeger (2005).

2.3 Parameters and Potential error Sources of Spatial TDR-Measurements

2.3.1 Technological components and setup of a Spatial TDR

A TDR100 by Campbell Scientific Inc. is used to generate TDR pulses. Coated three-rod probes of type SUSU03 with a length of 0.60 m developed by Schädel (2006) are used as wave guides. These consist of a stainless steel core of 6 mm diameter with a 1 mm thick PVC coating. The distance between the rods is 0.03 m. The rods are screwed into the probe head that is connected to a 50 Ω coaxial cable of type RG213.The probes are connected to an eight channel multiplexer of type SNAPMUX (Becker, 2004) with coaxial cables of type RG213 with an impedance of 50 Ω and a length of 15 m. The TDR100 is controlled and the data are logged by an ARCOM VIPER 1.2 Industrial-PC with embedded LINUX operating system.

2.3.2 Calibration of probe parameters

The pulse velocity of the TDR signal v is given by

Eq. 3

$$v = 2l / \Delta t ,$$

where l is the probe length and Δt the time difference between the first two main reflections in the reflectogram.

The equation to link v to ε with $v = c_0 / \sqrt{\varepsilon}$, with c_0 as the speed of light, does not apply for coated probes because here the signal depends on an effective ε which is composed of the dielectric properties of the coating and of the surrounding medium and would lead to an underestimation of soil moisture (Ferré et al., 1996). Becker (2004) and Huebner et al. (2005) suggested that the pulse velocity $v(\varepsilon)$ can be best expressed by the constant inductance L of the probe and the effective capacitance $C(\varepsilon)$ of the system probe and medium:

Eq. 4

$$v(\varepsilon) = 1/\sqrt{L \cdot C(\varepsilon)} .$$

In a second step ε of the medium is estimated with a relationship between $C(\varepsilon)$ and ε in the case of the three rod TDR probe described by a simple circuit model consisting of a series of capacitors, representing the capacitor between the rods filled with the surrounding medium C_1 and describing the constant capacitance of the coating C_2 (Figure 2):

Eq. 5

$$1/C(\varepsilon) = 1/(\varepsilon \cdot C_1) + 1/C_2 .$$

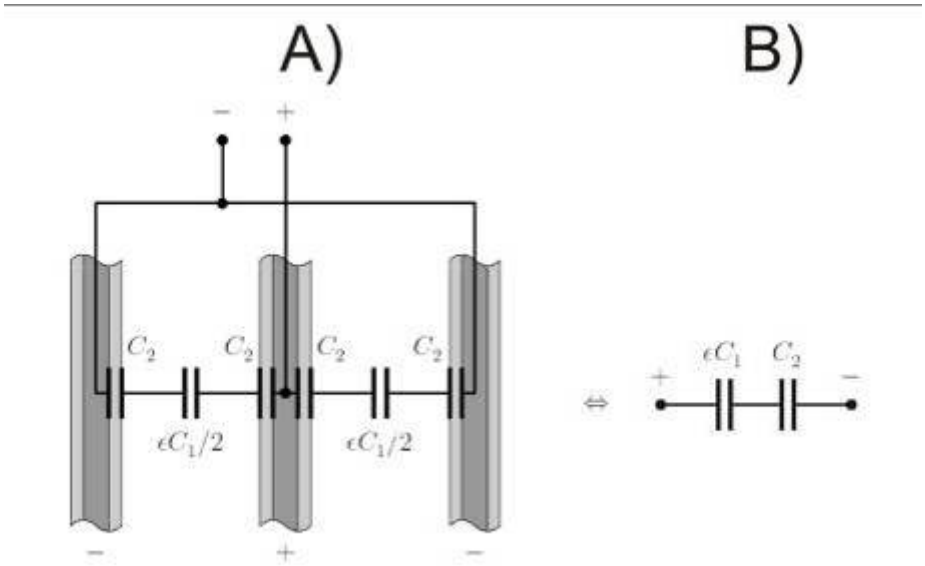

Figure 2: Total capacitance C of a 3-rod-probe as a function of the soil's dielectric permittivity ε. (A) segment of three parallel rods immersed in soil; light grey: PVC coating; dark gray: metallic core; (B) equivalent circuit. C1, C2: constant capacitance parameters determined by the probe's geometry (Becker, 2004).

According to Eq. 4 and 5 the probe is characterized by the three parameters C_2, C_1, and L, which have to be estimated by calibration measurements. C_1 and L are affected by the probe geometry, especially the distance of the wave guide rods. For parallel rods, the parameters are assumed to be constant. Becker (2004) found a good correspondence in the relationship between ε and C derived from full wave numerical simulations of coated three rod probes and the capacitance model shown in Eq. (5). Further laboratory observations corroborated the applicability of this capacitance model to parameterize the relationship between ε and C.

Becker (2004) suggested a calibration approach based on measuring TDR pulse velocities $v_i = v(\varepsilon_i)$ for two different media with well known dielectric permittivity values ε_1 and ε_2 (water and air) to determine C_2, C_1, and L. Combining Eq. 4 and Eq. 5 for the two media and solving them for C_1 and C_2 yields:

Eq. 6

$$C_1 = (\varepsilon_2 - \varepsilon_1)/(\varepsilon_2\varepsilon_1(v_1^2 - v_2^2)\cdot L), \text{ and } C_2 = (\varepsilon_2 - \varepsilon_1)/((\varepsilon_2 v_2^2 - \varepsilon_1 v_1^2)\cdot L).$$

Finally, L is estimated with the relationship to the rod impedance:

Eq. 7

$$Z(\varepsilon) = \sqrt{L/C(\varepsilon)}.$$

The jump between the impedance of the probe plus the surrounding medium $Z(\varepsilon)$ and the impedance of the connecting cable Z_0 causes a partial reflection of the TDR signal at the junction of cable and probe. By measuring the amplitudes of incoming and reflected signal, denoted by A_I and A_R, the reflection coefficient will be obtained that is linked to the impedance as follows:

Eq. 8

$$r(\varepsilon) = A_R / A_I = (Z(\varepsilon) - Z_0)/(Z(\varepsilon) + Z_0),$$

Substitution of Eq. 4 and Eq. 7 into Eq. 8 and solving for L yields:

Eq. 9

$$L = (1 + r(\varepsilon))/(1 - r(\varepsilon))\cdot Z_0 / v(\varepsilon).$$

Table 1: Probe parameters estimated based on Eq. 5 and 9 and absolute errors calculated with Gauss' law.

Parameter	Value	Abs. Error
L [nH m^{-1}]	625.0	23.0
C_1 [pF m^{-1}]	22.4	0.9
C_2 [pF m^{-1}]	304.6	30.0

Based on Eq. 6 and Eq. 9, the probe parameters C_1, C_2, and L have been derived from TDR reflectograms obtained in de-ionized water (ε = 80 at 20°C) and air (ε = 1) with parallel rod

geometry for all probes, as presented in Table 1. Based on the standard deviation of the dielectric permittivity values, the relative measurement error to 5 % can also be quantified.

2.3.3 C-G relation

As coated rods do not allow direct measurements of the electrical conductivity, an empirical function that relates $C(x)$ to $G(x)$, as proposed by Hakansson (1997), to close the set of equations is employed:

Eq. 10

$$G(C) = \begin{cases} G_\infty \cdot (1 - \exp(-(C - C_0)/C_d), & \text{if } C \geq C_0, \\ 0, & \text{if } 0 \leq C \leq C_0. \end{cases}$$

G_∞ is the conductance at saturation, C_0 is a capacity threshold below which conductance is zero and C_d determines how fast C reaches its maximum value. Becker (2004) showed with numerical simulations that Eq. 10 is a suitable model. In general, C_d, G_∞, and C_0 have to be determined empirically. Furthermore, in a clay-rich soil one could expect G to be non-zero for a C smaller than C_0. The parameter estimation requires manual calibration during the inversion of a known soil moisture profile.

2.3.4 ε-soil moisture relationship

Different models linking ε and soil moisture are reviewed by Cassiani et al. (2006) and Lesmes and Friedman (2005). Because of different geochemical and geophysical properties it is difficult to find a universal petrophysical relationship for the unsaturated zone (Paasche et al., 2006). In this study, the soil moisture from ε is calculated using the empirical relation proposed by Topp et al. (1980) for sand and glass beads. The ε-soil moisture relationship is developed using 11 undisturbed soil samples in a plastic core cylinder (diameter = 0.057 m, length 0.10 m) from different horizons of the study area. In the laboratory, samples are saturated and in each sample a 3-rod 0.075 m long TDR probe (CS640-L connected to a TDR100, both Campbell Scientific Inc.) are inserted. The samples are slowly dried. Once or twice a day the soil moisture is estimated by gravimetric method and the dielectric permittivity by TDR measurements. Different approaches to link ε and θ soil moisture are tested (Alharthi and Lange, 1987; Roth et al., 1992; Malicki et al., 1996; Friedman, 1997). For the soils in the study area, the linear relationship between the refractive index and soil moisture (Herkelrath et al., 1991) is found to be most suitable:

Eq. 11

$$\theta = a + b \cdot \sqrt{\varepsilon}\,.$$

The parameters a and b are fitting parameters.

2.3.5 Probe deformations during installation

It is investigated whether Spatial TDR clusters allows assessment of distributed soil moisture profiles under natural conditions in the headwater of the Weißeritz catchment close to the village of Rehefeld in Saxony, Germany. Soils are mainly Cambisols in periglacial weathering strata. In the summer of 2006, two Spatial TDR clusters were installed at two hillslopes close to the village of Rehefeld. Table 2 shows the mean soil characteristics determined from 20 undisturbed soil samples extracted in profiles excavated up to a depth of 0.70 m close to one of the clusters. Additional details of the project context, the spacing of TDR probes and the catchment are discussed in Section 3. The importance for the present study is that the installation of the 0.60 m long Spatial TDR probe at this field site is a challenging task, due to the large amount of gravel of up to 0.4 kg kg^{-1} (Landesamt für Umwelt, Landwirtschaft und Geologie, 2006), the increasing density with depth and the heterogeneity of the soils. Similar problems are documented by Spittlehouse (2000). A steel template with three holes set at the right distance between the rods is used, as well as a power drill with a 0.60 m long auger. Several attempts (on average about two) are necessary to drill three holes with the appropriate distance and depth due to gravel blocking. Nonetheless, difficulties occur in ensuring that the rods of the probes are parallel. Figure 1 illustrates typical deformations of the probes; the rods converge (Figure 1A) or diverge (Figure 1B) towards the end with increasing depth. As the theory of the inversion assumes parallel geometry of the rods, these deformations will likely cause errors in the estimated soil moisture profiles, because C_l and L cannot be assumed as constant over the profile. In section 3.2, the experimental setup to investigate the influence of simple rod deformations on the inversion is described.

Table 2Soil texture (following the United States Department of Agriculture (USDA), 1993 classification), bulk density θ_b, saturated soil moisture θ_S and permanent wilting point (*PWP*) of the dominating Cambisol at the Rehefeld study area, and experimental glass beads. ϱ and θ_S are estimated for 1.00 m³ soil cores with grain density of 2.65 g cm^{-3}. *PWP* is the soil moisture at 160 m pressure head. The glass beads have a grain size ranging from 0.25 to 0.5 mm in diameter. Standard deviation is abbreviated as STD.

Soil type	Sand [%]	Silt [%]	Clay [%]	ρ_b [g cm^{-3}]	STD ρ_b [g cm^{-3}]	θ_S [m^3m^{-3}]	*PWP* [m^3m^{-3}]
Cambisoil Rehefeld	52	32	16	1.15	0.11	0.56	0.08
Glass beads	100	-	-	1.50	0.05	0.38	0.03

2.3.6 Gravel and stones

The pulse velocity measured with TDR is related to the average volumetric soil moisture. This can, as suggested by Topp and Davis (1982), lead to misinterpretations when abrupt water content changes along the transmission lines are present. Knight et al. (1997) discussed theoretically the influence of "gaps" in the integration volume which are filled with materials with either a lower than average or higher than average permittivity. They found materials with lower

than average permittivity to have stronger impacts on TDR measurements. From a soil physical view, coarse gravel and stones in the integration volume of the TDR probe reduce the total volume of the pore space Φ at that depth.

2.4 Laboratory experiments to quantify error sources

This section shows the setup of the five different laboratory experiments and the results are presented. In Experiment 1 to 4, glass beads with a grain size of 0.25-0.5 mm diameter are used to ensure that the performance test took place in a medium with homogeneous pore space. In Experiment 5, disturbed soil from the field as described in Table 2 is used to test the method within a heterogeneous medium.

2.4.1 C-G relation, ε-soil moisture relation and constraining of inverted moisture profiles

The three parameters C_d, G_∞, and C_0 of Eq. (10) are estimated within Experiments 2 and 5. The results are listed in Table 3. The parameters of Eq. (11) a and b are estimated at -0.2291 and 0.1324, respectively. The coefficient of determination R^2 is 0.9837.

Table 3: Parameter sets characterizing the *C-G* relations for inversion of the reflectograms into soil moisture profiles both for glass beads and soils.

Exp.	Name	G_∞ [mS m^{-1}]	C_0 [pF m^{-1}]	C_d [pF m^{-1}]
1	Glass beads	1.5	50	18
2	Rehefeld soil	2.0	50	18

The last crucial step to ensure that the inverted soil moisture profiles complied with soil physics is to constrain the inversion within a physical range. The upper end is defined by soil saturated water content (θ_s) and the lower end by the permanent wilting point (*PWP*). This can easily be achieved by using the inverse ε to θ and the inverse C to ε relationships to obtain upper and lower limits for C. The parameters for the different soil substrates are listed in Table 2.

2.4.2 Experiment 1: effect of uncoated and coated probes on the reflectogram in field soils

Two SUSU03 probes are compared, one of each with and without coating. Experiments are accomplished in a plastic box with a height of 0.70 m and edge length of 0.30 m by 0.30 m (Figure 3A). Both probes are installed in the middle of the box and a wooden template is placed at 0.59 m depth to secure ideal probe geometry (Figure 3A). The box is carefully filled with glass beads that are moderately compacted to ensure good contact between soil and TDR probes

(Table 2). The experiment is conducted at two different wetness conditions, namely 0.08 m^3m^{-3}-0.09 m^3m^{-3} (dry) and 0.20 m^3m^{-3}-0.21 m^3m^{-3} (wet).

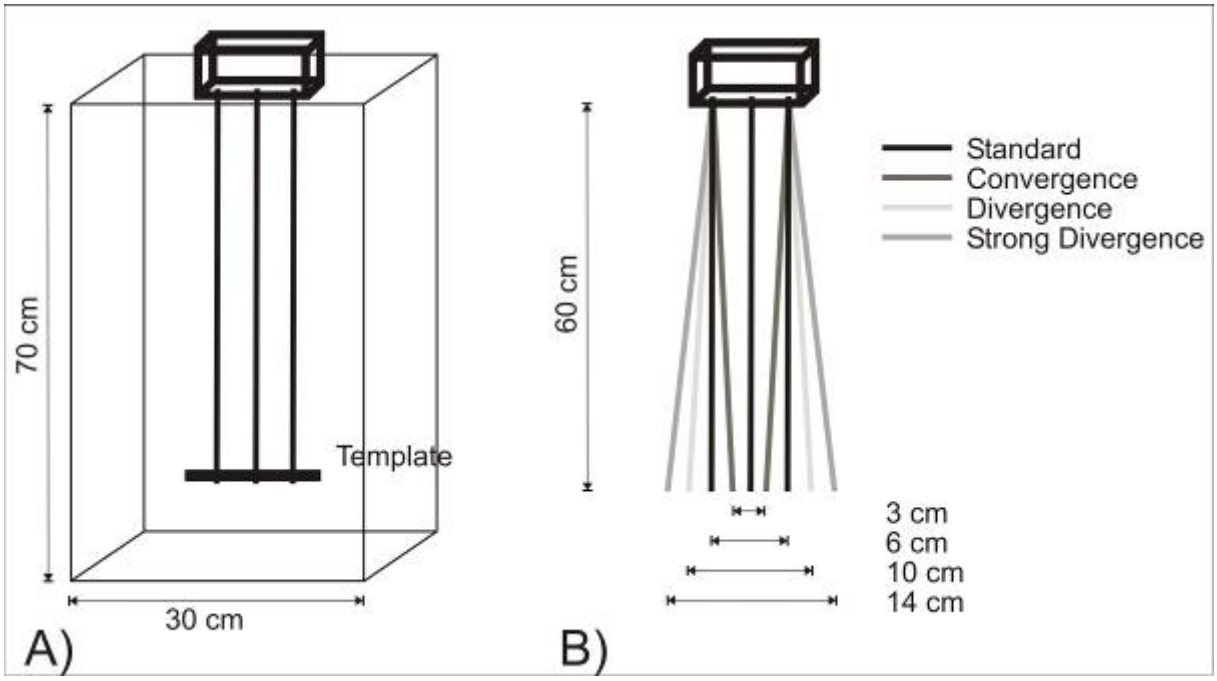

Figure 3: **Sketch of the plastic box with installed SUSU03 and position of the wooden template (A), and sketch of the four different probe geometries (B).**

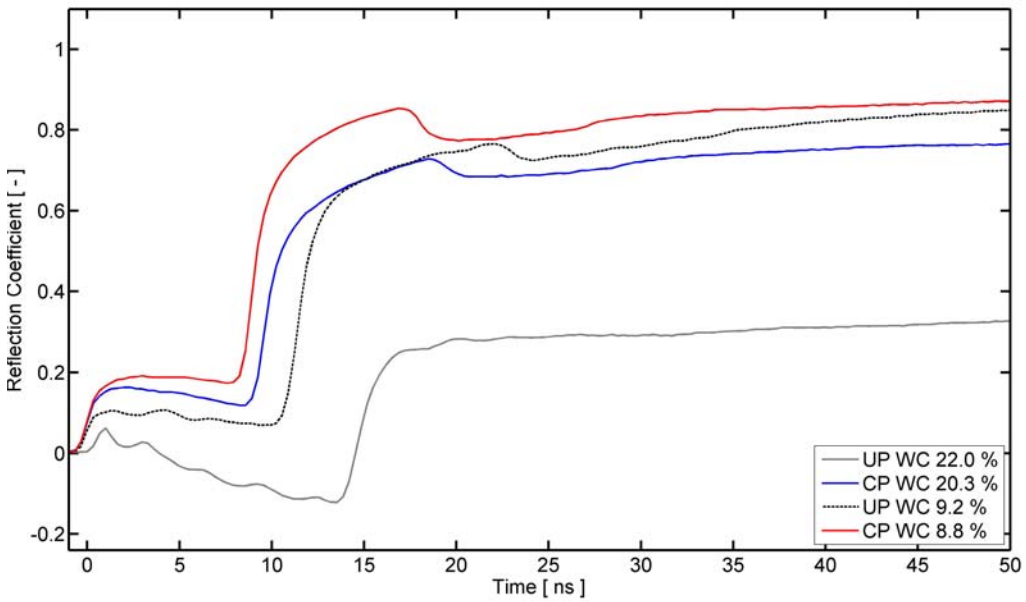

Figure 4: **Reflectograms obtained with coated (CP) and uncoated (UP) SUSU03 probes with 0.60 m rods at two different soil moistures, measured in an experimental box with glass beads (Table 2). Bulk electrical conductivity is 1.0 10^{-2} dS m^{-1} for the dry case and 6.7 10^{-2} dS m^{-1} for the wet case.**

Figure 4 shows the reflectograms of a coated and an uncoated rod probe at two different soil moistures in glass beads. In both cases the travel time of the coated probe is smaller compared to

the uncoated which is an effect of the isolating PVC coating. Estimated bulk electrical conductivity based on the method suggested by Huisman et al. (2008) and Lin et al. (2007) yielded values of 1.0 10^{-2} dS m^{-1} and 6.7 10^{-2} dS m^{-1} for the dry and wet case, respectively. For the case of uncoated rods, even a low electrical conductivity has already a strong influence on the shape of the reflectogram. Especially in the wet case, there is a strong attenuation between 2 and 14 ns that is much less pronounced for the coated rods. Despite the low value of bulk electrical conductivity, its influence on the uncoated probe is significantly strong. Coated rods will deliver the more reliable reflectograms and should be used in these soils when using a probe length of 0.60 m.

2.4.3 Experiment 2: performance in homogeneous media during transient conditions

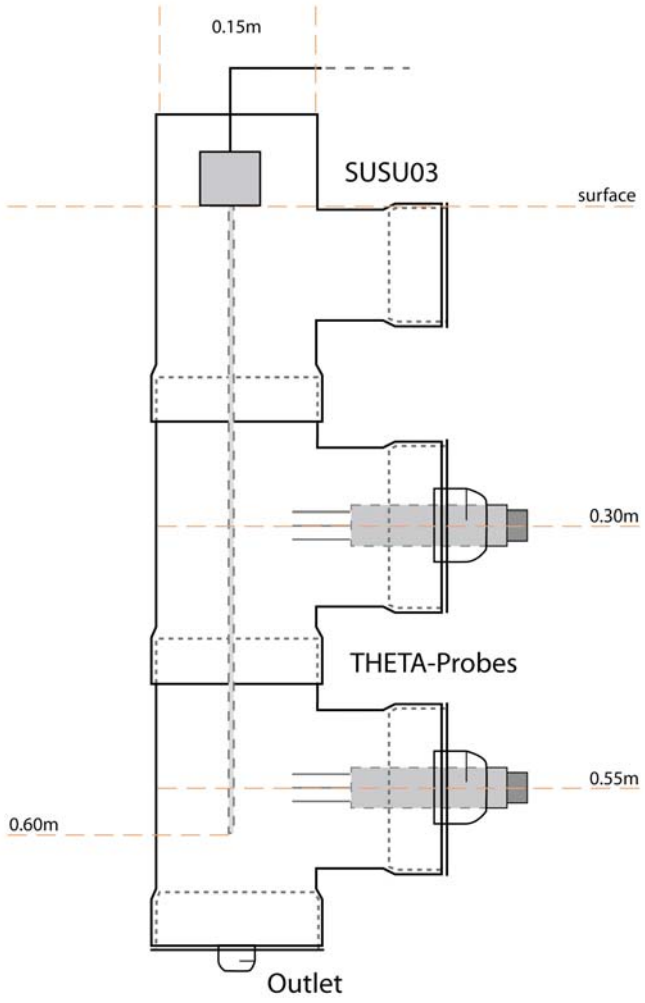

Figure 5: **Sketch of the setup of Experiment 2. A SUSU03 probe and two FDR probes (THETA probes, Delta-T-Devices) are installed in PVC tubes and the tubes are filled with glass beads. At the bottom of the tube, an outlet permits the controlled and stepwise drainage of water in the tube.**

Figure 5 shows the experiment setup. The experiment is conducted in a 1 m high and 0.15 m wide PVC tube. Glass beads are filled into the tube and compacted, resulting in a bulk density of 1.51 g m^{-3} and a saturated water content of 0.38 $m^3 m^{-3}$ (Table 2). Two T-pieces with a diameter of 0.15 m and a length of 0.09 m in the tube allowed for the installation of FDR probes (THETA,

Delta-T-Devices) with a shaft length of 0.11 m, rod length of 0.06 m and a diameter of 0.04 m. One probe of type SUSU03 is installed in the centre of the tube with rods pointing from the upper edge of the tube to the bottom and the narrow side of the probe facing the T-pieces. Independent soil moisture measurements are obtained with two THETA probes placed at a depth of 0.30 m and 0.55 m, which work in the FDR domain with a measurement error of ± 0.01 m^3m^{-3} (Gaskin and Miller, 1996). The FDR probes reach 0.03 m into the centre tube. The rods of the THETA probes have a distance of 0.04 m from the rods of the SUSU03 to avoid interaction of the measured signal. The sample area of a coated probe is of low range outside the rods (Ferré et al., 1998). The reflectograms are additional proven if the FDR probes influence the measurement signal. The experiment is started with a tube that is fully saturated with de-ionized water and the soil moisture is reduced by sucking off 250 ml of water at the bottom of the tube every 6 hours. Soil moisture profiles are inverted at the different moisture conditions and compared to the FDR probes.

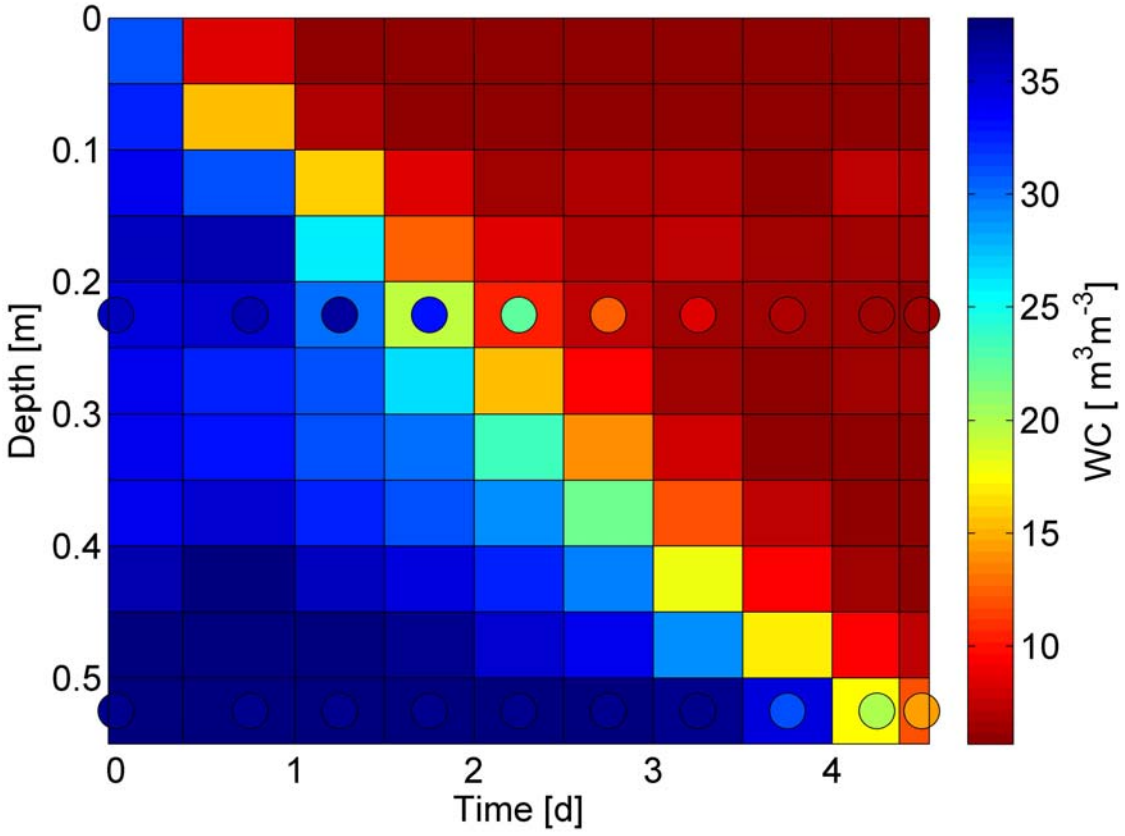

Figure 6: Comparison of inverted soil moisture profiles obtained within glass beads with independent soil moisture measurements by means of FDR probes (marked with circles). The colour coding is the same for both data sets.

Figure 6 presents inverted moisture profiles in comparison to the FDR probe obtained during the experiment. For the inversion, the parameter set "Exp. 1" in Table 3 is used. The profile data are aggregated to 0.05 m for a better comparability. Table 4 shows the absolute error of the inverted profiles to the FDR probes and goodness of fit criteria for the inversion calculated from observed and reconstructed reflectograms. Both data sets are generally in good agreement, except

for days 1.5 and 2.5. The higher values of the FDR probe measurements may result from effects of the T-pieces, which may have retained higher water content during drainage. Finally, it is important to stress that even a glass bead medium is not perfectly homogeneous. The reader should note the small variations in the moisture profile at the beginning of the experiment, which reflect small differences in saturated water content.

Table 4: Difference of inverted soil moisture to point measurements with FDR probes (THETA probe, Delta-T-Devices) as absolute error (AE) of the soil moisture in m^3m^{-3}; goodness of fit criteria calculated from observed and reconstructed reflectograms: root mean square error (RMSQ), mean error (ME), standard deviation of error (STDE), Nash-Sutcliffe efficiency (NSE) and the objective function (Eq. (2)).

Time [d]	0	1.5	2.5r	3.5	4.5
AE 0.30 m	-0.022	-0.032	0.022	-0.002	-0.003
AE 0.55 m	0.003	0.000	0.010	-0.029	0.019
RMSQ	$1.50\ 10^{-3}$	$4.52\ 10^{-3}$	$6.18\ 10^{-3}$	$8.05\ 10^{-3}$	$6.65\ 10^{-3}$
ME	$-1.02\ 10^{-3}$	$-3.06\ 10^{-3}$	$-4.60\ 10^{-3}$	$-5.95\ 10^{-3}$	$-4.51\ 10^{-3}$
STDE	$1.10\ 10^{-3}$	$3.35\ 10^{-3}$	$4.02\ 10^{-3}$	$5.06\ 10^{-3}$	$4.81\ 10^{-3}$
NSE	0.995	0.994	0.992	0.990	0.993
Objective Function	$3.35\ 10^{-14}$	$3.06\ 10^{-13}$	$5.69\ 10^{-13}$	$9.63\ 10^{-13}$	$6.55\ 10^{-13}$

2.4.4 Experiment 3: effect of probe deformations

Table 5: Mean soil moisture observed with different probe deformations at soil moisture of approximately 0.04 m^3m^{-3}, 0.08 m^3m^{-3} and 0.20 m^3m^{-3} estimated with SUSU03 and FDR probes (THETA probe, Delta-T-Devices). Standard deviation is abbreviated as STD.

Type of deformation	Convergence	Standard	Divergence	Strong Divergence	Mean THETA probes	STD THETA probes
Distance between the outer rods [m]	0.03	0.06	0.10	0.14	-	-
0.04 m^3m^{-3}	0.036	0.038	0.039	0.039	0.040	0.005
0.08 m^3m^{-3}	0.077	0.081	0.079	0.073	0.080	0.010
0.21 m^3m^{-3}	0.207	0.199	0.200	0.195	0.200	0.020

The effect of probe deformation on the estimated soil moisture profile and the mean soil moisture are studied by deforming the two outer rods under controlled conditions with the assumption of a parameter set up for a correctly parallel installed probe. Here four different cases are studied: parallel rods, converged rods, diverged rods and strongly diverged rods (Figure 3B and Table 5). The experiment is conducted with glass beads in a plastic box and a template to ensure the probe deformation (Figure 3A). The experiment is conducted at three soil moisture levels: 0.04-0.05 m^3m^{-3}, 0.07-0.09 m^3m^{-3}, and 0.20-0.23 m^3m^{-3}. The values are cross-checked with

FDR probe measurements along the experimental box. A TDR measurement is performed and inverted into a soil moisture profile. The procedure is repeated for all selected deformations. Establishing a homogeneous soil moisture profile during a single experiment is rather difficult and could only be achieved approximately.

Figure 7 presents the reflectograms and the inverted soil moisture profiles at different average soil moistures of 0.05 m^3m^{-3} (Figure 7A and D), 0.08 m^3m^{-3} (Figure 7B and E) and 0.20 m^3m^{-3} (Figure 7C and F) for the four different rod geometries shown in Figure 3B. During inversion the parameter set for glass beads (Table 3) are used. It has to be noted that due to installation and de-installation of the probe, which required refilling of the box, the soil moisture and bulk density profiles varied slightly between different experiments (Table 5 and Figure 7A-C) when comparing the different geometries.

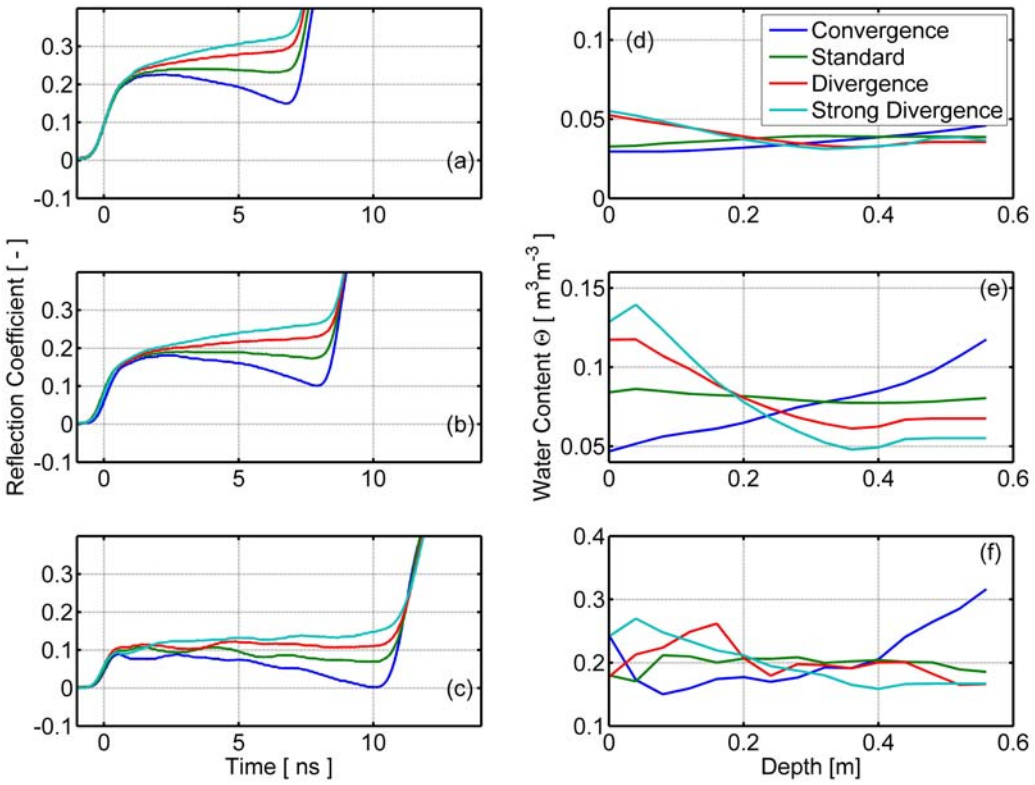

Figure 7: **Reflectograms and inverted soil moisture profiles obtained with different probe deformations at a soil moisture of approximately 0.04 m^3m^{-3} (A) and (D); 0.08 m^3m^{-3} (B) and (E); and 0.20 m^3m^{-3} (C) and (F). 'Standard' denotes according to Figure 3 ideal geometry, 'Convergence' means convergent rods with increasing depth, 'Divergence' and 'Strong Divergence' values signify a divergent probe as described in Figure 3.**

A decreasing distance between the wave guide rods means an increasing capacitance of the transmission line. Hence, the probe parameters C_l and L should vary along the transmission line. However, they are currently assumed to be constant, because the effect of rod deformation on the retrieved soil moisture profile is studied by the supposition of a parallel geometry on *de facto* different geometries. For convergent rods, the average soil moisture is measured correctly

compared to the measurement with parallel rods. However, the soil moisture along the rod increases with depth in all three cases, implying an underestimation of soil moisture in the upper half and an overestimation of soil moisture in the lower half. This becomes especially apparent for intermediate conditions and wet conditions.

For the case of divergent rods, the apparent soil moisture profile is just flipped in comparison to the convergent case. Thus, in the upper half an overestimation and in the lower part an underestimation of the soil moisture is observed. It is important to note that the average soil moisture calculated from the travel time with constant parameters is in most cases within the error range almost unaffected by deformations of the probe (Table 5). The experiments are also repeated in coarse sand of 0.06 to 0.60 mm grain size, with similar results (not shown). Thus, it can be stated that unknown changes in probe geometry will lead to a systematic bias in inverted soil moisture profiles, but will leave the average values largely unchanged in the case of the SUSU03 probe used.

As a first step, a simple quality measure is tested to identify probe deformations by introducing the coefficient of amplitude *CA*, defined as:

Eq. 12

$$CA = (V_{\max 1} - V_{\min}) / V_{\max 1},$$

where V_{max1} = maximum voltage of the first reflection and V_{min} is the inflection point before the second reflection in the reflectogram. The corresponding values for the deformation cases are listed in Table 6. In the convergent case, *CA* has positive values and is negative in the standard and divergent case. With increasing divergence *CA* values become larger. This is consistent with the theory of a plate capacitor, as an increasing distance between the rods corresponds to a decreasing conductance. The amplitude at the end of the reflectogram will thus increase, which yields a negative value for *CA*. In the convergent case the conductance increases at the end of the probe, which means a small amplitude and thus a positive *CA*. However, in the case of layered soils, where the lower part can be systematically drier/wetter than the upper soil, or in the case of gradients in salt, clay or organic content, identification of probe deformations using Eq. 12 is not that straight-forward.

Table 6: Amplitude coefficient (*CA*) for different probe deformations at soil moisture of approximately 0.04 m^3m^{-3}, 0.08 m^3m^{-3} and 0.20 m^3m^{-3}.

Type of deformation	Convergence	Standard	Divergence	Strong Divergence
Distance between the outer rods [m]	0.03	0.06	0.10	0.14
0.04 m^3m^{-3}	0.11	-0.33	-0.58	-0.75
0.08 m^3m^{-3}	0.22	-0.20	-0.66	-0.80
0.21 m^3m^{-3}	0.46	-0.25	-0.58	-1.31

2.4.5 Experiment 4: effect of solid objects in the integration volume

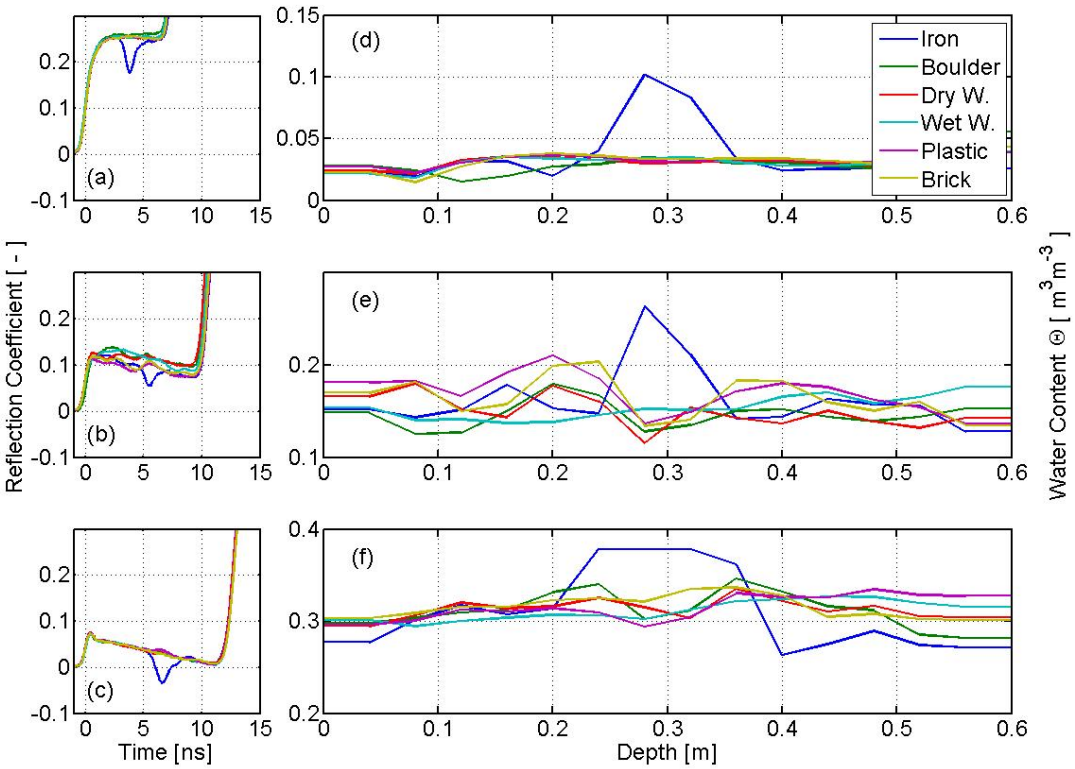

Figure 8: **Reflectograms and inverted soil moisture profiles with an iron block, dry and wet wood, PVC block, brick and boulder with a volume of approximately 1.5 l at a depth of 0.30 m. All probes are measured with ideal geometry. The mean soil moisture is about 0.04 m^3m^{-3}, (A and D, dry case) 0.16 m^3m^{-3} (B and E, intermediate case) and 0.30 m^3m^{-3} (C and F, wet case). Wood is abbreviated to W.**

The purpose of this experiment is to study the influence of different solids on the reflectogram and the estimated soil moisture profile. A coated SUSU03 probe is installed in the same box used in Experiment 1 (Figure 3A); ideal parallel geometry is ensured by installing a wooden template at a depth of 0.59 m. An iron block (a conductor), a dry and a saturated piece of wood (insulator), a PVC block (insulator) and a brick or a boulder from the study area, all with a volume of approximately 1.5 l, are placed close to the probe at a depth of 0.30 m. The box is filled with glass beads (Table 2). TDR measurements are performed at three different soil moisture levels: 0.04 m^3m^{-3} (dry case), 0.16 m^3m^{-3} (intermediate case) and 0.30 m^3m^{-3} (wet case).
Figure 8 presents the reflectograms as well as the inverted soil moisture profiles for the brick, the iron block, the dry and saturated wood, and the boulder block. Table 7 lists the soil moisture observed with FDR probe measurements along the profile, the mean soil moisture estimated with the SUSU03 and the soil moisture in the area of the object. During inversion, parameter set "Exp. 2" (Table 3) is used to characterize the transmission line. Similar to Experiment 3 it has to be noted that due to installation and de-installation of the probe, soil moisture and bulk density profiles varied slightly between different experiments. This leads to a non-constant profile in the inverted profiles, especially in the intermediate and wet case (Figure 8E and F).

As the iron block is an ideal conductor, the electric conductivity is strongly increased at a depth of 0.30 m. Consequently, soil moisture appears to be higher at that depth in the soil moisture profile, which is indicated in the reflectogram by the pronounced decrease in the amplitude at 5 ns in Figure 8C. The inversion yielded a soil moisture value of 0.37 m^3m^{-3} at 0.30 m, whereas the true soil moisture is approximately 0.30 m^3m^{-3}. The other objects, with the exception of the wet piece of wood, show up as a slightly drier region in the reflectogram, marked by the small increase in normalized voltage at 5 ns in Figure 8B and C. The wet piece of wood has no influence in the dry and intermediate case and less effect on the profile in the wet case, although slight heterogeneities in the pore space could be observed and have similar impact on the reflectograms. Inversion yields slightly lower soil moisture at 0.30 m when compared to the values below and above. The effect of the iron block and the other objects agree with the expected behaviour.

Table 7: Mean soil moisture observed with FDR probes (THETA probe, Delta-T-Devices) and estimated with the different objects and the soil moisture in the area of the object.

	Soil moisture between 0.28-0.33 m depth [m^3m^{-3}]						
T	Mean THETA probe	Iron	Boulder	Dry Wood	Sat. Wood	Plastic	Brick
dry	0.04	0.094	0.034	0.031	0.034	0.031	0.034
intermediate	0.16	0.240	0.131	0.135	0.152	0.142	0.140
wet	0.30	0.378	0.306	0.308	0.307	0.299	0.328
		mean soil moisture SUSU03					
dry	0.04	0.037	0.034	0.034	0.033	0.034	0.035
intermediate	0.16	0.160	0.147	0.147	0.154	0.166	0.161
wet	0.30	0.310	0.313	0.313	0.312	0.315	0.316

It is important to stress that an ideal conductor in the integration volume has the same influence on the reflectogram and the inverted moisture profiles as a convergent probe geometry (compare Figure 7A and Figure 8A). Both lead to a strong decrease in the amplitude of the reflectogram. Fortunately, gravel, boulder blocks and other solid objects of low electric conductivity and low permittivity seem to be not as critical as is expected. Their effect on the reflectogram is rather small.

2.4.6 Experiment 5: measurement of soil moisture in disturbed soil

The applicability of TDR in soils of high clay content is generally hampered because of relaxation phenomena and high energy losses along the transmission line (Chen et al., 2007; Kupfer et al., 2007). As the soil at the field sites contains about 16 % clay, irrigation experiments are performed using field soil material (Table 2) in the box described in Experiment 1 with the wooden template to guarantee an ideal probe geometry. The plate at the base is perforated to allow for exfiltration of irrigated water. To set up the experiment, the box is first filled to 50 % with disturbed soil material from the field site, the SUSU 3 probe is installed in the template, two FDR probes installed at depths of 0.25 m and 0.50 m and then the remaining volume filled. Additionally, a

0.30 m uncoated TDR probe of type CS610 (Campbell Scientific Inc.) is installed vertically from the top into the box to measure the bulk electrical conductivity. After filling and probe installation, the soil material is compacted to avoid air gaps between the rods and the surrounding soil. The spin-up time of the experiment is two months and irrigated with 74 l m^{-2} every fourth day to achieve stable initial conditions. The actual irrigation experiment lasted 10 h, with a temporal sampling interval of the soil moisture data before irrigation of 20 min and during and after irrigation of 10 min. The soil is irrigated twice (74 l m^{-2} 4 min^{-1}) using de-ionized water. During the inversion the profile information of the previous time step is used as the initial condition for the following step. Inverted soil moisture profiles obtained with Spatial TDR are compared to measurements with the FDR probes at two different depths.

Figure 9 presents the temporal development of the inverted soil moisture profile during two irrigations of approximately 74 l m^{-2} in a period of 4 minutes at 5:20 h and 6:40 h (A), the absolute error of inverted profile compared to FDR probe measurements (B), the objective function of the inversion (C), and the inverted profiles (D). The range of the bulk conductivity measured with a CS610 is 0.04-0.10 dS m^{-1}. The spatial resolution is aggregated to 0.05 m length for a better comparability with the FDR probe measurements. During inversion, parameter set "Exp. 2" (Table 3) is used to characterize the transmission line.

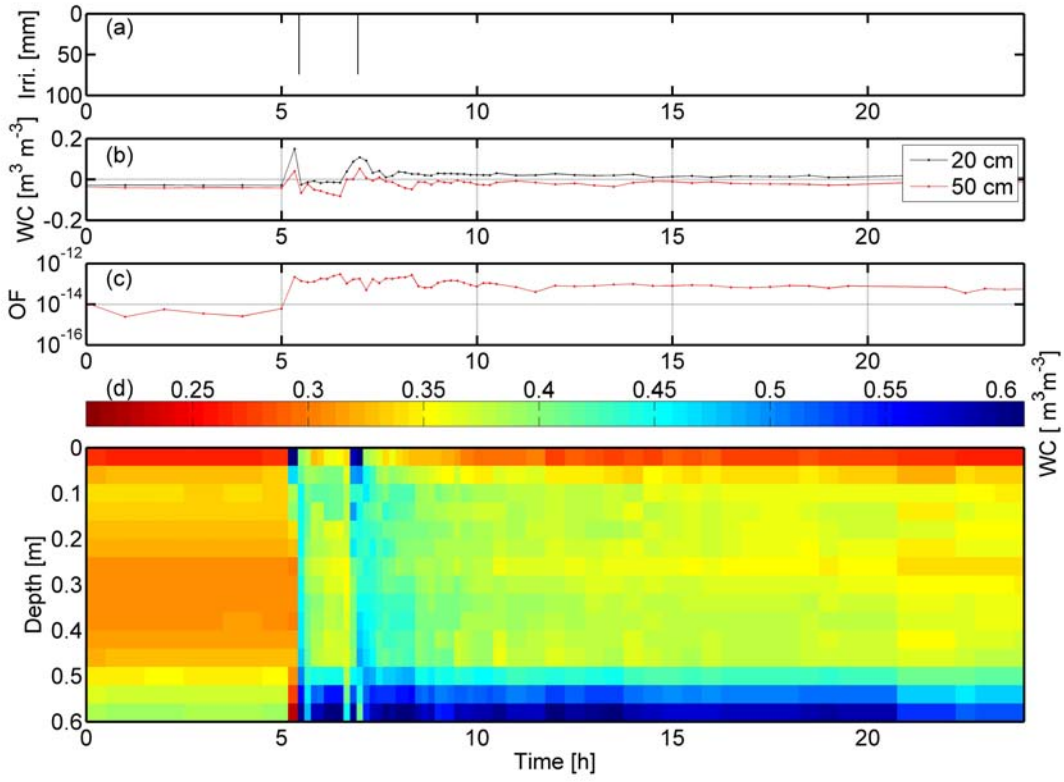

Figure 9: **Inverted soil moisture profiles obtained in an experimental box filled with soil from Rehefeld with A) the irrigation, B) the absolute error of inversion compared to measurement with FDR, C) the objective function (shortened with OF) of the inversion and D) the inverted profiles to a depth of 0.55 m.**

The soil column is relatively dry before the irrigation, with a dry top layer and a slight increase in soil moisture towards the bottom. During the irrigation, the infiltration front reaches a depth of approximately 0.15 m in the first 10 min, and then the infiltration front reaches the bottom after further 10 min. Exfiltration starts at the bottom of the soil column, with some 10 l m^{-2} leaving the column in the first few minutes after the infiltration front has reached the bottom. In the top layer, up to a depth of 0.10 m, the soil moisture decreases while the lower layers remain saturated for 2 hours, after which the second irrigation experiment is initiated. The wetter soil reacts much faster upon irrigation. Drying then starts again, mainly forced by evaporation, and the profile evolves to the initial conditions. First, the soil moisture decreases from 0.56 m^3m^{-3} to 0.25 m^3m^{-3} in the top layer up to a depth of 0.08 m within a few hours. The deeper parts have lower rates of drying depending on the depth, and at the end of the experiment the lowest 0.12 m are still saturated.

The estimated absolute error (Figure 9B) of the inverted value minus the measured soil moisture with FDR probes in the depths 0.20 m and 0.50 m shows that the inverted value slightly underestimates the soil moisture measured with the FDR probes before the irrigation. During the irrigations, the inversion overestimates the soil moisture, and during the drying the soil moisture is underestimated again. Especially during the irrigation phase, the absolute error is larger for the upper probe (0.15 m^3m^{-3}) than for the lower one (0.05 m^3m^{-3}). During the drying phase, the soil moisture for the upper probe is slightly overestimated, and for the lower it is underestimated. One explanation for the differences of < 0.03 m^3m^{-3} between inverted soil moisture and FDR probe measurements during the experiment is small scale heterogeneity in the soil column.

Figure 9C shows the temporal development of the objective function for the inversions, which is an uncertainty measure for the inverted soil moisture values. A higher value of the objective function implies a high uncertainty of the measurements. The objective function slightly decreases at the beginning of the experiment. It increases with the start of the irrigation. Between the two irrigation events, the objective function remains constant, but increases again after the second irrigation. Finally, the objective function value decreases continuously with decreasing soil moisture content. The increase in the objective function and the large difference to the upper FDR probe during the irrigation indicate that fast soil moisture changes are problematic for the inversion procedure, which applies especially for the upper part of the probe.

2.5 Discussion and Conclusions

Different laboratory experiments are carried out to investigate the feasibility of retrieving soil moisture profiles with Spatial TDR technology in glass beads and heterogeneous loamy soils with substantial clay content.

This study shows that deformation of the probe geometry, which can be assumed to be the rule rather than the exception when installing long TDR probes in heterogeneous soils, influence both the reflectogram and the inverted soil moisture profile. In the case of divergent or convergent rods, neither the inductance L nor the capacitance C_l can be assumed to be constant along the transmission line. Fortunately, probe deformations leave the average moisture content

along the probe almost unchanged. The average value is determined from the pulse travel time between the first and second main reflections in the reflectogram. Their location is not affected by probe deformations, because of the use of coated probes here. Average soil moisture values obtained with uncoated probes are, however, more sensitive to probe deformations, as shown by Bänninger et al. (2008) and Spittlehouse (2000). Spittlehouse observed a reduction in average soil moisture in the divergent case and predicted an underestimation of the sampling volume for the convergent case. Ferré et al. (1998) showed that coated probes have a clearly smaller sampling volume than uncoated probes and that three rod probes have a smaller sample volume than two rod probes. A decreasing/increasing of the sample volume in the case of convergent/divergent probes has thus a smaller effect when using coated three rod probes, which explains the robustness of average soil moisture contents obtained here. A much stronger deformation than has been investigated here could surely have an effect on the average soil moisture values. However, in the present study just realistic rod deformations are investigated that are observed in a related field study (Chapter 3).

It is also good news that solid objects like gravel, wood or boulder blocks only have a small effect on the inverted soil moisture profiles. They show up as slightly drier regions in the reflectogram. However, when a solid electrical conductor (an iron block) is present, soil moisture in this region is strongly overestimated by the inversion. Similar problems could occur in soils with a high content of iron-rich minerals, as discussed by Robinson et al. (1994) and Van Dam et al. (2002).

Finally, observations with THETA probe-type FDR probes and soil moisture values retrieved from the same depths are generally in good accordance, both in glass beads and disturbed natural soil from the field site. It should be noted that during infiltration or withdrawal, the accuracy of the inverted profile decreases. It is demonstrated furthermore that Spatial TDR is capable of monitoring fast infiltration and redistribution of irrigation water in soil.

The sources and subsequent impacts of different kind of errors are analysed. The biggest problem is certainly the bias that is introduced by probe deformations. The suggested *CA* measure allows the assessment of whether the probe is convergent or divergent. During the experiments, positive values are found in the case of convergent rods; negative values are observed for parallel and divergent rods. The absolute value of the negative values increases with increasing divergence. Thus, if the reflectogram of a probe shows strongly negative or positive values under different conditions, it is likely that the probe geometry is deformed. In the case of a small negative *CA*, the function is not able to give clear information about the probe geometry if the probe is parallel or slightly divergently installed. This could lead to a biased inversion with a slight underestimation of the depth. This error source can only be identified by excavation of the probe. In the case of layered soils where the lower part can be systematically drier/wetter than the upper soil, or the case of gradients in salt, clay or organic content, identification of probe deformations using Eq. 12 is not that straight-forward. The amplitude coefficient should to be evaluated for different wetness states: if the amplitude coefficient remains unchanged while observed, a probe deformation is likely. It can be recommended, furthermore, that assessment of detailed information on the soil profile and the soil's physical properties within different layers be used to assist interpretation of the amplitude coefficient.

Future steps should further enhance the calibration of transmission line parameters. Especially for soils rich in fine particles, Eq. 10 should be revisited, to check whether the assumption of zero conductivity is reasonable when C drops below C_0. Independent data on the electrical conductivity of the soil will facilitate solving this problem. Furthermore, information about soil chemical properties and mineral content could be used as a pedo transfer function in supplementary work. It might also be necessary to introduce separate parameterization of the C-G relationship in Eq. 10 for strongly different soil horizons.

CHAPTER 3 SOIL MOISURE DYNAMICS AND RUNOFF GENERATION IN HEADWATER CATCHMENTS: LEARNING FROM FIELD DATA

3.1 Introduction and Motivation

3.1.1 How to observe the spatial distribution of soil moisture

Soil moisture is a key state variable that controls hydrological dynamics at various spatial scales. There is experimental evidence that the onset of point scale threshold processes such as fast preferential flow in soil (Zehe and Flühler, 2001a ; Blume et al., 2009), Hortonian overland flow initiation (Zehe et al., 2007), or the switch between hydrophilic and hydrophobic conditions are strongly controlled by antecedent soil moisture conditions (Dekker et al., 2005). Furthermore, various studies suggest that the antecedent soil moisture state exerts crucial control on rainfall-runoff response at the field and headwater scale (Bronstert and Bárdossy, 1999; Gurtz et al., 1999; Jayawardena and Zhou, 2000; Montgomery and Dietrich, 2002; Meyles et al., 2003; Chirico et al., 2003; Zehe and Blöschl, 2004; Zehe et al., 2005; Blöschl and Zehe, 2005) or on the preferred flow regime in small catchments (Grayson et al., 1997). However, most of the listed studies rely to a large degree on modelling. Experimental studies that relate observations of spatiotemporal soil moisture dynamics at the field or headwater scale to observed flows, either at the surface or in the stream, are rare (Burt and Butcher, 1985, Grayson et al., 1997; Starr and Timlin, 2004; McNamara et al., 2005; Lin, 2006; Frisbee et al., 2007). This is notwithstanding that they could offer additional – probably unexpected – pieces of information to the puzzle that up to now has largely comprised model extrapolations. The reason for the limited number of field studies is well known. Soil moisture at the headwater scale exhibits huge spatial variability and single or even distributed TDR measurements yield non-representative data.

Promising technologies to assess spatially distributed three-dimensional soil moisture proxies at the field scale are ground penetrating radar (GPR) (Binley et al., 2002; Roth et al., 2004) or electrical resistivity soundings (ERT) (e.g. Kemna et al., 2002; Graeff et al., 2009). The former yields the subsurface pattern of the dielectric permittivity, the latter the subsurface pattern of the apparent specific resistivity. The difficulty for both methods is that there are no general petrophysical relationships available to transform the observed variables into soil moisture content (Paasche et al., 2006). A draw-back of both methods is that observations are – in most cases – restricted to field campaigns and therefore provide only a coarse temporal resolution.

Most past and recent studies have largely relied on distributed TDR observations. One approach is to use a set of fixed TDR sensors to monitor temporal soil moisture dynamics at selected points, as for instance suggested by Bárdossy and Lehmann (1998) in the Weiherbach, Germany, Anctil et al. (2008) in the Orgeval watershed, France or Blume et al. (2009, 2008 a, b) in the Malalcahuello catchment in Chile. The advantage of using fixed stations is that they allow a high temporal resolution, which allows either comparison of observed point soil moisture dynamics to event scale discharge response and piezometers response as suggested by Blume et al. (2008a), or to use this information to improve discharge predictions as recently shown by Anctil et al. (2008).

The drawback of this approach is that a high spatial resolution with this approach cannot be achieved, simply because of the high costs. Other authors thus prefer spatially highly resolved soil moisture sampling by means of mobile or portable TDR sensors, as for instance Grayson et al. (1997) or Grayson and Western (1998) in different catchments in Australia or Brocca et al. (2007, 2009) for three field sites in Italy. Spatially distributed sampling allows identification of temporal changes in correlation structure and spatial variability depending on the average near surface wetness. Albertson and Montaldo (2003) and Western et al. (2004) found, for instance, a reduction in variance and an increasing correlation length with increasing wetness of a field site in Australia. Similarly, Brocca et al. (2007) report that at their rather homogeneous site soil moisture variance reduced during wet conditions and soil moisture is normally distributed in the flat valleys areas. Furthermore, Brocca et al. (2007) and Grayson and Western (1998) defined representative sites whose soil moisture values are always close to the overall average. Brocca et al. (2009) found further that the ranks of their distributed measurements in the univariate soil moisture distribution at a fixed time did not change much between different observation times. This temporal stability of the ranks suggests that the moisture pattern reflects the pattern of stationary soil properties, at least at the seasonal scale. Blume et al. (2008 a, b) found, however, at a much more heterogeneous and forested site, partly contradicting results. The main drawback of using mobile TDR sensors is the limited temporal resolution that is too coarse for relating observed soil moisture dynamics to systems behaviour under rainfall-driven conditions.

In this study, in a headwater catchment in the Ore Mountains, another approach is suggested to assess representative soil moisture data for typical landscape units and to explore subsurface wetness control on runoff generation. The idea is to combine advanced Spatial TDR technology (Schlaeger, 2005; Becker, 2004; Graeff et al., 2010) that allows retrieval of soil moisture data with an innovative sampling strategy, that combines the advantage of both approaches discussed above. Before further elaboration on this sampling strategy, it is helpful to define precisely what is the meaning of "soil moisture variability" and what determines a "soil moisture ensemble" in a statistical sense. Spatiotemporal variability of soil moisture is determined by a multitude of spatial patterns that interact in a nonlinear way in space and time. During and after extreme precipitation events the spatial rainfall pattern can be expected to be dominant. Hence, soil moisture is expected to be spatially uniform (Grayson et al., 1997, Grayson and Western, 1998; Brocca et al. 2007). With increasing dryness, terrain, soil types and vegetation begin to dominate more and more and soil moisture variability is expected to increase as shown by Brocca et al. (2007), Grayson et al. (1997), Grayson and Western (1998) or Western et al. (2004). Thus, a soil moisture ensemble is defined as an area - that is uniform with respect to soil type, terrain properties and vegetation class (Wilson et al., 2004), but also rainfall and radiation forcing. At least the first moment of the soil moisture pattern – the mean – should be constrained by soil type, vegetation and terrain. Understanding this deterministic part of spatial soil moisture variability requires therefore the determination of representative mean values within different ensembles or strata. In heterogeneous systems this is, however, highly complicated by local scale statistical soil moisture variability within such an ensemble that stems from local fluctuations in soil hydraulic properties, macropores and micro topography. For instance, Zehe and Blöschl (2004) found the variance of soil moisture observed within a cluster of 25 TDR measurements at a 4 m^2 large field plot is, at 0.04 $(m^3m^{-3})^2$, as large as the soil moisture variance observed at 61 locations in the 3.2 km^2

Weiherbach catchment. However, they showed furthermore that the first two moments observed within a different cluster of 25 TDR measurements at a different plot are, within the confidence limits, identical to those obtained at the plot. Similarly Brocca et al. (2007) found that 9 to 35 measurements allow assessment of a stable mean soil moisture values.

Therefore clustering of several TDR probes within different ensembles/strata could thus be a promising strategy to discriminate different sources of soil moisture variability (deterministic and stochastic) and combine the advantages of high temporal and locally high spatial resolution. A set of fixed TDR stations equally distributed in a catchment would mix these sources of variability because it will cover several ensembles. As long as the total spatial extent of the network is small enough to neglect spatial variability in rainfall and radiation, both sources of variability may still be un-revealed using appropriate geostatistical methods and a stratified sampling (Bárdossy and Lehmann, 1998; Zehe et al., 2005). However, the sampling size in the individual classes may become too small to allow representative estimates of prior distributions, even when up to 100 TDR stations are installed, as reported in the study of Bárdossy and Lehmann (1998). A TDR cluster may furthermore be operated at a sampling interval of 10 minutes for up to 40 sensors and may cover an area of up to 500 m^2. This can be deemed as sufficient to investigate soil moisture control on runoff generation and to shed light on a possible dependence of field scale soil moisture variance on the average wetness state or on the spatial pattern of soil moisture changes under different conditions. The ideal case is that the individual TDR probes within such a cluster yield soil moisture profiles instead of an integral value along the probe. This would allow assessment of highly resolved infiltration data to test and improve the current generation of soil hydrological models for flow in the unsaturated zone (compare Chapter 2). The drawback of operating Spatial TDR clusters is, however, that a single one costs roughly 12-15 k€.

This study presents an application of the outlined TDR technology (the underlying theory is explained in detail in Chapter 2), in a headwater of the Weißeritz in the German eastern Ore Mountains, where two TDR clusters have been installed since autumn 2006. In principle, one may obtain two types of soil moisture data from these clusters: (1) the standard vertically averaged soil moisture values at the individual probes based on the travel time of the TDR signal as is used here, and (2) inverted soil moisture profiles based on the approach suggested by Schlaeger (2005), as explained in Chapter 2. Identification of reliable soil moisture profiles in these soils is, however, complicated by unexpected error sources such as very strong probe deformations, strong vertical gradients in porosity and density, and the presence of gravel and stones in the integration volume, which all arose when installing the TDR probes in these highly heterogeneous soils. Chapter 2 reports in detail how these error sources affect retrieval of soil moisture profiles in these soils. It is found that the vertically averaged soil moisture is not affected by these errors but inverted soil moisture profiles may be strongly biased.

3.1.2 Investigation of the dominating runoff processes

One key challenge during rainfall driven conditions is to understand the fingerprints in the response time or residence time for tracer distributions at the plot (Beven and Germann, 1982; Germann and Beven, 1985; Zehe and Flühler, 2001a, b; Vogel et al. 2005a, b) and hillslope

(Tromp-van Meerveld and McDonnell, 2006a; Weiler and McDonnell, 2007; Lehmann et al., 2007) that are caused by vertical and lateral preferential flow. Here, the response time for the response by the measurement device (e.g. gauge or TDR probe) and residence time i.e. the time water and solute spend travelling from its entry point to a certain depth, interface or the catchment outlet, are key signatures to characterise flow and transport at all scales (McGuire and McDonnell, 2006). Depending on the system state, the interactions between catchment characteristics and precipitation may cause abrupt changes, both in internal process patterns and the way they transform into integrated catchment response (Zehe and Sivapalan, 2009). Such threshold behaviour in catchment response is often caused by preferential flow in subsurface connected structures, which may even extend over entire hillslopes, and its interaction with deep percolation into the bedrock (Tromp-van Meerveld and Weiler, 2008; Wienhöfer et al., 2009). Different authors have investigated residence time and the dominating processes within sprinkling experiments. Cassiani et al. (2009) observed fast infiltration through the soil into the subsurface and regolith. Bronstert (1998) detected mainly overland flow in a loess dominated catchment. Montgomary et al. (1997) and Montgomary and Dietrich (2002) did not observe surface runoff on a very steep hillslope but could observe runoff response in all sprinkling experiments and explain that by subsurface processes on impermeable layers. Tromp-van Meerveld and McDonnell (2006a) and Wienhoefer et al. (2009) monitored lateral subsurface storm flow only on the bedrock surface. Sprinkling experiments in combination with different soil moisture measurements and dye tracer experiments are used to understand the dominating processes.

The main objective of the present study is thus to:

- Investigate how different clusters determine the mean, variance and correlation length (range) of vertically averaged soil moisture values and whether the variance and range depends on the average wetness within the ensemble.
- To explore the relationship between spatial average soil moisture dynamics obtained within one TDR cluster and the discharge response at the outlet of the 16 km^2 large catchment.
- To compare observations with long-term simulations from the physically based hydrological model CATFLOW to investigate soil and vegetation controls on observed soil moisture dynamics and explore whether the spatial extent of the TDR clusters does indeed allow for an assessment of a representative mean soil moisture dynamics.
- Identify the dominating hydrological processes during an irrigation experiment.

3.2 Research area and additional data sets/methods incl. CATFLOW

3.2.1 Research area

The research area is the headwaters of the Weißeritz River. The Weißeritz basin is located in the eastern part of the Ore Mountains, Czech Republic/Germany, between 50° 40' and 50° 49' northern latitude and 13° 35' and 13° 45' eastern longitude. It consists of two main channels, the Red and Wild Weißeritz, which jointly contribute to the Elbe River at the city of Dresden. The

area is selected because basins of the Ore Mountains are typically well known for their sensitivity to flash floods response and the direct effect of the Weißeritz River on the city of Dresden (LFUG, 2004; Pöhler, 2006; Guse et al., 2009; Uhlemann et al, 2010). The basin covers an area of 384 km^2 and stretches over 15 km from north to south. The work is focusing on the headwater catchment of the Wilde Weißeritz down to the gauge at Ammelsdorf, which lies above the storage reservoir Lehnmühle. The complete catchment of the Weißeritz is not under investigation because of the effect of three storage reservoirs in the downstream part of the catchment and their strong influence on the runoff evolution. The catchment is ranges from 910 m at Pramenáč to 527 m at its outlet. The area is characterized by plateaus with only gentle slope divided by steep valleys. The metamorphous bedrock is mostly covered with a strongly heterogeneous periglacial soil structure covering layers of loamy soils with Podzol-Cambisoil associations (Heilmann and Symmangk, 2008). Conifer forest dominated by *Picea abies* (European spruce) and arable land appear in approximately equal shares in the catchment to the Ammelsdorf gauge (Table 8). The watershed of the Rehefeld gauge is dominated by forests and the Becherbach has only a small amount of pasture.

Table 8: Landuse in the three sub-basins

Subbasin	Land use
Ammelsdorf	50% forest, 13% arable land, 3% bogs, 30% pasture, 4% settlements
Rehefeld	61% forest, 11% bogs, 26% pasture, 2% settlements
Becherbach	80% forest, 20% pasture

For more than 20 years water levels have been observed at the Rehefeld and the Ammelsdorf river gauges operated by the Federal State of Saxony (Landestalsperrenverwaltung Sachsen). The small watershed of the Becherbach is a typical steep tributary of the Weißeritz river network (Table 9) and is instrumented with a capacitance water level measurement device of the type "TruTracks" (Intech Instruments LTD.). Different events are sampled using NaCl as a tracer to estimate the runoff volume. A rating curve is calculated and used to transform water stages to runoff.

Table 9: Topographic and hydrological (of the period 2000–2010) characteristics of the nested watersheds.

	Catchment size [km²]	mean Slope [°]	std Slope [°]	Mean q $l\ s^{-1}km^{-2}$	q05 $l\ s^{-1}km^{-2}$	q95 $l\ s^{-1}\ km^{-2}$	Mean Q m^3s^{-1}	Q05 m^3s^{-1}	Q95 m^3s^{-1}
Becherbach	2	7.5	4.8	17.63	0.81	151.11	0.043	0.002	0.366
Rehefeld	17	6.3	4.4	19.56	1.33	98.9	0.339	0.023	1.712
Ammelsdorf	49	7.9	5.1	19.28	1.96	89.23	0.988	0.101	4.574

The mean flow rate at the Ammelsdorf gauge is about 0.99 m^3s^{-1} and the specific discharge 19 $l\ s^{-1}km^{-2}$, at the Rehefeld gauge it is 0.34 m^3s^{-1} with a specific discharge of 20 $l\ s^{-1}km^{-2}$ for the period 2000-2010, and at the Becherbach gauge it is 0.04 $m^3\ s^{-1}$ with a specific discharge 18 $l\ s^{-1}km^{-2}$ for the period 2007-2010. Average annual precipitation at the meteorological station Zinnwald (877 m a.s.l.) (Figure 10) is 1000 mm during the period of 2000-2009 and the average

precipitation amount for the summer half year is approximately 600 mm. Average annual temperature is between 4-5.5 °C.

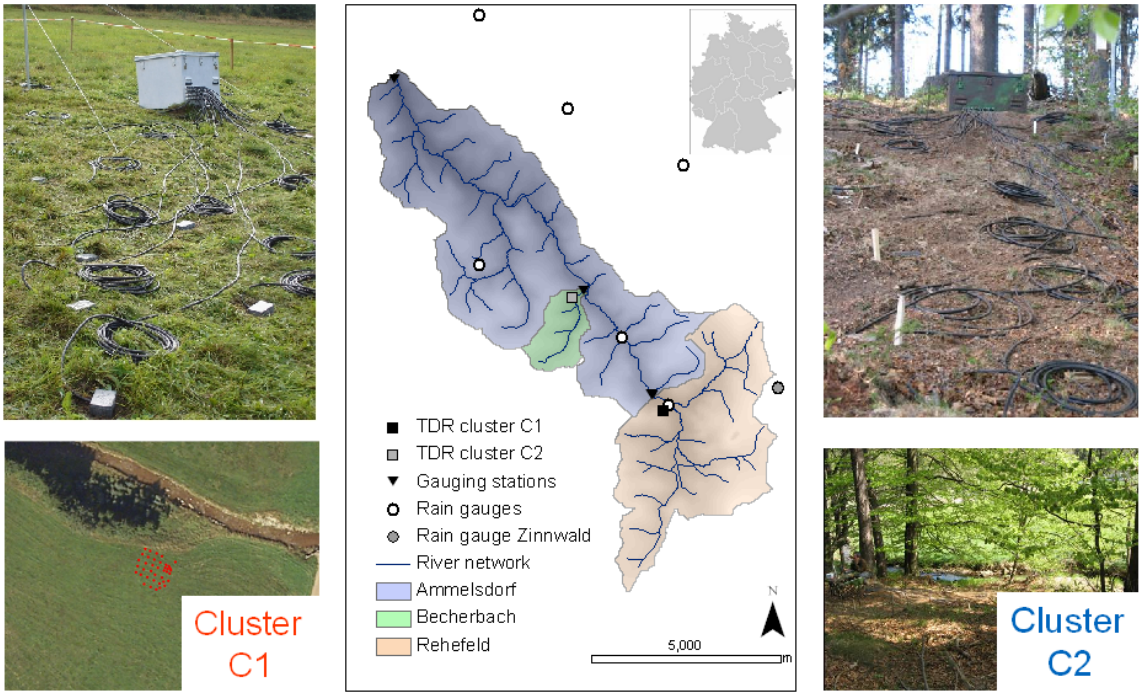

Figure 10: **Map view of the headwaters of the Wilde Weißeritz (50°43'-50°49' N; 13°38'-13°45' O) with instrumentation, as well as photos to highlight the differences between the two TDR cluster sites of C1 (left) and C2 (right).**

The headwater is additionally instrumented with six rain gauges, a meteorological station positioned at the grassland site, several "TruTracks" to observe shallow groundwater, tensiometers, profiles of FDR probes (THETA probes, Delta t) as reference measurement and two TDR clusters. Figure 11 shows the spatial extend of the installed probes at the two study sites.

Cluster C1 is installed in open grassland and consists of 39 TDR probes (Figure 3.1). There is an elevation difference of 5 m between the upper and lower part of the study site with a mean slope of 12°. Cluster C2 has been installed at a forested site and consists of 31 sensors. The TDR sensors used are 60 cm long insulated three-rod probes of type SUSU03 (Schädel, 2006. The probes are connected to a TDR100 (Campbell Scientific Inc.) via an eight channel multiplexer of type SNAPMUX (Becker, 2004) by means of coaxial cables of type RG213 with an impedance of 50 Ω and a length 15 m. The TDR100 is controlled by ARCOM VIPER 1.2 Industrial-PC with embedded LINUX operating system that also serves as data logger. A combination of a HS-L 130 solar panel (Siemens) with a power rating of 130 W and a 12 V gel battery guided by a solar controller SLR 2016 provides an independent power supply in the field even under winter conditions. Data collection of soil moisture data started in May 2007 at a sampling interval of 1/2 h. Installation, which is done from the surface, of the 60 cm long TDR probes at both sites is a challenge, mainly due to the large amount of gravel as well as high soil stability. Even when using a steel template with three holes at the right distance and an electric drill, on average about two attempts are necessary to drill three holes down to a sufficient depth. Soil profiles that are

excavated to check for proper installation showed that TDR probes are often deformed. Probe deformations affect the capacitance of the transmission line which is crucial in the context of TDR inversion (Becker, 2004; Schlaeger, 2005). In Chapter 2 the laboratory study showed that probe deformations have a minor influence on TDR travel times and therefore on the vertically averaged soil moisture. However, retrieved soil moisture profiles can be seriously corrupted by rod deformations.

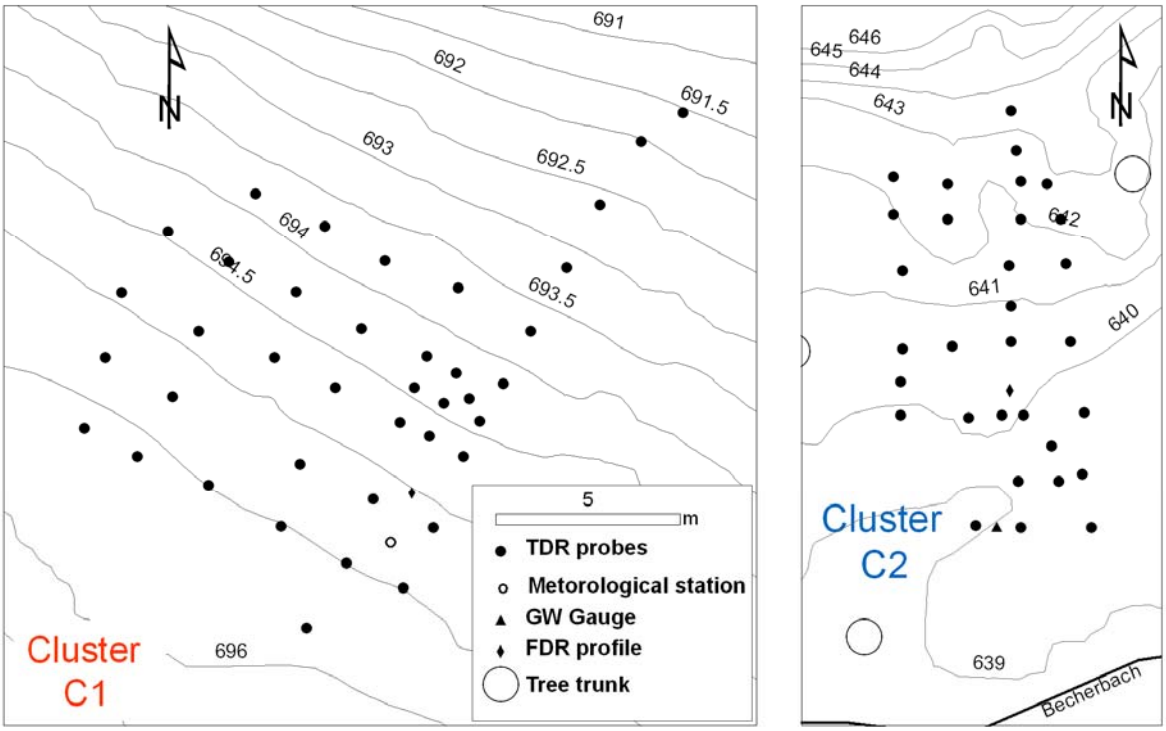

Figure 11: Spatial extent of installed TDR probes with elevation lines and additional instrumentations at the two study sides, C1 (grassland) and C2 (forest).

The soil at C1 was investigated through 4 soil pits, 40 auger drills to a depth of 1 m and 39 pits to depth of 0.7 m after the dismounting of the TDR probes in November 2009. At C2 10 auger drills to a depth of 1 m were conducted and 3 pits to a depth of 70 cm. 120 soil samples were collected at different depths to estimate the grain sizes. At both sites the soils were classified as Cambisoils (Table 10) and the parent bedrock at C1 consists of Cambric phylite, at C2 of Palaeozoic red gneiss. 250 soil samples in 1.00 cm^3 soil cores taken to estimate the bulk density (ϱ) and porosity (Table 11). In situ measurements of hydraulic conductivity were taken close to the TDR for different depths between 20 cm, 40 cm and 80 cm by means of an Amoozimeter (Ksat Inc., Raeigh, North Carolina). The principle is to maintain a constant water level in an auger hole and measure the discharge through the walls of the hole, based on the decrease in a water table with time (Amoozegar, 1989a). After a steady state is established, k_s is calculated according to Amoozegar (1989b). The support volume of the measurement is in the order of 10-40 $H \times r^2$ where H is the level of water maintained in the auger hole and r is the radius. Gravel content is quantitatively estimated using photogrammetric analysis of the soil pits.

Table 10: Soil profiles at the two locations C1 and C2

	Horizon	Type	Munsell Colour	colour	accuracy	Humus content	Hollows	Pro-portion of macro-pores	Rooting [fine roots/m²]	Substrate	Parent material	Skeletal fraction
Grass land site C1	0-30 Ap	top soil horizon characterised by cultivation	10YR 3/5	grey brown	planar diffuse	medium humus content	Earth worms	2%	15	loamy sand	Upper Layer	15
	30-45 Bv	Brunification	7.5YR 4/6	brown orange	planar diffuse		Earth worms	2%	4	sandy loam	Upper Layer	30
	45-100 Cv	parent material	10 YR 4/6	orange					0	sandy loam	Basal Layer	40
Forest site C2	0-10 Of	organic horizon with plant remains										
	10-25 Ah	top soil horizon	10YR 3/5	grey black	planar diffuse	medium humus content	Earth worms	2%	25	loamy sand	Upper Layer	15
	35-50 Bv	Brunification	7.5YR 4/6	brown orange	planar diffuse		Earth worms	2%	4	loamy sand	Upper Layer	30
	50-100 Cv	parent material	10 YR 4/6	yellow					2	loamy sand	Basal Layer	40

Table 11: Average soil properties obtained at grassland site C1, ϱ is the bulk density, k_s is saturated hydraulic conductivity, θ_s is saturated water content and OC is organic content. ϱ and θ_S are estimated on 1.00 cm³ soil cores with grain density of 2.65 g cm^{-3}.

Depth [m]	S [g g^{-1}]	U [g g^{-1}]	Cl [g g^{-1}]	k_s [mm d^{-1}]	ρ [g cm^{-3}]	θ_s [m³m^{-3}]	OC [g g^{-1}]	Gravel content [m²m^{-2}]
0.00				8,640.00				
0.10	0.37	0.49	0.14	1,884.73	1.04	60.59	0.11	0.02
0.30	0.38	0.52	0.09	89.16	1.15	56.45	0.09	0.07
0.50	0.35	0.52	0.12	449.21	1.09	58.70	0.02	0.02
0.70	0.48	0.39	0.13	142.15	1.19	55.05	-	0.05
0.90	0.38	0.46	0.17	34.56	1.65	37.74	-	0.12

The soil at the grassland site of C1 is a sandy loam (Table 11). The upper 20 cm exhibit a high content of organic matter which is reflected in the low bulk density of 1 g cm^{-3} and large porosity of 0.63. Soil stability is nonetheless high due to the large amount of gravel and aggregated material. Consequently, soil hydraulic conductivity in the top layer is large, around 2,000 mm d^{-1}, and decreases by one order of magnitude in 30 cm depth. Surface infiltrability measured with a constant head infiltrometer is at around 8,640 mm d^{-1} with a high variance (Figure 12). The soil at the forested site of C2 has an even higher infiltrability - beyond the measurement range - which is explained by the dominating grain sizes of loamy sand, lower bulk density and higher organic content of the top soil (Table 12).

Table 12: Average soil properties obtained at forested site C2, , ϱ is the bulk density, k_s is saturated hydraulic conductivity, θ_s is saturated water content and OC is organic content. ϱ and θ_S are estimated on 1.00 m³ soil cores with grain density of 2.65 g cm^{-3}.

Depth [m]	S [g g^{-1}]	U [g g^{-1}]	Cl [g g^{-1}]	k_s [mm d^{-1}]	ρ [g cm^{-3}]	θ_s [m³m^{-3}]	OC [g g^{-1}]
0.10	0.87	0.08	0.05	172,800.00	0.75	71.70	0.13
0.30	0.88	0.08	0.04	486.79	0.85	67.77	0.09
0.50	0.91	0.06	0.03	34.02	1.14	57.03	0.03
0.70	0.92	0.04	0.04	43.20	1.30	50.94	-
0.90	0.86	0.09	0.05	25.92	1.35	49.06	-

At both sites gravel content increases with depth, which is for C2 only qualitatively observed. In the laboratory study in Chapter 2 it is shown that gravel within the integration volume has a minor influence both on TDR travel times (and thus average soil moisture) as well as on retrieved soil moisture profiles.

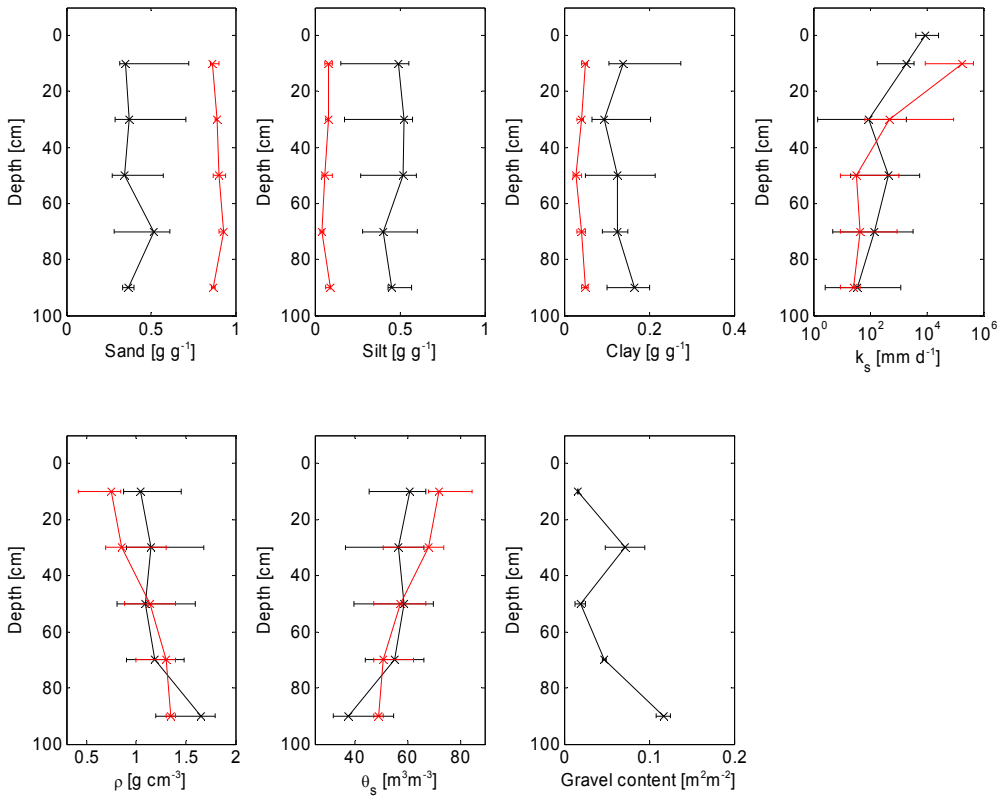

Figure 12: Distribution of the median of hydraulic conductivity k_s, grain size distribution (the prevailing texture following the United States Department of Agriculture, USDA notation), bulk density ϱ, saturated water content θ_s and gravel content at grassland site C1 Rehefeld (black line) and C2 Becherbach (red line) with the confidence intervals 0.25 and 0.75.

3.2.2 Data Analyses and Modelling

3.2.2.1 TDR travel times, depth integrated soil moisture and outliers

This study will be focus on data observed in the period between the 3rd May 2007 and the 26th October 2007, which is the frost-free period in 2007. TDR travel times are determined by detecting the time of steepest ascent in the first (signal entry) and second main reflection (reflection at the open end of the probe) in the reflectogram (Becker, 2004). Although there is a large amount of data gathered within an automated procedure, reflectograms of each individual probe are visually inspected frequently for their quality. Based on the calculated average dielectric permittivity, the average soil moisture is calculated after Herkelrath et al. (1991); compare Chapter 2. The data underlying this study are hence time series of vertically averaged soil moistures obtained within the two clusters and the related time series of temporal soil moisture changes.

3.2.2.2 Statistical and geostatistical analysis

First, for both sites the time series are cleaned of outliers that are defined as values that drop outside the 99.9% range observed at an individual probe. Next, time series of the spatial mean

and standard deviation, both of the soil moisture values and the hourly soil moisture changes, are computed. Periods where the number of TDR probes producing measurements dropped below 10 are excluded from this procedure.

The spatial covariance structure of vertically integrated soil moisture is analyzed in two steps. First the temporal means and standard deviations for the individual TDR probes in a cluster are calculated, simply to reduce noise that is introduced by small-scale variability in surface and subsurface water flow during individual events. Based on these values, dry and wet days are selected where the individual soil moisture values at the TDR probes differed more than plus/minus one standard deviation from the mean and then these values averaged in time to assess average conditions during dry and wet conditions for the individual probes. The resulting values reflect the average spatial distribution of soil moisture during average wet and dry conditions. In a second step, experimental variograms are calculated using the Matheron estimator and fitted to a spherical variogram function by minimizing least squared differences. Minimum lag is 1.1 the minimum probe distance; lag tolerance is set to 50%. Lag classes with less than 30 pairs are not included in the fit. As necessary conditions for second-order stationarity, the residuals are proven on a Gaussian distribution with zero mean. This is fulfilled in all cases. Due to the small extent of a TDR cluster, geostatistical analysis is somewhat limited as the maximum detectable range corresponds roughly to 50% of the maximum lag. The maximum lag distance is 15 m.

3.2.2.3 Rank stability

Rank stability plots (Teuling et al. 2006; Lin 2006; Starks 2006; Brocca et al., 2009, 2010) are used to understand the temporal persistence of spatial soil moisture patterns on the one hand and can help in identifying representative sites, where the measured soil moisture closely resembles that of the spatial mean.

The relative differencing technique scales the measurements from each location against the associated field mean, thus stabilizing the variance due to the changing value. The relative difference δ_{ij} with location i and time j is calculated by:

Eq. 13

$$\delta_{ij} = \frac{\theta_{ij} - \overline{\theta_j}}{\overline{\theta_j}},$$

where $\overline{\theta_j}$ is the mean of each time step j:

For each location i, the mean and $\overline{\delta_i}$ and standard deviation $\sigma(\delta_i)$ of the relative differences are:

Eq. 14

$$\overline{\delta_i} = \frac{1}{M}\sum_{j=1}^{M}\delta_{ij}$$

Eq. 15

$$\sigma(\delta_i) = \sqrt{\frac{1}{M-1}\sum_{j=1}^{M}\left(\delta_{ij} - \overline{\delta_i}\right)^2},$$

with *M* the number of time steps.
A stable location in time is characterised by a low value of $\sigma(\delta_j)$. The $\overline{\delta_j}$ is a measure for the bias of the soil moisture for each location. By combining the values with the root mean square error ($RMSE_\delta$) the locations of higher temporal stability can be identified by low $RMSE_\delta$ values and $\overline{\delta_j}$ close to zero (Joshi et al., 2011).

Eq. 16

$$RMSE_\delta = \sqrt{\overline{\delta_i}^2 + \sigma(\delta_i)^2}$$

The results from Eq. 14 to 15 are sorted by rank and plotted from the lowest mean to the highest to identify the location with the highest stability.
The estimated values are compared with topographic values of elevation, slope and topographic wetness index of the two hillslopes by the Spearman rank correlation with,

Eq. 17

$$\rho = 1 - \frac{6\sum_{i=1}^{n}\left(R(x_i) - R(y_i)\right)^2}{n(n^2-1)},$$

where the variables *x* and *y* are ranked separately, given $R(x_i)$ and $R(y_i)$. *n* is the sample size. The coefficient is based on the sum of difference between the corresponding ranks of *x* and *y* and reach values between -1 to 1. The topography is measured with a differential GPS (DGPS, Trimble 5700/5800) at C1 and because of the canopy coverage with a levelling instrument at C2 with a point density of 50 cm and a measurement accuracy of +/- 2 cm.
The topographic wetness index (*TWI*; Beven and Kirkby, 1979) is used to investigate if there is correlation to that index on the small scale. The index describes the affinity of a subarea to saturate as long as the total extend of the elevation model is large enough to describe the local catchment size (A_s) of the subarea.
It is calculated as:

Eq. 18

$$TWI = \ln\left(\frac{A_s}{\tan(\beta)}\right),$$

where is β the local slope. Large values are an indicator for areas with a tendency to saturation and results from large local catchment size and small angle.

3.3 Vegetation control on soil moisture dynamics: learning form physically based simulations

The water balance of the grassland site and the forested site is simulated using the physically based hydrological model CATFLOW and averaged simulated and observed soil moisture dynamics compared at both sites. The idea is to investigate concurring influences of soil and vegetation parameters on the model results as well as to test the hypothesis that the spatial extent of the TDR clusters is large enough to assess an unbiased spatial average soil moisture at both sites during the observation period. The latter is the case, if a spatially homogeneous model setup that uses observed soil hydraulic data allows unbiased reproduction of the mean dynamics.

3.3.1.1 Model description

CATFLOW allows physically-based simulations of flow and solute transport at the hillslope and small catchment scales (Maurer, 1997; Zehe et al., 2001). The model represents a hillslope along the steepest descent line as a 2-dimensional cross section that is discretized by 2-dimensional curvilinear orthogonal coordinates. The hillslope is thus assumed to be uniform perpendicular to the slope line. Soil water dynamics is described by the Richards' equation in the potential form that is numerically solved by an implicit mass conservative Picard iteration (Celia & Bouloutas 1990). Accordingly, the model allows simulation of subsurface flow under saturated and unsaturated conditions. Soil hydraulic functions are described after van Genuchten (1980) and Mualem (1976). Evaporation and transpiration is simulated using an advanced approach based on the Penman-Monteith equation, which accounts for annual cycles of plant morphological and plant physiological parameters, albedo as a function of soil moisture and the impact of local topography on wind speed and radiation. In the case of infiltration excess or saturation excess, surface runoff is routed along the main slope line and using the convection-diffusion approximation of the one-dimensional Saint-Venant equation. It is numerically solved by an explicit upstream finite difference scheme.

Enhanced infiltration due to preferential flow and macroporosity is represented by a simplified, effective approach motivated by experimental findings of Zehe and Flühler (2001a). If soil saturation at a surface node exceeds field capacity, effective soil hydraulic conductivity is increased by a macroporosity factor. Detailed explanation of the macroporosity is given by, Zehe et al. (2001) and Zehe and Blöschl (2004).

The model, including the effective approach to account for enhanced infiltration, has been successfully applied to simulate the long term water balance and the effect of soil moisture variability on flooding in the Weiherbach catchment, Germany (Zehe et al., 2001; Zehe and Blöschl, 2004; Klaus and Zehe, 2010) as well as to simulate the rainfall-runoff response in a small alpine catchment (Lindenmaier et al., 2005) and in the Malalcahuello catchment in Chile (Blume, 2008).

3.3.1.2 Model setup and simulation variants

The concurring influences of soil hydraulic parameters and plant morphological parameters on soil moisture are investigated in a two step procedure to find the most parsimonious model setup that allows a successful prediction of the time series of observed average soil moisture at both sites.

Table 13: The parameters θ_r (residual water content), α (air entry value) and n (width parameter) for the different layers are estimated based on the pedo transfer function of Carsel and Parrish (1998). The values are kept constant during simulation.

Depth [cm]	θ_r [$m^{-3}m^{-3}$]	α [m^{-1}]	n [-]
0-20	0.065	7.5	1.89
30-120	0.078	3.6	1.56
120-200	0.095	1.9	1.31

The 35 m long hillslopes are discretized into a two-dimensional finite difference grid. Vertical resolution is 2 cm in the upper 0.60 cm and 0.20 m down to 2 m depth. Lateral resolution is 0.5 m. Surface model elements extend over a width of 26 m which corresponds to the width of the hillslopes. Both model hillslopes are thus assigned a homogeneous three-layer soil profile, neglecting stochastic variability of soil parameters as first guess. In a first step three different soil profiles A, B, C and the vegetation parameters for forest and grassland that are determined in the Weiherbach catchment (Zehe et al., 2001) (see next section) are compared. The van Genuchten parameters θ_r (residual water content), a (air entry value) and n (width parameter) in the different layers are estimated based on the available texture data using the pedo transfer function of Carsel and Parrish (1988) kept constant during the simulations (Table 13). The saturated hydraulic, k_s, conductivity and porosity, θ_s, varied within the three soil profiles. Profile A and B used the average values observed at the grassland and the forested site, respectively, for the upper two layers. The deep layer is parameterized according to Carsel and Parrish (1988). Profile C used values derived by Carsel and Parrish in all layers, assuming that only texture data are available (Table 14). Please note that the porosities and hydraulic conductivities of the pedo transfer function are clearly smaller compared to the measured values. Simulation results are evaluated using the root mean square error (RMSE), the absolute bias (Bias) and the correlation coefficient R.

Table 14: Saturated hydraulic conductivity (k_s) and porosity (θ_s) used in the different profiles.

	Profile A		Profile B		Profile C	
Depth [m]	k_s [$m\ s^{-1}$]	θ_s [m^3m^{-3}]	k_s [$m\ s^{-1}$]	θ_s [m^3m^{-3}]	k_s [$m\ s^{-1}$]	θ_s [m^3m^{-3}]
0-0.20	4.16×10^{-5}	0.63	$1.23\ 10^{-4}$	0.68	$1.23\ 10^{-5}$	0.50
0.30-1.20	1.58×10^{-6}	0.61	$2.89\ 10^{-6}$	0.66	$2.89\ 10^{-6}$	0.52
1.20-2.00	7.22×10^{-7}	0.41	$7.22\ 10^{-7}$	0.41	$7.22\ 10^{-7}$	0.41

In the next step the most suitable soil profile and adjusted vegetation and landuse parameters are selected. The latter include the annual cycles of plant morphological parameters (leaf area index *LAI*, plant cover, root depths, plant height, as well as plant roughness), several parameters that control the evapotranspiration model such as plant albedo, minimal stomata resistance, a factor and an inflexion point parameter of the soil moisture weighting function for stomata resistance computation (Zehe et al., 2001). These parameters as well as the annual cycles of plant morphological parameters are determined for different crops, forest and grassland in the Weiherbach catchment in South West Germany, based on detailed field survey, remote sensing

and process model studies (Zehe et al. 2001). Plant physiology may be assumed to be independent from the catchment setting. Thus the complete corresponding parameters sets are taken over. However, the annual cycles of plant phonological parameters such as *LAI*, plant cover and also root depth depend of course on the climate setting and climate in the Rehefeld is on average three degrees cooler than in the Weiherbach catchment. Thus the annual cycles of plant morphological parameters from the Weiherbach dataset by dividing the daily values by their annual maxima are normalised. *LAI*, plant cover and root depth of these normalised annual cycles range thus from zero to one. By multiplying these normalised annual cycles by slightly different annual maxima of *LAI*, plant cover and root depth, slightly different annual cycles during different simulations can be tested. The combinations of *LAI* maxima, plant cover maxima and root depths that are used are presented in the results section. Again, RMSE, the bias and correlation coefficient are used as quality criteria.

The upper boundary condition during simulation is atmospheric, based on the observed precipitation and meteorological data observed at C1. At the lower boundary, gravity flow is established. The left boundary condition at the hill top is set to zero flow; the right boundary condition is a seepage interface to allow subsurface flow to exfiltrate from the hillslope. Simulation started on 1st March 2007, which is already snow free, to assure a sufficiently long initialization period and lasted up to 26th October 2007. The focus lies on the period from 1st May to 26th October 2007.

3.4 A field scale irrigation experiment to explore fast vertical and lateral flow processes

A sprinkling experiment was carried out to understand the dominating runoff processes on the grassland hillslope C1. Before the experiment was initiated, the vegetation is cut to a length of 3 cm, to avoid channelling of overland flow in the existing herbal layer. The last precipitation event occurred three days prior and had an amount of 12 mm. The median soil moisture of the TDR probes one day before the irrigation experiment was 0.37 m^3m^{-3}.

3.4.1 Irrigation rates and sprinkling

Two irrigation experiments were carried out. Using a groundwater pump (MP1, GRUNDFOS, Bjerringbro, Denmark) water from the Wilde Weißeritz was allowed to irrigate an area of 13 m by 8 m (Figure 13) through two oscillating sprinklers. The intensity of 12 mm h^{-1} thus corresponds to a return period of half a year due to the KOSTRA atlas (Bartels et al., 1997) in the region. The first irrigation of 36 mm d^{-1} has a return period of ½ a and the second with 60 mm d^{-1} of 2 a. The absolute irrigation amount was measured with 10 rainfall accumulators (13 cm diameter, 10 cm height).
To investigate interactions of subsurface and surface processes with emphasise of lateral flow, only the upper part of the instrumented field was irrigated. Thus it will be distinguish four classes of TDR probes in operation: a) irrigated directly, b) at a down slope distance of 0.1 m to 0.5 m to the irrigated plot, c) at a down slope distance of 1.4 m to 1.7 m distance, and d) at a down slope distance of larger than 2.0 m.

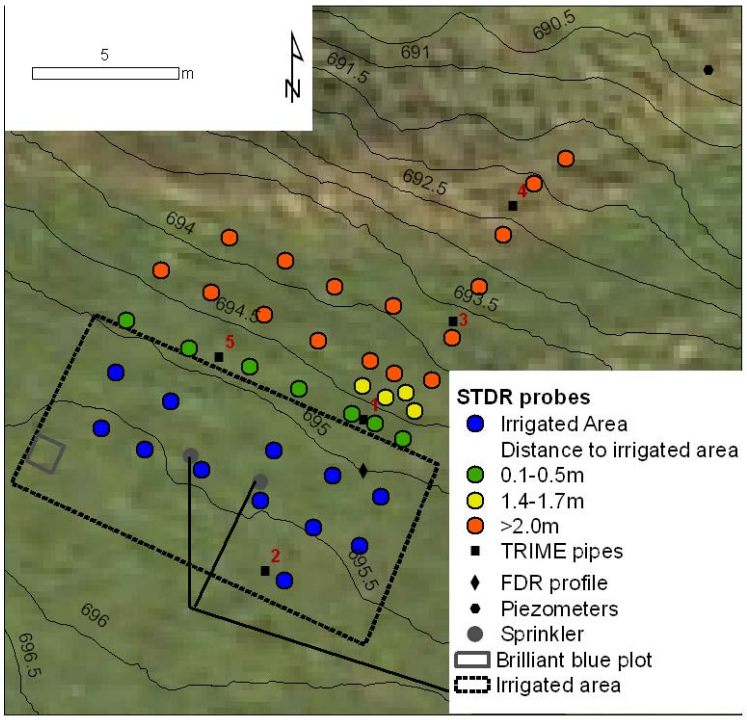

Figure 13: Sprinkling experimental subset on the grassland site C1 Rehefeld.

3.4.1.1 Installation of soil moisture profile sensors

The hillslope was additionally instrumented with access tubes of a TRIME T3C pipe probe (IMKO GmbH) up to a depth of 3 m. Laurent et al. (2005) and Evett et al. (2006) have discussed in detail the accuracy of the method. With a COBRA drill hammer auger holes were prepared half a centimetre in diameter less than the TRIME pipes (4.4 cm) to guarantee a good contact to the soil. The tubes were than driven into the soil by a hammer. Gaps around the access tube that occur during the installation process at the surface were filled in with soil material from the drilling. The installation was completed 2 months before the experiment.

Five tubes were installed on the experimental field (see Figure 1). The installation depth varied between 1.9 m and 3.0 m depending on the gravel content. Two were located in the irrigation field, one just below the plot and two were installed at a distance of 5 m and 10 m. Measurements taken at each 10 cm in three directions determined the mean soil moisture. These snapshots of soil moisture profiles were measured at irregular intervals, as the assessment of the entire profile proved to be very time consuming.

3.4.1.2 Dye tracing

The dye tracer brilliant blue is a widely used labour intensive and invasive method to understand the near surface flow processes (Zehe and Flühler, 2001b; Stamm et al., 2002; Weiler and Flühler, 2004; Kim et al., 2006; Blume et al., 2008; Anderson et al., 2009, Van Schaik et al., 2010). On an area of 1 m^2 (Figure 1) using a dye concentration of 4 g l^{-1}, 40 l of water and dye was injected before the second irrigation and excavated one day later. Vertical profiles were opened each 10 cm to depth of 80 cm - 90 cm. All profiles are photographed with a digital camera, rectified with WGEO (DHI-WASY GmbH, Berlin, Germany) and enhanced with GIMP (GNU Image

Manipulation Program) by disaggregating the image into the channels of the colour space of HSV (Hue- Saturation- Value). The tone curves were adjusted to increase the contrast between stained and non-stained areas and the grey scale image analyzed where light grey represents the stained area and dark grey the unstained (Blume et al, 2008).

3.4.2 Control of pre-event conditions and rainfall characteristics of flood events

3.4.2.1 Estimating runoff coefficients

The runoff coefficient (C_r) is the classical measure for describing the catchment runoff response at the annual or event scale (Mosley and McKerchar, 1992). Blume et al. (2007) gave a broad overview of the different methods to estimate the event-based C_r. Here, the ratio of direct runoff and total precipitation amount at the event scale is used. There are different concepts of how to separate the direct runoff from baseflow, each of them based on a considerable amount of conceptualisation and all of them bear systematic errors (Blume et al. 2007). Exclusively tracer methods do allow a realistic quantification of the baseflow component (Hoeg et al., 2000; Ladouche et al., 2001). However, this is laborious, expensive and restricted to a small number of events and catchments which is insufficient for a statistical analysis. The main difficulty is to define the end point of the flood event when no tracer data are available (Nathan and McMahon, 1990; Merz and Blöschl, 2003; Blume et al. 2007). In the present study Blume's method is employed for base flow separation which assumes that at the end of the event the catchment starts to drain like a linear reservoir. The areal precipitation amount is estimated with the inverse distance weighting method.

Only those events with >5 mm precipitation are included in the sample, which corresponds to the 5% quantile of the sample, and a ratio of peak discharge to pre-event discharge larger than 0.5 for the Rehefeld and Ammelsdorf gauges and 0.6 for the Becherbach, similar to Noribiato et al. (2009). The minimum time to define separate events was set to 6 hours. Events that occurred closer in time are aggregated to a multi-event. In general, runoff coefficients are estimated only for the snow-free period, as the density of the snow measurement network is too low to adequately represent the liquid water content in the snow store.

3.4.2.2 Estimators of catchment wetness and the meteorological forcing

In general, predictor variables are classified into those estimating the catchment's antecedent wetness and those which can be determined *a priori*, from those that characterise the meteorological forcing which can only be estimated based on *a posteriori* observations or based on predictions (both with uncertainty).

The catchment's state is characterised by pre-event runoff q_0 as a proxy for the wetness of the deep subsurface. Pfister et al. (2003) and McIntyre et al. (2007) used q_0 to predict runoff volume and peak of an arid and a humid catchment using statistical models. Additionally, soil distributed moisture observation areas – if available – are often used for characterising near surface catchment wetness (Meyles et al., 2003; Blume, et al. 2009; Brocca et al. 2009b; Zehe et al., 2010; and Penna et al., 2010). In the present study the spatial average soil moisture (WC_0) is used as well as the coefficient of variation of soil moisture within the cluster (CV). Additionally, the

antecedent precipitation index *API* is as a widely used measure of the antecedent catchment state (Brocca et al., 2009b). However, the *API* remains a subjectively determined and implemented parameter (Heggen, 2001), defined by *N* days before the event and *a*, the decay constant.

Eq. 19

$$API(t_0) = \sum_{i=1}^{N} P(t_{0-i}) \cdot \alpha^i$$

The *API* has the disadvantage of not representing any soil and geological specific difference, which is of importance in a heterogeneous subsurface and depends on the density of the measurement network. Longobardi et al. (2003), Brocca et al. (2008), and Graeff et al. (2009) have documented that *API* did not improve their predictions. However there are other studies which have presented the contrary: Xia et al. (1997), Descroix et al. (2002), and Berthet et al. (2009) have all shown that considering *API* improved the quality of their runoff and stream flow estimations.

Furthermore, the antecedent precipitation *AP,* i.e. the cumulated rainfall sum over a defined fixed period without a decay factor is tested. Although this parameter is sometimes criticized (Heggen, 2001), several studies have shown that it might be useful for small catchments (e.g. Ali and Roy, 2010). Several AP^N and API_a^N in the ranges of N =5d - 60d and a = 0.8 - 0.99 are tested but will only results for best estimators (AP^{60} with a temporal window of 60 days and $API_{0.95}^{30}$ with a window size of 30 days and a = 0.95) will be presented here for sake of briefness.

The meteorological forcing is characterised by the accumulated event rainfall *P*, cumulative rainfall in the first two hours of the event *P2h*, mean hourly rainfall intensity *I*, and duration of rainfall *DP*. Proxies for pre-event evapotranspiration *ET* are daily evapotranspiration of the previous day (Ali and Roy, 2010; Hrnčíř, et al., 2010) and antecedent sunshine duration index (Graeff et al., 2009). However, these parameters are less relevant at the event time scale and are not considered in this study.

3.5 Results

3.5.1 Average dynamics and spatial variability of soil moisture at the two clusters

Figure 14 gives a first overview on the precipitation input and temperature forcing (A and B) during the period 5rd May 2007 and end at the 1th of October 2007 at a meteorological station installed close to the cluster C2 as well as on the time series of vertical average soil moisture for the individual probes for cluster C1 at the grassland site (C) and C2 at the forested site (D). The period of missing data is due to a break-down of the multiplexers that took a while to be fixed. The total range of soil moisture values within the probes of cluster C2 is smaller compared to cluster C1. The most downslope TDR probe at C2 is influenced by shallow groundwater and is consequently very wet during the entire period. The probes at the dry end of the spectrum are installed in a debris-rich, fast-draining spot. At both sites there is a small diurnal variation in

measured soil moisture. The amplitude is of the order of 0.002 m^3m^{-3}, correlation with air temperature is negative and strongest at a lag of 12 h. The negative correlation could be explained by evaporation and transpiration loss during the day which is regained due to dew formation during the night. A daily fluctuation of 0.002 m^3m^{-3} in soil moisture at porosity of 0.6 and along a length of 60 cm corresponds to an evaporation loss of 0.8 mm during daytime. This appears to be reasonable.

Figure 15 A) and B) compares time series of the first two spatial moments at both clusters. The temporal dynamics of the spatial means at both sites looks similar to a hydrograph, with fast rising "peaks" and long "recessions". Average soil moisture at the grassland site is significantly larger than at the forested site as can be seen from the box plots in Figure 15 C). Coefficients of variations (not shown) at both sites are pretty constant at the grassland site with on average 0.22 and a narrow range between 0.23 and 0.2 compared to C2 where the relative spatial variability is fluctuating between 0.22 and 0.15 with an average around 0.18. The Spearman rank correlation coefficient between the time series of spatial average soil moisture at both sites is 0.73. Thus, 50% of the temporal soil moisture variance observed at one site may be explained by the variance observed at the other site. As the climate forcing is supposed to be very similar it can be concluded that 50% of the soil variance is determined by climate conditions, the rest is determined by soil and vegetation.

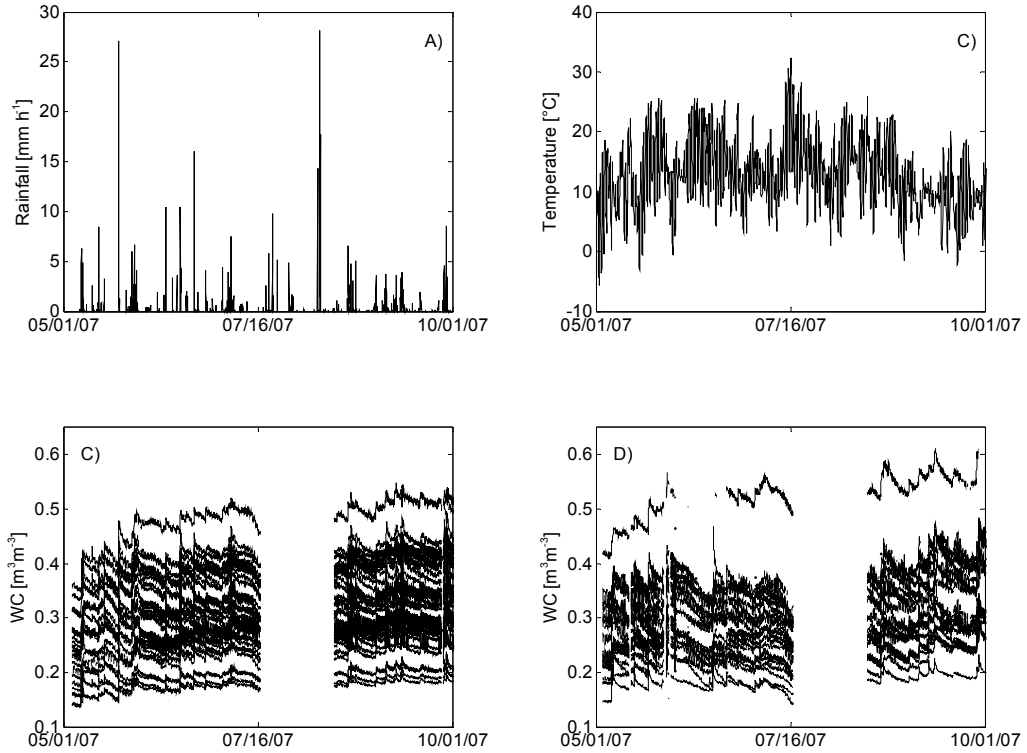

Figure 14: **Precipitation (a) and air temperature (b) in the observation period, vertically average soil moisture at probe locations at C1 (c) and C2 (d). Period starts at 5rd May 2007 and end at the 1th of October 2007.**

As can be seen from the box plots in Figure 15 C), the spatial mean of soil moisture within the upper 60 cm is on average 0.04 m^3m^{-3} larger than at the forested site C2. The marginal soil moisture distribution at C2 is clearly skewed towards the right; at C1 it is rather symmetrical. Hourly soil moisture changes at both sites are on average zero (Figure 15 D). Their marginal distributions appear rather similar. The second spatial moments of hourly soil moisture changes are small, at around 0.001 m at both sites. The coefficients of variation of hourly soil moisture changes are, however, very large, with values up to 100. This highlights that the relative spatial variability of the hourly soil moisture changes are large when compared to the relative spatial variability of the absolute moisture values, which underlines the heterogeneity of this site.

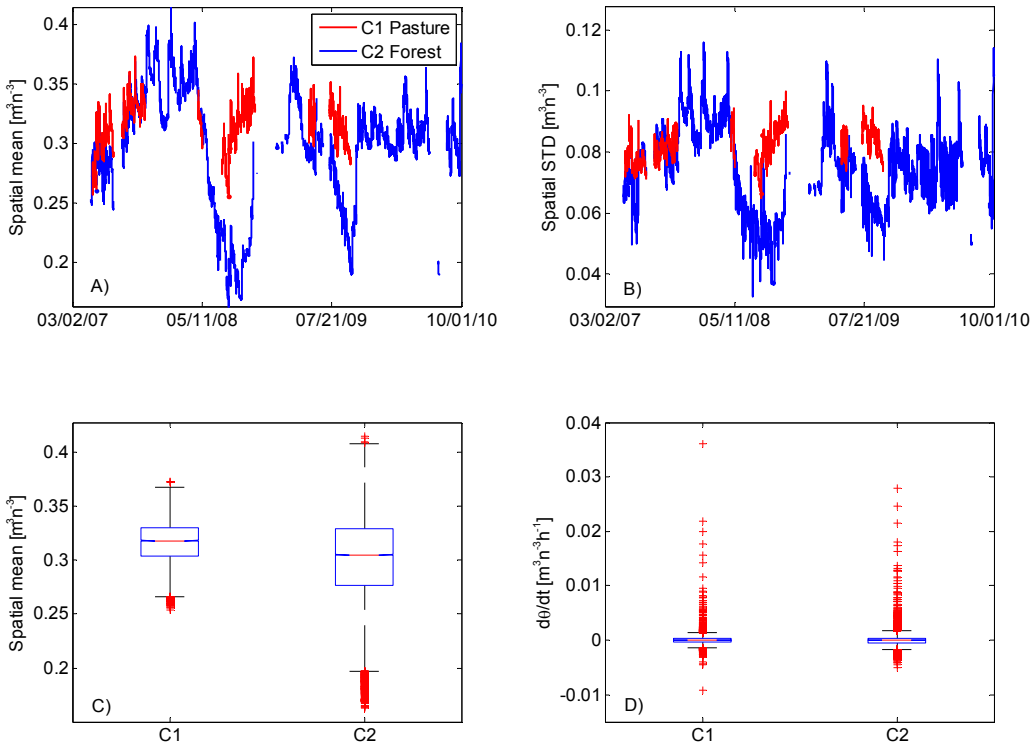

Figure 15: **Time series of spatial average soil moisture (A) and spatial standard deviation at both clusters (B), box plots of spatial average soil moisture (C) and of the spatial average soil water increments (difference between values at two adjacent time steps (D).**

3.5.2 Average covariance structure

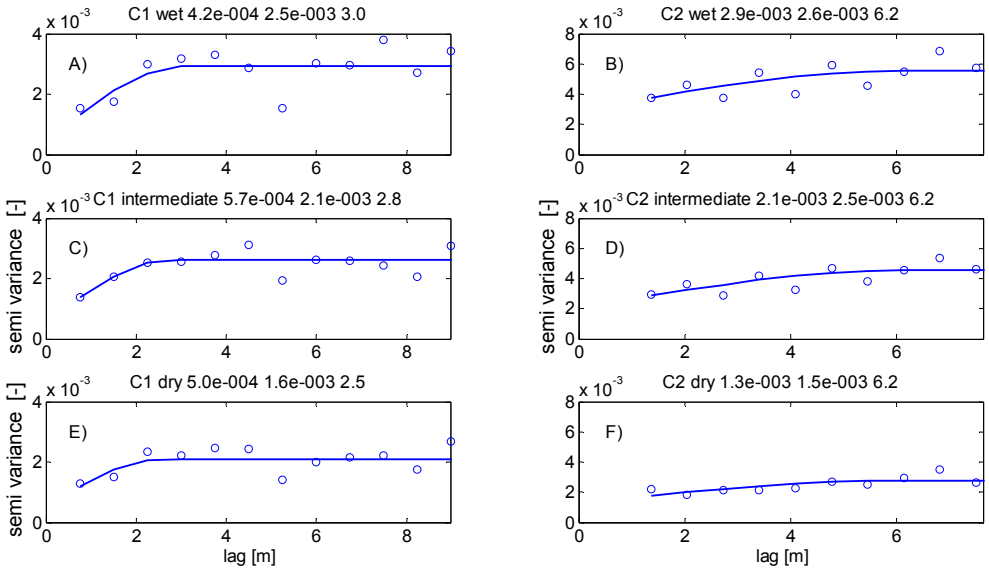

Figure 16: Experimental variogram and fitted spherical variograms for both sites (left column of panels is C1, the right is C2). Upper panels represent average wet conditions, middle overall average conditions and lower panels average dry conditions. The panel headers list the nugget, sill and range of the fitted spherical variogram function.

The correlation length of the long-term averages of soil moisture at individual probes at C1 turned out to be 2.8 m (Figure 16 C). This small value is not astonishing due to the extensive small-scale heterogeneity observed at this site. Gravel content and porosity especially vary strongly between neighbouring plots. For wet/dry conditions the range shows a slight increase/decrease of 0.2 m. The sill to nugget ratio – a measure for the part of the variability that is explained by the variogram - increases from dry to average to wet conditions as 3/1 over 4/1 to 5/1. This finding, and the increasing correlation length with increasing wetness, is consistent with findings of Western et al. (2004) or Grayson et al. (1997). However, contrary to their findings, in the case total soil moisture variance (nugget + sill) in C1 increases with increasing average wetness (Figure 16 A). This due to the fact that a few probes are located in gravel-rich soil spots which drain very fast due to the high permeability and low water retention. These probes stay relatively dry even when the rest of the field wets up during rainfall events. Brocca et al. (2007) found at their grassland site in the upper Tiber valley effective ranges that are approximately 28 - 35 metres and also a nugget of sill ratio that changed with average saturation.

At the forested site, C2 correlation length does not vary with average wetness and is - at 6.2 m - roughly 50% of the maximum probe distance (Figure 16 B, D, E). Also the sill to nugget ratio is almost constant at approximately 1 : 1. Also here total variance is maximum in the wet case and minimum in the dry case. The reason is the same as in the case of C1: some spots of high permeability never really wet up due to fast drainage. The constant correlation length and the constant nugget to sill ratio reflect the stationary pattern of throughfall within this spring/summer period. Disturbances due to large rain events are simply filtered out to deal with

temporally-averaged data that reflect average dry, total average and average wet conditions at the probes.

3.5.3 Rank stability of soil moisture time series

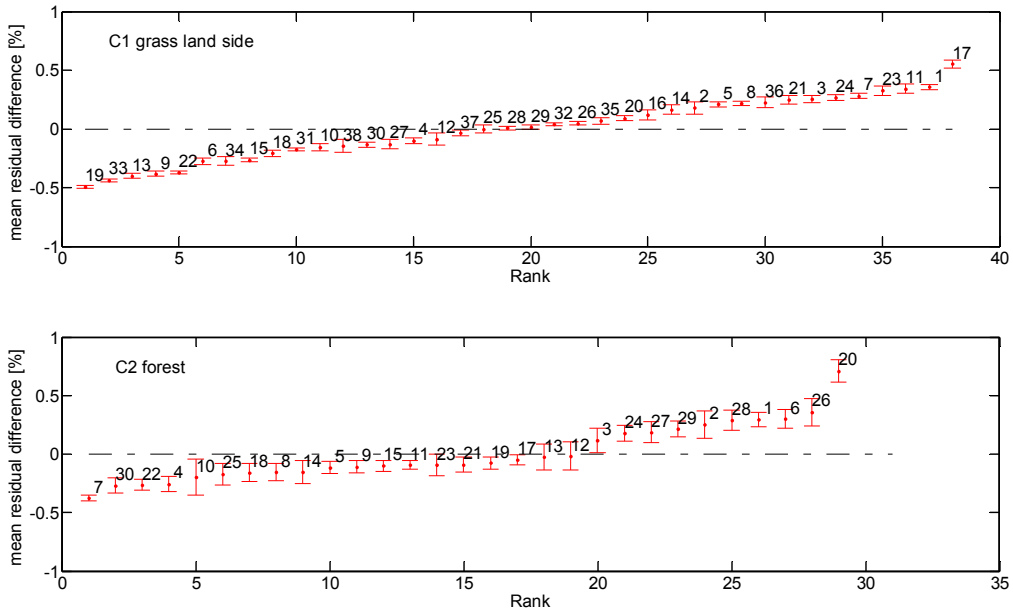

Figure 17: Ranks of the deviation of the spatial mean for the different probes. A is the lot for C1 and B) for the C2.

Figure 17 shows the rank ordered mean relative difference for the two sites and each probe to show how individual site values deviate from the mean during the complete measurement. Winter periods are not included. The variability of the probes in C1 and the variation of each single probe are smaller compared to the forest site C2. Probe 20 is located close to the channel and is affected by groundwater. The dryer locations are because of higher gravel content examined by auger drills.

As Figure 18 shows, there is in C1 no visible relationship with topographic factors. Texture and geomorphologic features should here be the controlling factors.

For C2 with increasing elevation (ϱ = -0.46) and decreasing angle (ϱ = -0.35), wetness increases but not strongly. The *TWI* has no gaining of cognition about soil moisture patterns for both sides. The microtopography is not adequately represented in DEM and soil moisture is more controlled by soil type.

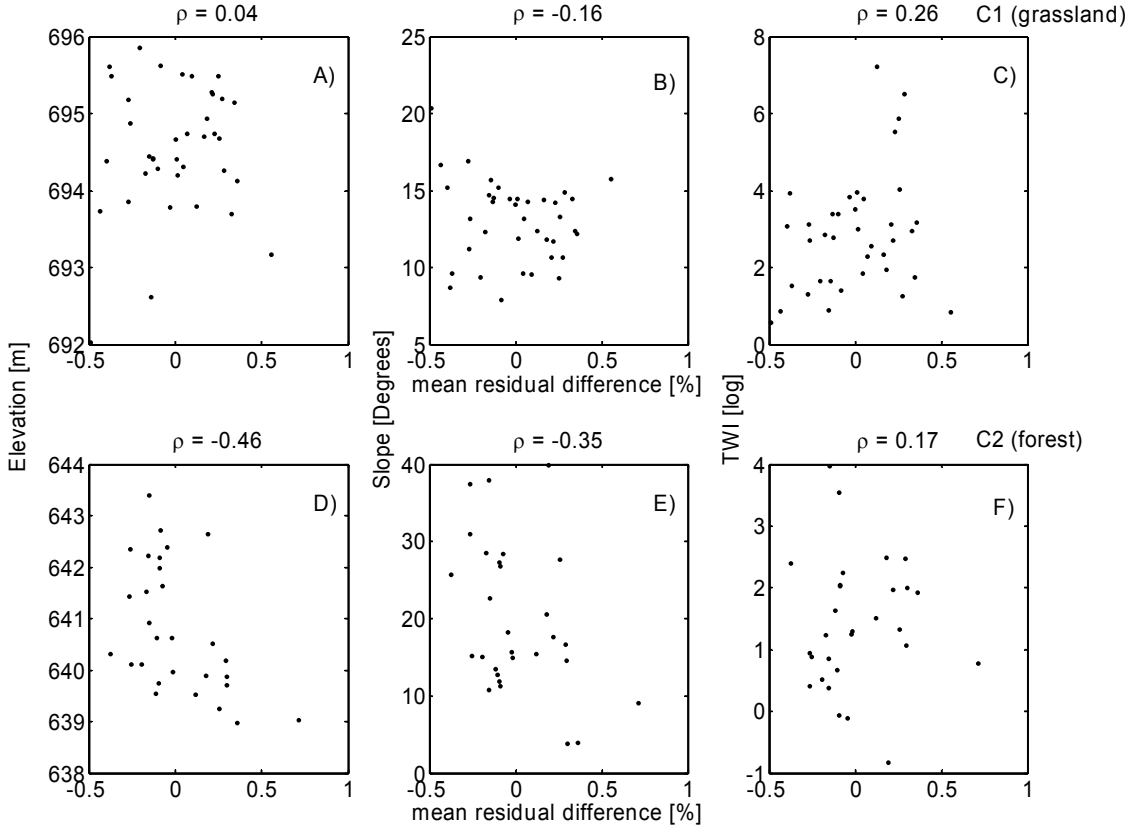

Figure 18: Relationship of the two clusters' mean residual difference to topography (A and D), slope (B and E) and topographic wetness index (C and F) for C1 (A to C) and for C2 (D to F). In the header Spearman's rank correlation ϱ is given.

3.5.4 Vegetation and soil control on hillslope scale soil moisture regimes

3.5.4.1 Model sensitivity to different soil profiles

As can be seen from Table 6, soil profile A) yields the best model performance for the grassland site, whereas profile B) yields the best model performance for the forested site. This underlines the value of observed soil hydraulic data, as both profiles use data that are measured at the respective sites. Profile C), which has a smaller porosity and smaller k_s, causes - at both sites - the highest bias, the worst correlation and RMSE, respectively.

Table 15: Root means square error (RMSE, scale is 10^{-4}), bias (scale is 10^{-3}) and correlation between simulated and observed average soil moisture obtained with the three different soil profiles (compare Tables 13 and 14 for soil parameters)

	Grassland			Forest		
Profile	RMSE×10^{-4} [-]	Bias×10^{-3} [m^3m^{-3}]	R [-]	RMSE/10^{-4} [-]	Bias/10^{-3} [m^3m^{-3}]	R [-]
A	6.9	14	0.753	78.2	47	0.725
B	27	-60	0.010	10.4	32	0.850
C	33	-74	0.169	18.0	-54	0.630

3.5.4.2 Model fine tuning with LAI, plant cover and root depth

Table 16: Annual maxima of leaf area index (*LAI*), plant cover and root depth run through during the model fine tuning and corresponding model goodness parameters root means square error (RMSE, RMSE, scale is 10^{-4}), bias (scale is 10^{-3}) and correlation. The annual maxima observed in the Weiherbach catchments are in bold italics, the best parameter sets are in bold (compare Figure 19).

Site	*LAI* [m^2m^{-2}]	Plant cover [-]	Root depth [m]	RMSE×10^{-4} [-]	Bias×10^{-3} [m^3m^{-3}]	R [-]
Forest	13.5	0.9	1	5.4	11	0.892
Forest	14.0	0.8	1	10.4	32	0.850
Forest	***14.0***	***0.9***	***1***	***10.4***	***32***	***0.850***
Forest	14.0	0.85	1	8.1	23	0.876
Forest	13.5	0.8	1	5.1	9.2	0.891
Forest	**13.5**	**0.85**	**1**	**4.7**	**5.7**	**0.889**
Grassland	4	1	0.2	7.0	-12	0.727
Grassland	5	1	0.2	7.2	-14	0.716
Grassland	6	1	0.2	7.5	-16	0.71
Grassland	4	1	0.3	10.1	-24	0.655
Grassland	**5**	**0.9**	**0.2**	**6.8**	**-8**	**0.749**
Grassland	5	0.9	0.3	9.2	-19	0.700
Grassland	6	0.9	0.2	7.0	-10	0.743
Grassland	6	0.9	0.3	9.5	-20	0.695
Grassland	***4***	***1***	***0.1***	***6.9***	***14***	***0.753***
Grassland	4	.95	0.1	7.3	16	0.763
Grassland	4	0.9	0.1	8.4	20	0.780
Grassland	3.5	1	0.1	7.0	15	0.751
Grassland	3.5	0.95	0.1	7.6	17	0.763
Grassland	3.5	0.9	0.1	9.2	22	0.788
Grassland	3.0	1	0.1	7.6	16	0.762
Grassland	3.0	0.95	0.1	8.5	20	0.776

Table 16 lists the annual maxima of leaf area index, plant cover and root depth run through during the model fine tuning as well as corresponding model goodness parameters. The annual maxima observed in the Weiherbach catchments are printed in bold italics, the best parameter sets are obtained at both site are printed in bold (compare Figure 19). As can be seen from Table 16, slight changes in the annual maxima of *LAI* and plant cover yielded a clear improvement in the model's performance. Figure 19 B) highlights the surprisingly good accordance of the averaged simulated soil moisture in the upper 60 cm with the averaged soil moisture observed at the forested site. Despite small overestimation of the soil moisture peaks during rainfall events, the averaged simulated soil moisture is most times within the confidence interval of the observed average soil moisture. The confidence interval is estimated by dividing the standard deviation within a cluster by the square root of the number of sensors that are available at this date. It is furthermore remarkable that simulated averaged soil moisture is still a good match for the observations, even after the period of missing data. A good prediction of soil moisture at the forested site is possible when using the normalised annual cycles of plant morphological parameter observed in the Weiherbach catchment and a slight adaptation of the annual maxima of *LAI* and plant cover.

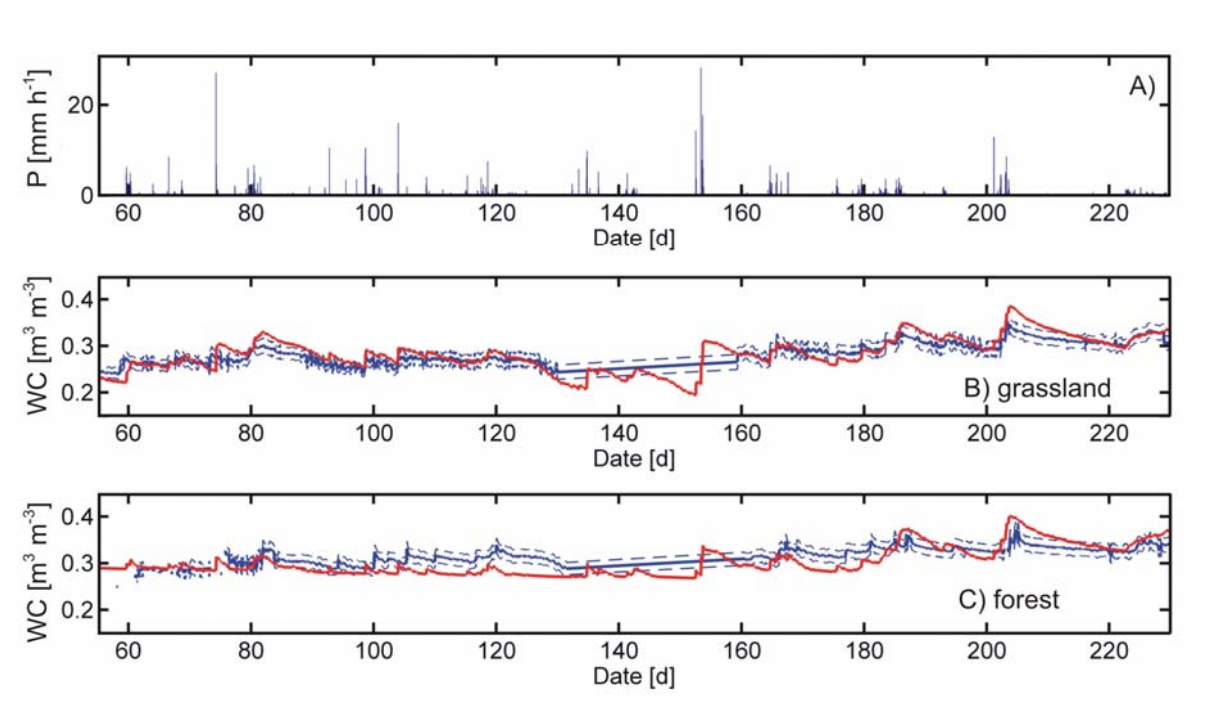

Figure 19: **Precipitation observed at grassland site C1 (a), spatially averaged soil moisture in the upper 60 cm simulated with CATFLOW (solid red line), observations (solid blue line) and confidence interval of the spatial average soil moisture (dashed blue line) for the grassland site C1 (c) and the forested site C2 (b). The confidence interval is estimated by dividing the standard deviation within a cluster by the square root of the number of sensors that are available at this date. The plotted period starts at 5th May and ends at 26th October 2008. Please note that the period between day 120 and 160 is a period of missing data.**

Reproduction of the observed average soil moisture time series at the grassland site is not that straightforward, although other parameters are observed, including variations in root depth (Table 16). The best simulation, parameters printed in bold, has higher RMSE, larger bias and smaller correlation coefficient when compared to the best simulation at the forested site. Figure 19 C) shows that the model systematically underestimates soil moisture between day 100 and day 160 which corresponds to the period between mid-June to the start of September. Even a strong variation of the annual maxima of *LAI*, plant cover and root depth, while leaving the normalised annual cycle unchanged, is obviously not sufficient to match observed soil moisture dynamics as well as at the forested site.

3.5.4.3 Simulated average soil moisture dynamics

Based on the model results, it can be concluded that a homogeneous soil setup that uses local observations of k_s and porosity produces as good a model performance at both sites as using soil profiles that are completely parameterized through the pedo transfer function of Carsel and Parrish (1998). This is not surprising but underlines on one hand the value of local k_s and porosity observations for setting up physically based models. And it shows on other hand that the residual water content, *a* the air entry value and *n* parameter estimated based on the pedo transfer function of Carsel and Parrish (1998) are sufficient to achieve a good model acceptable performance. This is good news as direct measurement of these parameters is laborious.

At the forested site furthermore, a small adjustment of the annual maxima of *LAI* and plant cover can be found, while assuming that their normalised annual cycles are the same as observed in the Weiherbach catchment (Zehe et al., 2001) leads to a strong improvement of the model bias and RMSE. Simulated averaged soil moisture is for almost the whole period within the confidence interval of the observed spatial average soil moisture. It can be concluded that the best model setup (soil profile A, *LAI* = 13.5, plant cover = 0.85) is a promising representation of key areas in the Rehefeld headwater, that could serve as building blocks to represent forested areas in a catchment model. Further it can be concluded that the extent of the sampling grid is large enough to assess the dynamic spatial average soil moisture in an almost unbiased way. At the grassland site, fine tuning of the model results based on adjusting the annual maxima of root depth, *LAI* and plant cover is not as successful. The normalised annual cycle of grass morphological parameters in Rehefeld must differ from those in the Weiherbach. Negative bias in the model is not due to non-representative sampling but due to insufficient representation of vegetation. A better model performance requires survey of the annual cycles of these plant morphological parameters, especially during periods of obviously bad model performance (in early May and in summer).

3.5.5 Irrigation experiment for the identification of the dominant runoff processes

3.5.5.1 Spatial pattern of sprinkling rates

Because of wind drift and the fact that an oscillating irrigation system was in use, homogeneous irrigation of the field could not be achieved (Figure 20); furthermore, the mean pumping rate was in both cases higher than the median irrigation sum in the totalisators. During the irrigation the surface of the irrigated field is saturated and overland flow occurred. During the first experiment the maximum extent of overland flow was 0.3 m and during the second 0.5 m downhill from the lower border of the irrigated plots.

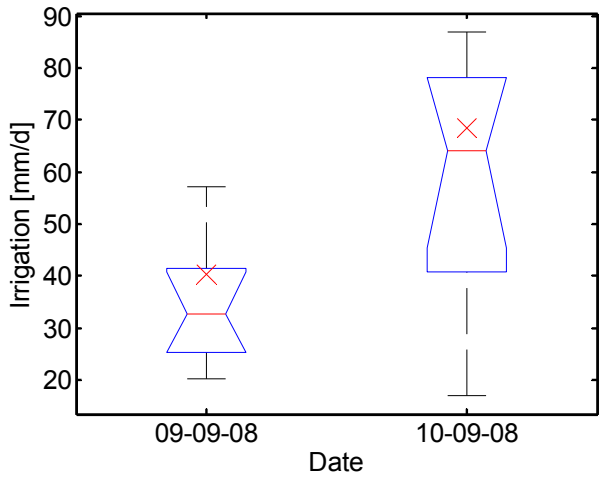

Figure 20: Distribution of the two irrigation fields. The red X is the mean irrigation measured by the amount of pumped water. The sample size is for both experiments 10.

3.5.5.2 Soil moisture dynamics from Spatial TDR and FDR observations

The TDR probes within the irrigated plots and the FDR probe at 0.2 m depth showed an immediate reaction to the irrigation pulse (Figure 21). The shallow subsurface reached a state

close to saturation in one hour. The range in soil moisture increases was from 0.05 m^3m^{-3} - 0.10 m^3m^{-3} for the TDR probes and much higher for the FDR probes, 0.07 m^3m^{-3} - 0.20 m^3m^{-3}. The strongest response was observed in the deepest probe. Soil moisture dropped immediately after irrigation ended, without any detectable lag.

Probes located at a downhill distance of 0.1 m to 0.5 m reacted with a lag time of 0.5 to 1 hour. The total soil moisture increases ranged between from 0.05 m^3m^{-3} - 0.15 m^3m^{-3}. At this distance overland flow was detected by eye during the two irrigation experiments and measured with handheld FDR probes (THETA probe, Delta-T-Devices). The maximum down slope distance at which probes outside the field reacted to the irrigation is 1.7 m. The observed lag time was 2.5 to 3 hours for the 4 probes at this location. Total of soil moisture increases were between 0.05 m^3m^{-3} and 0.10 m^3m^{-3}. Probes with a distance >2.0 m did not show any response to the irrigation. In the recession of soil moisture all probes reacted differently due to their specific soil physical properties.

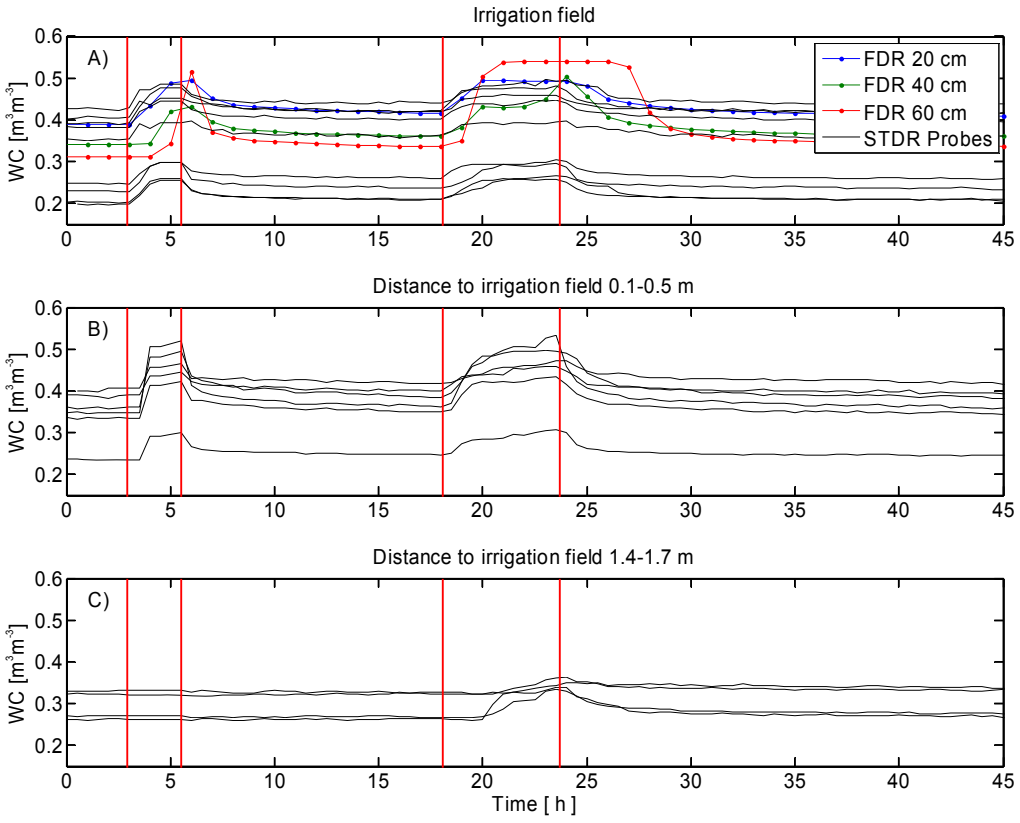

Figure 21: Probe response during irrigation of A) the direct irrigated TDR and FDR probes, the down slope probes are at a distance of 0.1 m - 0.5 m (B) and 1.4 m - 1.7 m (C) to the irrigation field.

The FDR sensors within the profile reacted generally with stronger soil moisture increases compared to the TDR probes. Here it has to be taken into account that the integration volume of a FDR probe(type THETA) is only 0.37 l while the TDR probes have a sampling volume larger than 3.0 l (see Chapter 2). The FDR probe at 0.2 m depth responds directly to the irrigation. The

two deeper FDR probes reacted with a lag of one hour for the first irrigation pulse and zero for the second pulse. This suggests that fast preferential flow pathways became active during the first event and there activation threshold was still exceeded when the second pulse started.

3.5.5.3 Soil moisture profiles

Pre-event soil moisture was wet in the top 0.2 m of the profile, dropping to low values at depths of 0.4 m to 0.5 m and remained dry in the lower parts of the profile (in Figure 22 as changes in soil moisture, Appendix, Figure 1 shows the measured absolute values). In tube 4 a water table was observed at a depth of 2.5 m.

During the irrigation, the soil moisture response differed from location to location, which reflects the complex structure of the subsurface and the variable flow process. All access tubes in the irrigation field (1 and 2) and close to the field (3 and 5) showed a response in the top layer to a depth of 0.1 m to 0.3 m.

Tube 1, located in the centre of the irrigation field, showed a response only to a depth of 0.2 m during the first event but the reaction reached greater depths and was still ongoing after the experiment for the second pulse of irrigation. Tube 2, which is located at the upslope edge region of the irrigation field, responded to a depth of 0.3 m during both experiments. Deeper parts of the profile were not connected. After the experiment soil moisture at a depth of 2.6 m showed a positive increase which can be explained by water transport through preferential flow pathways which were not within the sampling volume of the tube. Tube 3 was located at a down slope distance of 0.4 m to the irrigation field. During the first experiment no data were obtained from the tube and it showed little response to the second.

Tube 5 was installed with a similar distance to the irrigation field as tube 3. It responded in the top horizons to a depth of 0.3 m and in the bottom at a depth of 2.4 m during the first irrigation. The response time occurred 1.5 hours from the start. Soil moisture returned to the initial conditions before the second irrigation and then the soil moisture increased from the depth upward during the experiment to a depth of 1.5 m after the event. The first response was observed 2 hours after onset of the irrigation.

Tube 4, located at a distance of 10 m down slope, showed no response to both irrigation inputs at the near surface. At the end of the second irrigation pulse the water table rose by 0.05 m to a level of 2.45 m and soil moisture increased, which is a clear hint of a lateral transport component.

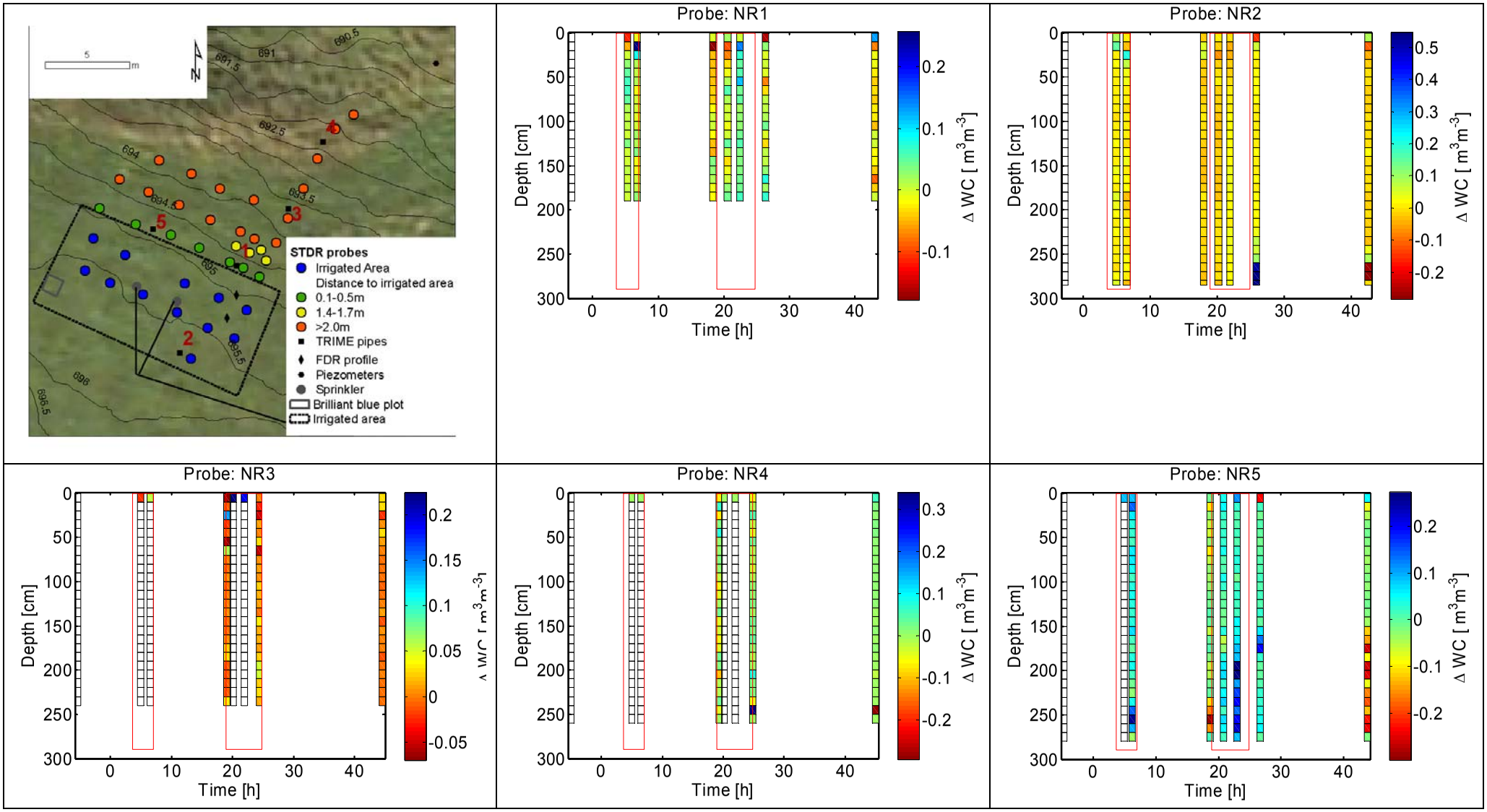

Figure 22: Soil moisture changes in profiles measured with TRIME probe for the five access tubes. The red boxes mark the irrigation period. Because of the heterogeneous response, colour bars are for each plot different.

3.5.5.4 Dye tracer experiment

One dye tracer experiment was carried out in the irrigation field and soil profiles excavated directly after the second irrigation. The excavation depth was limited to a depth of 0.8m because of a large boulder at that depth. High pixel values indicate flow pathways and the relative dye coverage along the depth on the left panel shows the distribution along the profile. The upper profile, to a depth of 5 cm to 15 cm, was dominated by homogeneous infiltration (Figure 23 A and B). Preferential flow then controlled the transport of the dye to the bottom of the profile and even deeper than the excavated level. In Figure 23 A) the infiltration was dominated by flow through gravel on the left hand side. Flow through macropores located at 0.4 m and 0.65 m at a depth of 0.4 m was a secondary flow path. Macropores from earth worms burrows and root channels were observed up to a depth of 0.4 m in all the profiles investigated. Figure 23 B) shows infiltration in discontinuous patterns governed by the presence of gravel. Between 0.5 m and 0.8 m depth and 0.3 m and 0.6 m, macropores dominate flow.

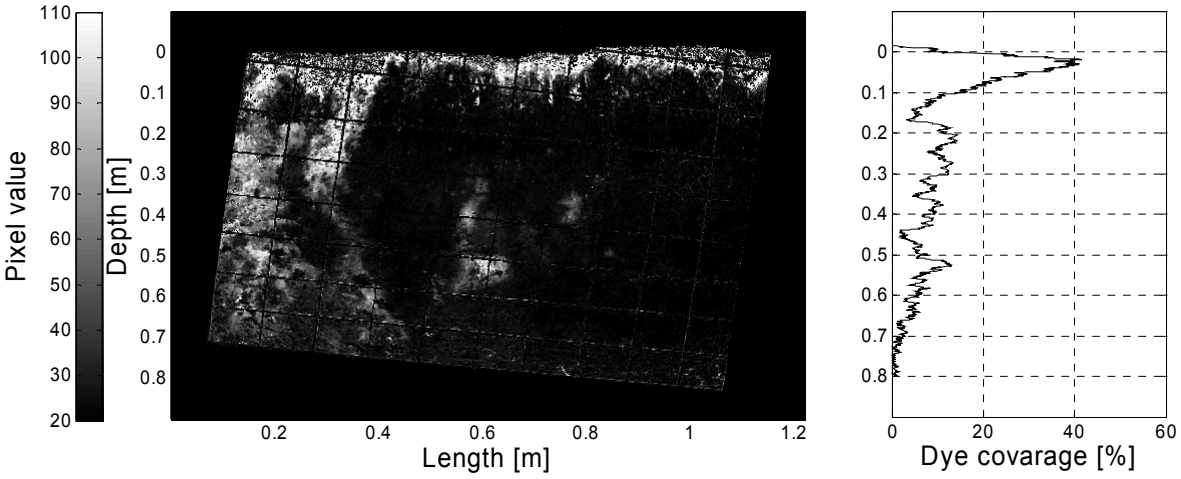

A)

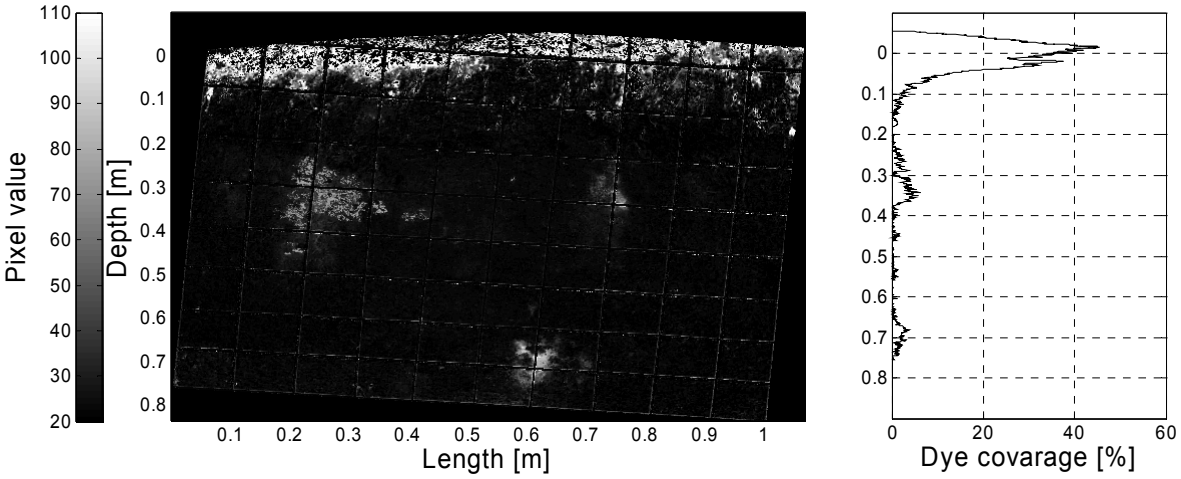

B)

Figure 23: Dye tracer profile and dye coverage of the vertical profiles at 30 cm and 70 cm. Areas with higher pixel values (brighter colour) have higher dye coverage which is an indicator for flow pathways.

3.5.6 Control of pre-event conditions and rainfall characteristics of flood events

Figure 24 shows scatter plots of the observed runoff coefficient C_r against selected meteorological predictors for the three nested catchments (the correlation matrix is in the Appendix, Table 4-6). Please note that individual events at the different catchments have different characteristics and runoff data are not always available for all three gauges. Rainfall intensity (I) has obviously no influence on the runoff coefficient, as can be seen from the scatter plots in the second and third row. This corroborates that Hortonian overland flow is not a relevant process in these catchments. Runoff coefficients in each catchment show some dependency on total rainfall amount P and rainfall duration DP. In the Becherbach catchment, this relationship suggests a threshold dependence: rainfall events with a duration shorter than two hours and an amount less 25 mm did not cause any flood formation. However, the sample size at the Becherbach is still too small to infer general behaviour and derive something like a general response threshold.

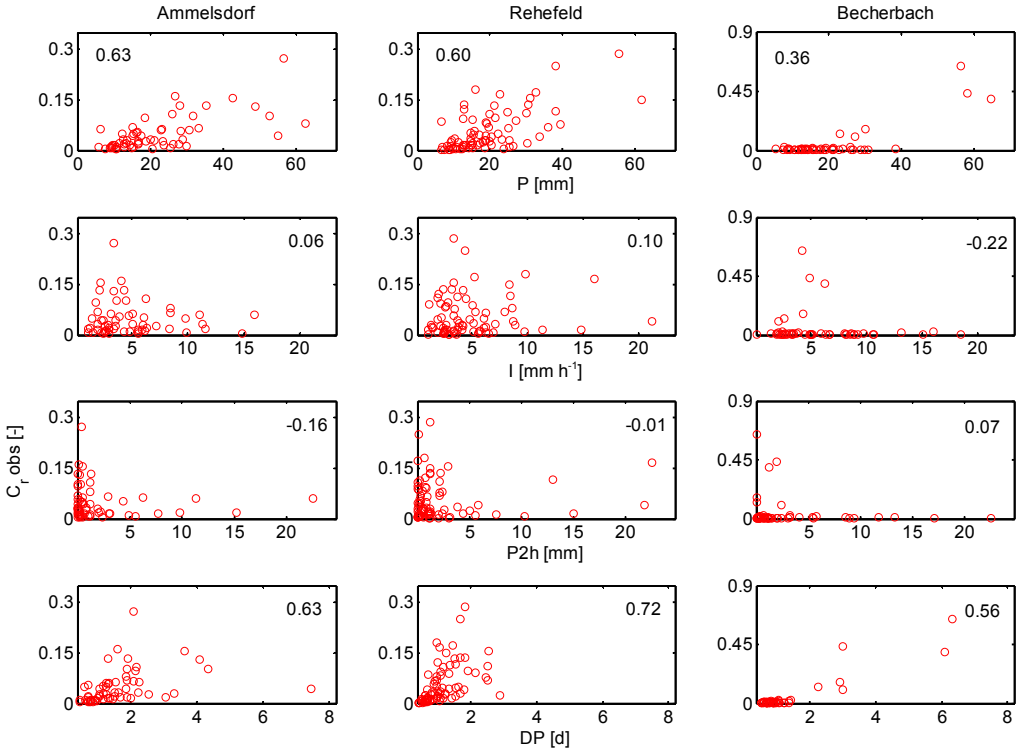

Figure 24: Scatter plots of meteorological forcing variables rainfall (*P*), mean rainfall intensity (*I*), 2-h-sum of precipitation (*P2h*), and duration of rainfall (*DP*) compared to the runoff coefficient (C_r). The Spearman rank correlation between predictor and C_r is plotted in each panel.

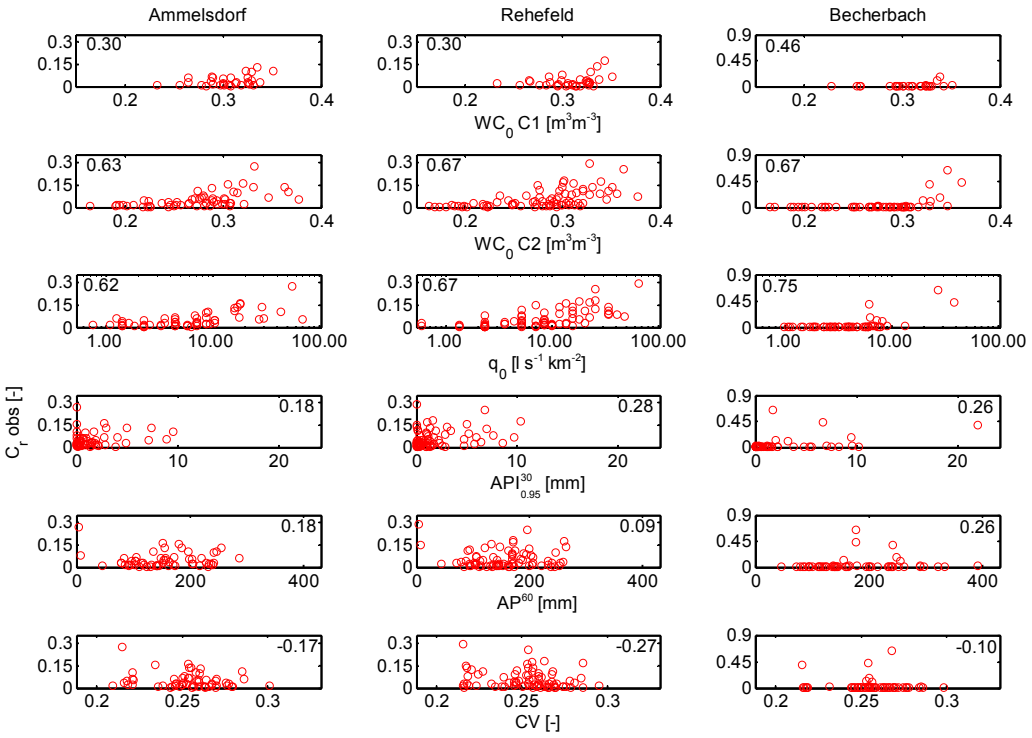

Figure 25: Scatter plots of the pre-event conditions predictor variables pre-event WC_0 for the STD clusters C1 (grassland) and C2 (forest), pre-event runoff (q_0), antecedent precipitation index ($API^{30}_{0.95}$), antecedent precipitation (AP^{60}) and coefficient of variation of WC_0 (CV) compared to the runoff coefficient (C_r). The Spearman rank correlation between predictor and C_r is plotted in each panel.

Figure 25 presents C_r plotted against the measures for antecedent catchment wetness. Again, a threshold-like dependence of C_r on pre- event discharge q_0 and WC_0 can be observed when looking at the Becherbach. When soil water saturation at the forest cluster reaches 0.33 m^3m^{-3} and specific discharge reaches 10.0 $ls^{-1}km^2$ the system's response is clearly enhanced. Hereby WC_0 shows a clearer trend compared to q_0 above the threshold value. As can be seen from the other scatter plots in Figure 25, none of the other predictors of the pre-event conditions are useful to explain the observed runoff coefficients.

Soil moisture observed at the forest C2 is a better predictor for the strength of the flood response than soil moisture at the grassland site. It could be due to the fact that high runoff coefficients are simply missing for C1. However, it could also be due to the fact that TDR cluster C2 is closely located to the riparian zone (Zehe et al. 2010) and a high average soil moisture in this cluster could indicate that upslope forested areas get connected to the riparian zone and will thus contribute to runoff formation in case of a precipitation event. James and Roulet (2007) suggested a similar a threshold-like change for the Westcreek catchment.

3.5.7 Analysis of bimodal runoff response

As demonstrated in Figure 25, a WC_0 of 0.33 m^3m^{-3} the Becherbach causes much higher runoff coefficients. This is further enlighten by a closer look at the rainfall runoff events from 9th May

2007, 15th June 2007, 11th September 2007, and 28th September 2007 (Figure 26). All these events had a similar rainfall input but show a completely different runoff response. The first event (Figure 25 A) consisted of 30 mm of rainfall, but the specific discharge volume was Q volume of 0.3 mm, which correspond to a C_r of 0.004. The respective WC_0 is 0.25 m^3m^{-3}, a specific prevent discharge q_0 of 1.2 l $km^{-2}s^{-1}$. The third event (Figure 25 C) behaves completely different during initial conditions (WC_0 0.33 m^3m^{-3}, q_0 8.2 l $km^{-2}s^{-1}$): 27 mm of rainfall produced a C_r of 0.10 and the runoff response shows a bimodal hydrograph. After the direct response to rainfall a second peak occurs with its maximum two days after the rainfall and producing more than 2/3 of the complete runoff volume.

These bimodal events are the typical response above the threshold value of 0.33 m^3m^{-3} WC_0. Similar runoff response characteristics are observed in adjacent head watersheds (Prange, 2010) but not in the Weißeritz itself (gauge Rehefeld and Ammelsdorf).This is a clue that that event type is triggered by a catchment condition analogous to that in the Schäfertal (Graeff et al., 2009) and Löhnersbach (Zillgens et al., 2007) and that the observed small tributaries in the headwater area of the Wilde Weißeritz produce a much higher response in streamflow above a certain threshold in antecedent wetness conditions.

A closer look at the relationship of discharge (*Q*) to soil moisture and groundwater level below ground (*GWL*) reveals hysteretic effects (Figure 26). The relationship is plotted from the beginning of the rainfall to the ending of the event in hourly time steps. The event from 7th May 2007 shows a clockwise response in *WC* to runoff. Runoff directly reacts to rainfall and returns to the baseflow level afterwards, whereas the *WC* response is slower and longer, and also decreases much slower before it returns to the starting level. The *GWL* shows no direct response to rainfall and only a small increase of 5 mm after 6 hours. The relationship between *Q* and *GWL* is also clockwise. During the event with wet antecedent conditions (11th September 2007) the hysteretic response shows a reverse response in the *WC-Q* relationship. The response of WC is only a small increase from 0.25 m^3m^{-3} to 0.28 m^3m^{-3} and WC returns back to starting conditions faster than *Q*. The bimodal response is not observed in *WC*. *GWL* reacts more slowly but is long-lasting and decreases less fast compared to runoff. Similar findings can be found for two other examples. During dry conditions, clockwise hysteresis between *WC* and *Q* is observed and during wet conditions anticlockwise.

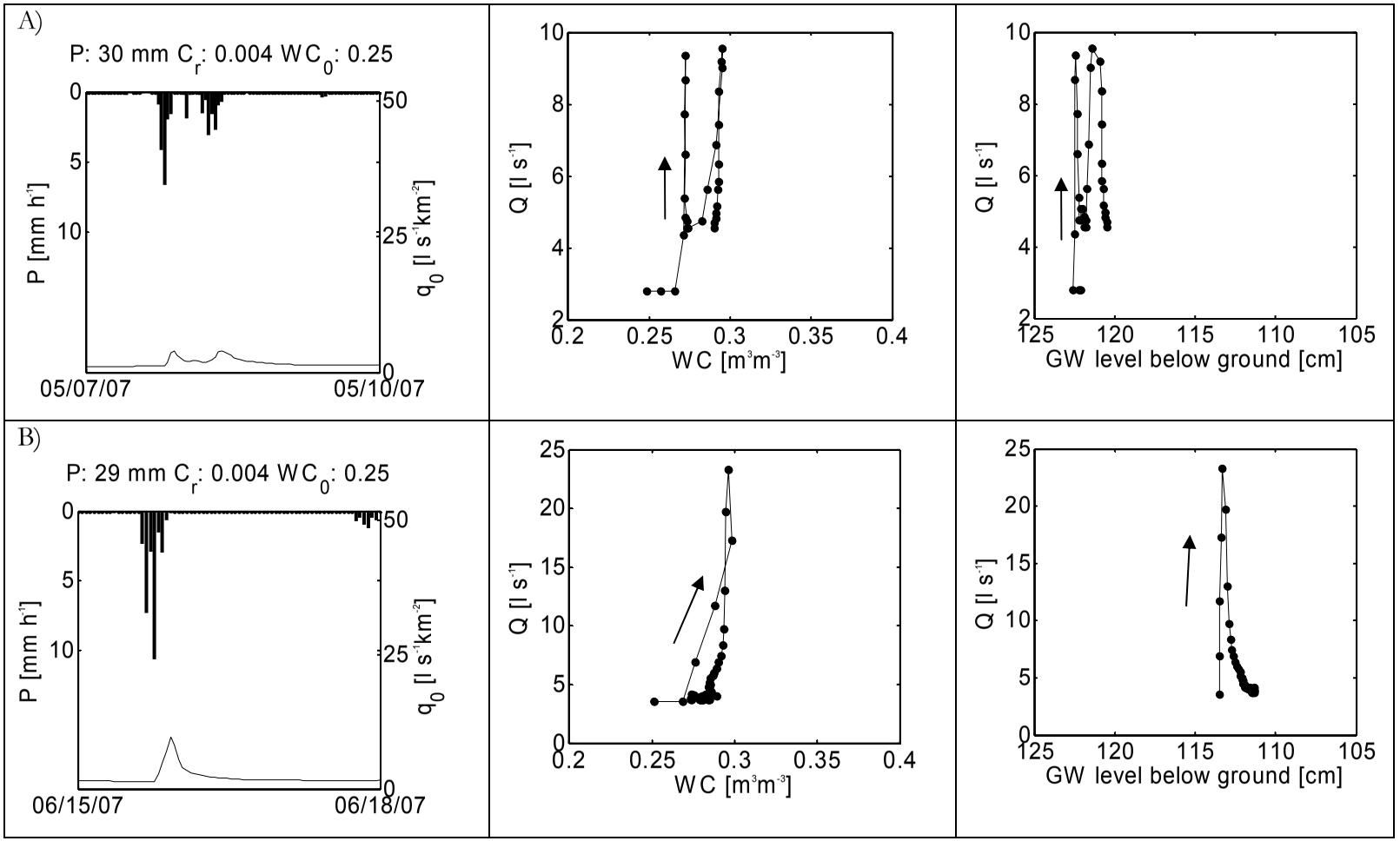
A)
P: 30 mm C_r: 0.004 WC_0: 0.25
P [mm h-1]
q0 [l s-1km-2]
05/07/07
05/10/07
Q [l s-1]
WC [m3m-3]
GW level below ground [cm]
B)
P: 29 mm C_r: 0.004 WC_0: 0.25
06/15/07
06/18/07

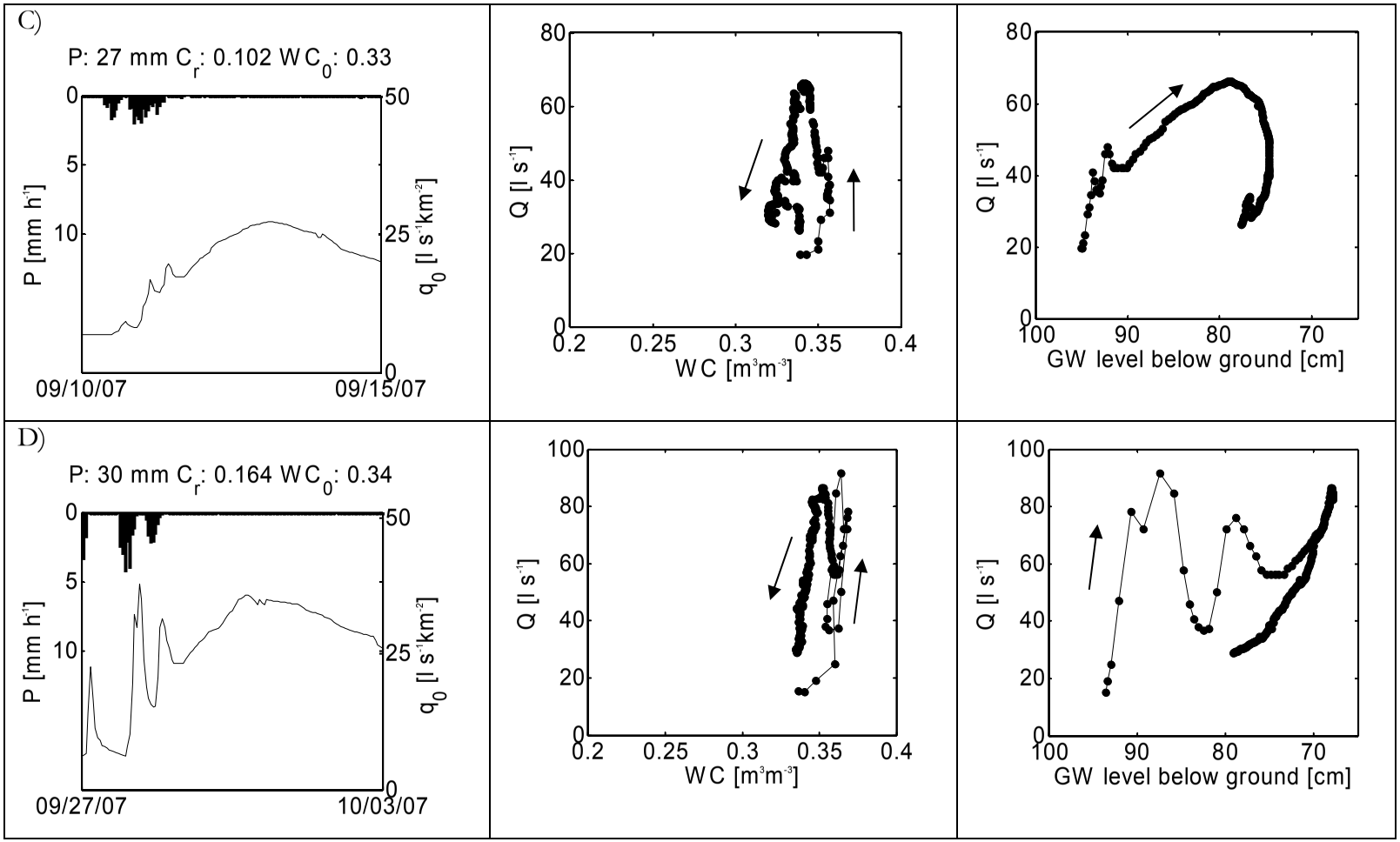

Figure 26: Runoff responses of the Becherbach for different wetness conditions with hysteretic characteristics of soil moisture and groundwater level below ground to runoff. The time steps are hourly.

The hysteresis between *GWL* and *Q* is always clockwise and the reaction has a lag time of 4 to 6 hours under dry conditions and occurs directly but slower under wet ones.

Under dry conditions the fast runoff component is faster compared to the soil storage. Under wet conditions the soil storage does not increase over a value 0.37 m^3m^{-3}. For the presented events the rainfall intensity under wet condition is below 5 mm h^{-1} and therefore smaller compared to the dry conditions (7-12 mm h^{-1}). However, the response in groundwater occurs simultaneously to *Q*, which indicates fast bypassing of the unsaturated zone under wet conditions and fast mobilisation of groundwater. On the other hand, under dry conditions only a small response in *GWL* can be observed and the unsaturated zone absorbs nearly all of the input rainfall.

A possible hypothesis is that vertical preferential flow and thus bypassing of the unsaturated zone dominates wet conditions. Unsaturated k_s has already reached high values due to higher soil moistures and macropores are connected. Water is directly transferred to the groundwater and fast groundwater flow contributes to runoff generation.

3.6 Discussion and Conclusions

3.6.1 Deterministic and stochastic soil moisture variability

The analysis presented gives clear evidence that clustering of TDR probes, even if they simply yield the usual vertical average, allows identification of deterministic soil moisture variability, i.e. the difference between the first and second moment, and even allows a first glimpse of the differences in higher moments such as skewness of the two soil moisture ensembles. Spatial variability in soil moisture values is quite large at both sites, between 0.07 m^3m^{-3} and 0.08 m^3m^{-3}. This is considerably larger than that which has been observed in the Weiherbach catchment in Germany (Bárdossy and Lehmann, 1998), or in the upper Tiber valley, Italy (Brocca et al., 2007) but comparable to what Blume et al. (2009) observed in the Malalcahuello catchment in Chile. The total extent of the clusters at 400 m^2 is rather small. This underlines the fact that a single TDR probe is not very useful to assess the representative average soil moisture status in such a heterogeneous environment. On the other hand, Brocca et al. (2007, 2009b) reports are consistent with the findings of Grayson and Western (1998) on the existence of representative monitoring sites, where the observed soil moisture is, on the weekly scale, always close to the overall spatial average of the field/ catchment. However, such sites may not be identified *a priori*, which underlines the value of any kind of distributed soil moisture observations in general.

It is interesting and important to note that the soil moisture time series in Figure 14 do not intersect. The ranks of the soil moisture values observed at different locations in a cluster remain thus temporarally stable. Also Brocca et al. (2007) report temporal stability of the ranks within their soil moisture data sets. These findings suggest that the spatial variability in soil moisture measurements reflects spatial heterogeneity of stationary soil properties as well as of the micro topography. Soil moisture time series within each cluster are furthermore highly correlated (0.90), which underlines that the dynamics observed at a single probe is a good estimator for average soil

moisture dynamics at the small field scale in the Rehefeld catchment. Thus, a distributed set of single TDR stations may yield representative information on temporal soil moisture dynamics at the headwater scale, which can be very important information for many modelling studies and maybe even for flood warning purposes, as shown for instance by Anctil et al. (2008) in the Orgeval watershed.

Furthermore, clear evidence is found that clustering of TDR probes in combination with long-term monitoring allows identification of average spatial covariance structures at the small field scale at different wetness states. It has to be admitted that the small extent of cluster C2 likely gives only a limited picture of the spatial covariance of soil moisture at the forested site. The estimated range is almost 50% of the maximum probe distance, which is the theoretical limit. Distributed sampling that covers a larger extent is clearly desirable here. Spatial correlation length at the grassland site seems in contrast to be rather short, due to small-scale heterogeneity in soil properties. Zimmermann et al. (2008) found a similar small correlation length for the hydraulic conductivity at a steep grassland site in Ecuador. Brocca et al. (2007) found at their grassland site in the upper Tiber valley effective ranges that are approximately 10 times larger. The much shorter ranges at that site may be explained by the huge small scale heterogeneity due to the high gravel content of these soils. It is important to note that the small-scale heterogeneity of soil properties at the forested site is similar to the grassland site. Therefore it can be concluded that the correlation structure at the forested site is dominated by the pattern of throughfall and interception and therefore vegetation; at site C1 it is dominated by small-scale variability in soil properties. This is of course not astonishing for a forested site: the important point is that a cluster of TDR probes allows quantification of such a statement.

The investigation of temporal stability shows that variability of each probe is low at the grassland site (C1). Here six probes can be selected to represent the mean *WC*, but the location is not correlated with topographic characteristics. Soil physical properties are thus dominant. At the forested site (C2) variability is higher and two probes (12 and 13) are close to the zero line. There is clear negative correlation with elevation and slope with a low rang value. The highly heterogeneous soils are governing the distribution of *WC*.

3.6.2 Simulated average soil moisture dynamics

Based on the model results, a homogeneous soil setup that uses local observations of k_s and porosity gives a better model performance at both sites than when soil profiles are parameterized using the pedo transfer function of Carsel and Parrish (1988). This is not astonishing but underlines on one hand the value of local k_s and porosity observations for setting up physically based models. And it shows on other hand that the residual soil moisture, the air entry value and n parameter estimated using the pedo transfer function of Carsel and Parrish (1988) are sufficient to achieve an acceptable model performance. This is good news as direct measurement of these parameters is laborious.

At the forested site, a small adjustment in the annual maxima of *LAI* and plant cover, while still assuming that their normalised annual cycles are the same as those observed in the Weiherbach

catchment (Zehe et al., 2001), leads to a strong improvement in the model bias and RMSE. Simulated averaged soil moisture is within the confidence interval of the observed spatial average soil moisture for almost the whole period. The best model setup (soil profile A, *LAI* = 13.5, plant cover = 0.85) is a promising representation of key areas in the Rehefeld headwater, that could serve as building blocks to represent forested areas in a catchment model. The extent of the sampling grid is large enough to assess the dynamic spatial average soil moisture in an almost unbiased way. At the grassland site, fine tuning of the model results based on adjusting the annual maxima of root depth, *LAI* and plant cover is not as successful. The normalised annual cycle of grass morphological parameters in Rehefeld must differ from those in the Weiherbach. Thus it can be concluded that negative bias in the model is not due to non-representative sampling but rather to insufficient representation of vegetation. A better model performance requires a survey of the annual cycles of these plant morphological parameters especially during periods of obviously bad model performance (in early May and in summer).

3.6.3 Identification of dominating processes with an irrigation process

The sprinkling experiment gives a good view on the dominating flow processes at the grassland site C1 Rehefeld. The interaction in the TDR cluster shows that overland flow is of minor importance, similar to the findings from time series analysis. During the experiment an intensity of 12 mm h^{-1} was achieved and produced overland flow with a maximum length of 0.5 m. Subsurface flow between the probes could be observed to a length of 1.7 m, with a lag time of 2.5 to 3 hours which is an effective lateral hydraulic conductivity of approximately 10^{-4} m s^{-1}. That value is similar to the highest measured hydraulic conductivity. Lateral flow in the top layers was only observed in the second irrigation experiment which is indicative that specific soil moisture has to be reached and or the amount of precipitation must be above a specific value to initialise lateral fluxes. The FDR profile could hint at vertical transport for the top 0.6 m. Here a lag for the two deeper probes during the first experiment indicated a hydraulic conductivity of the same magnitude as for the lateral flow and during the second experiment they reacted instantaneously under wet conditions. The response to soil moisture on the second irrigation was faster in the interaction of the FDR profile.

The measurement in the access tubes show that all profiles react to the irrigation input in the top 0.2 m to 0.5 m, that the following horizons are not connected, and in the case of access tubes 2 and 5 that the deeper layers saturate from the bottom to the top upward. In case of tube 5 a response to the first irrigation was observed after 1.5 hours for the first irrigation and after 2 hours for the second, which led to the conclusion that a hydraulic conductivity > 5×10^{-4} m s^{-1} existed at that position. An impermeable layer below or the groundwater table could be the reason. Tube 4, which is at a distance of 10.0 m, reacted with a lag of <6 hours and here again, an effective hydraulic conductivity of approximately 10^{-4} m s^{-1} can be approximated.

The dye tracer showed that only in the upper horizon to a depth of 0.15 m was matrix flow dominant and that preferential flow could be observed to the end of the excavated profile. The transport from the B horizon to the groundwater surface was dominated by preferential flow paths with a high transport velocity. Wetting starts then from the groundwater surface upward, as the access tubes 2 and 5 show.

These findings are similar to the experimental results of Pöhler (2006), who has done infiltration experiments in the Weissbach which is another subcatchment of the Weißeritz further downstream.

Overall it can be concluded that the suggested sampling strategy of clustering TDR probes in typical functional units is promising for exploration of soil moisture control on runoff generation, as it yields dynamics of representative soil moisture states at a high temporal resolution. Long term monitoring of such critical landscape elements - the forested site here - could maybe yield valuable information for flood warning. Furthermore, TDR allows the unravelling of different types of stochastic and deterministic soil moisture variability within and between different soil moisture ensembles. Thus it can be concluded that TDR provides a good combination of the advantages of permanent sampling with spatially highly resolved soil moisture sampling using mobile rods. The main drawbacks of TDR are the high cost of a single moisture cluster (12-15 k€) as well as the challenge of installing 60 cm long TDR probes in heterogeneous environments. Monitoring should thus be carefully selected.

3.6.4 Soil moisture control on event runoff

Average antecedent soil moisture at the forested site has a high Spearman rank correlation to runoff coefficients of the three catchments (Becherbach = 0.63, Rehefeld = 0.67 and Ammelsdorf = 0.54) Duration of rainfall and precipitation volume have similar values. $API^{30}_{0.95}$, AP^{60}, CV and rainfall intensity have lower correlation values.
Pre-event runoff alone correlated also with the runoff coefficient to a high degree to and is strongly correlated with average soil moisture at both sites. Thus it can be concluded that subsurface storm flow or fast groundwater flow is the dominant feature of the runoff generating process, at least in the snow-free period. Saturation excess overland flow plays a large role due to the high permeability of the top soil, which is more than 10^{-4}m s^{-1}, and the large amount of gravel a minor role. Subsurface storm flow is reported to be the dominant runoff process in many other studies in forested areas (Zehe and Sivapalan, 2009) such as those of Uhlenbrook et al. (2002), Tromp-van-Meerveld et al. (2006a) and Blume et al. (2008a, b). Interestingly, the wetness state of the lower hillslope sector in forested sites seems to be of higher importance for event runoff production than average catchment wetness represented by pre-event discharge. In the Ammelsdorf and Rehefeld catchments, forested sites likely contribute more strongly to event scale runoff production than does grassland. This highlights that spatiotemporally highly resolved sampling of representative soil moisture in key landscape units yields very valuable information for explaining and predicting runoff production. The forested site close to the Becherbach is obviously such a key site - not to determine the average catchment wetness as suggested by Grayson and Western (1998) or Brocca et al. (2007) - but to determine the average wetness of landscape areas that contribute to flood formation.

Under dry conditions the unsaturated zone dominates runoff response and groundwater has a minor effect. If the catchment wetness increases over a threshold value of WC_0 the upslope areas are connected to the main catchment which results in a fast response in groundwater level while

the *WC* decreases to the starting level. This hypothesis will have to be validated with additional instrumentation and/or tracer techniques.
This hysteretic behaviour between streamflow/subsurface flow and soil moisture is found by several other authors (Graham et al. 2010, Hrnčíř et al. 2010, Penna et al. 2010). Spence et al. (2009) also found hysteretic patterns between discharge and storage. However, discovering hysteretic behaviour between storage and discharge is an indicator of system controls and time-variant dominant processes.

CHAPTER 4 SOIL MOISURE DYNAMICS AND RUNOFF GENERATION IN HEADWATER CATCHMENTS: LEARNING FROM MODELS OF DIFFERENT COMPLEXITY

4.1 Motivation: how can modelling help? Different models for different questions/scales (incl. Hillslope scale)

The field of hydrological modelling covers different approaches and a variety of applications (Singh, 1995; Beven, 2002). Physically based models are based on observable state variables and parameters. They may thus help to gain understanding of for instance how distributed processes and parameters control hydrological behaviour at larger scales (Tromp-van Meerveld and Weiler, 2008). They are also useful to shed light on how soil at the small scale control flow and transport processes (Klaus and Zehe, 2010). Physically based models are however data intensive, their setup is time consuming and needs experience and for that reason not popular in engineering hydrology. Conceptual models represent the process patterns and redistribution of water inside the catchment with simplified concepts and are often designed for a specific modelling target such as flood predictions or water balance calculations. Conceptual models allow simulations catchment scale streamflow response in an adequate way, which does not at all mean that the simulated dynamics inside the catchment is a good match of real internal dynamics. They are thus limited to a scale where errors due to simplified process conceptualisations may average out (Dooge, 1986).

By focusing only on the simulations of flood events, the researcher may have several different intentions such as to understand the processes and process interactions which control flood formation, to design and compare mitigation measures or to forecast timing, peak discharge or total volume of floods. Commonly, hydrologists use distributed conceptual hydrological models for real-time stream flow forecasting, flood warning purposes or to assess landuse change impacts on floods. Alternative approaches to continuous flood forecasting models are nonparametric models based only on stream flow series (Costa et al., 2011) or artificial neural networks (de Vos and Rientjes, 2008; Schmitz and Cullmann, 2008). Flood volumes, which are of key importance for operating storage reservoirs, can be predicted using regionalized runoff coefficients or linear regression models that are based on different predictors to characterise pre-event conditions (Pfister et al., 2002, 2003; Blume et al., 2007; McIntyre et al. 2007, Hrnčíř et al. 2010).

Even if the rainfall runoff model in operation is a perfect one, uncertainties in the observed and predicted meteorological forcing could cause errors in projected runoff and projected model state variables (Aubert et al., 2003). As representative data on the catchment scale soil moisture pattern are usually not available, state variables or model parameters of continuous flood forecasting models are usually updated by assimilating the observed stream flow prior to issuing a hydrological forecast (Refsgaard, 1997, Kneis et al., 2010). The past ten years, however, have witnessed a rapid development towards the direct integration of observed soil moisture data into rainfall runoff modelling. This comprises the use of distributed ground-based point data,

remotely sensed soil moisture patterns, or combinations of both. Soil moisture patterns have been used to initialize state variables (Goodrich et al., 1994; Jacobs et al., 2003; Zehe et al., 2005; Noto et al., 2008; Brocca at al., 2009a) and to update model state variables by assimilation techniques (Aubert et al., 2003; Francois et al., 2003; Crow et al., 2005). While these authors report that assimilation soil moisture data increased the quality of hydrological forecasts or flood predictions, Crow and Ryu (2009) argue that the improvements achieved from these efforts are relatively low. They stress that antecedent moisture conditions are of minor importance for very intense storm events and predictive uncertainty is dominated by the error introduced by rainfall estimation. Furthermore, Crow and Ryu (2009) criticize assimilation techniques such as the Kalmann filter as being ill-suited for updating the non-linear relationship between antecedent soil moisture and runoff.

Nonetheless, whether it is dealing with updating of continuous model states or regression of flood volumes, both procedures require representative data on the catchment wetness. Traditional approaches for event-based models consider the antecedent precipitation (*API*) or the pre-event discharge (q_0) as an integral indicator for the filling of the catchment scale groundwater store (Fedora and Beschta, 1989; Pilgrim and Cordery, 1993; Berthet et al., 2009). These approaches, however, yield no information about the spatiotemporal variability of soil moisture within the catchment. This information is clearly desirable as those areas that contribute to flood formation are variable in time. It is therefore essential to be interested in the wetness of those landscape elements that indicate whether upslope areas and subsurface storages connect to the riparian zone and start to contribute to the flood formation process (Zehe et al. 2010). Most strategies to assess distributed information on soil moisture dynamics still rely largely on distributed point measurement, by means of either FDR or TDR methods. One approach is to use a set of fixed TDR/FDR sensors to monitor temporal soil moisture dynamics at selected points, as for instance suggested by Bárdossy and Lehmann (1998), Anctil et al. (2008) or Blume et al. (2008 a, b). The advantage of using fixed stations is that they allow a high temporal resolution; the drawback is that spatial resolution is either coarse or the total extent of the network is small. Thus, other authors prefer spatially highly resolved soil moisture sampling by means of mobile or portable TDR sensors, as for instance Grayson et al. (1997) or Grayson and Western (1998) in different catchments in Australia or Brocca et al. (2007, 2009) for three field sites in Italy. Zehe et al. (2010) recently used a clustering design of soil moisture sensors to assess spatiotemporal highly resolved data to characterise soil moisture dynamics at typical hillslope units. The drawback of this approach is that it is limited to two to three clusters.

In summary, it seems there is neither a commonly accepted strategy for how to obtain useful data on distributed soil moisture dynamics or the antecedent wetness in headwater catchments nor whether such data might be helpful to predict runoff volumes or to update states of continuous states for improving food forecasts. The main objectives of the present study are thus:

1. To demonstrate that average soil moisture dynamics observed at a representative forested landscape element in Rehefeld catchment is of key importance for predicting runoff coefficients in three nested catchments by means of generalised linear models (GLM).

2. To investigate whether a distributed rainfall runoff model, which has been calibrated for these catchments, allows similar good predictions of the runoff coefficients compared to GLM. The model WaSiM ETH is used, which is frequently used in meso-scale catchments (Schulla, 1997; Niehoff et al., 2001; Gurtz et al., 2003; Krause and Bronstert, 2007; Bormann et al., 2008).
3. To compare soil moisture dynamics observed at the representative site to soil moisture simulated with WaSiM ETH at this location.
4. To compare the relationship of runoff coefficients and soil moisture at the representative location for both observed data and model results.

It is assumed that the distributed process oriented rainfall runoff model "which works for the right reasons" should not only match the observed rainfall runoff behaviour but also match the interplay between average soil moisture of representative sites and runoff coefficients that has been observed in the target catchment.

4.2 Model descriptions: WaSiM ETH, GLMs

4.2.1 Generalized linear models

The objective of this statistical analysis is to identify the best describing predictors that characterize the rainfall forcing as well as the near surface and deep subsurface wetness state of the catchment in order to predict the C_r. Generalized linear regression models (GLMs) are used with a binomial error distribution to estimate the relationship between the runoff coefficient as the response variable and different predictor variables. In the case of proportional data, Crawley (2002) recommended the use of binomial GLMs; because they weight the estimates depending on their binomial denominators (low weights to estimates with small binomial denominators), they use a maximum likelihood estimation compared to the sum of squares used for Linear Models (LMs). GLM may furthermore cope with non-normal and heteroscedastic residuals. It is adequate to use a binomial GLM to predict relative data without a direct countable context (e.g. McPherson and Jetz, 2007). Francke et al. (2009) discusses the pros and cons of LMs versus GLMs in detail. The above mentioned generalisations are here based on the logit transformation – a function that links linear predictor to the response variable (Crawley, 2007). The runoff coefficients are constrained to the range [0, 1] whereas their range on the logit scale is [-∞, +∞].The generalized linear regression model using the n predictors is shown in (Eq. 1)

The generalized linear regression model using the *n* predictors is shown in (Eq. 1)

Eq. 20

$$\log it(Cr) = \ln\left(\frac{p}{1-(p)}\right) = \beta_0 + \sum_{i=1}^{n} \beta_i x_i \,,$$

where the regression coefficients (β0…βi) are estimated to obtain an optimum fit. The predictor variables (xi...xn) are used without normalization, as shown in Appendix Table 1-3.

4.2.1.1 Predictor selection and development of the GLM

4.2.1.1.1 Estimators of catchment wetness and the meteorological forcing

As discussed in Chapter 3 *I* distinguished predictor variables that characterise/estimate the catchment's antecedent wetness and can be determined *a priori*, from those that characterise the meteorological forcing which can only be estimated based on *a posteriori* observations or based on predictions (both with uncertainty). The predictor variables and their relation to event scale runoff coefficients were already presented in Chapter 3.5.7.

4.2.1.1.2 GLM assessment

Multicollinearity or linear dependence among the predictors can be problematic when interpreting coefficients or for prediction, if the correlation structure is not constant (Fox, 2002; Dormann et al., 2011). To avoid this problem the predictors and the corresponding full models were assessed within a five-step analysis that was followed by a validation procedure:

1) Determination of the correlation matrix and classification of highly correlated parameters into two different subsets.
2) The resulting subsets of predictors are submitted to hierarchical partitioning where the independent predictive power of each predictor variable is computed. This results in a reduced subset.
3) The resulting possible general linear models built from all possible combinations of the parameters of the reduced subsets are compared with an exhaustive search method (Morgan and Tatar 1972) using the Bayes Information Criterion (BIC) as a measure of model performance.
4) Evaluation of the calibrated models: The two best models of the subsets are evaluated using different performance criteria.
5) Validation of the two models: Jack-knifing is used, i.e. leave-one-out cross validation, for internal validation to obtain an unbiased estimate of the model performance (Harrell, 2001; Blume et al., 2008; McIntyre et al., 2008).

The entire analysis is carried out for all three sub-basins and the five steps are further explained in the following:

Step 1): Predictors with a Spearman rank correlation $|\varrho| > 0.7$ (Green, 1979) are not used within the same model (cf. Appendix Table 4-6). Average soil moisture WC_0 and present runoff q_0 had the highest correlation to the runoff coefficient for all catchments. However, at the same time they are strongly correlated to each other. Thus two subsets of predictors are created, one including the antecedent water content and one including the pre-event runoff. These subsets included 8 predictors each: CV, AP^{60}, $API_{0.95}^{30}$, P, $P2h$, DP, I and WC_0 or q_0.

Step 2): The best parsimonious model for the three catchments is estimated with hierarchical partitioning (Mac Nally, 1996, Heikkinen et al., 2005) using the R-scripts (R-Team Development Core, 2009) of Walsh and Mac Nally (2009). In hierarchical partitioning, the independent predictive power of each predictor is computed and joint contributions to the model resulting from collinearity are separated (Olea et al, 2010). The predictors with a higher independent

explanatory power than 10% are selected, where 100% corresponds to the sum of the independent explanatory power of all predictors.

Step 3): As exhaustive search methods have the disadvantage that they do not account for multicollinearity between the predictors (Dormann et al., 2011), the search method is only used to identify the best models after the subsets have been submitted to hierarchical partitioning. Here the exhaustive search algorithm by McLeod and Xu (2010) was used. The Bayes Information Criterion (BIC) is chosen instead of the more commonly used Akaike Information Criterion (e.g. Reineking and Schröder, 2006) as it is stricter and more selective towards models with fewer predictors (parsimonious models). The BIC is defined as:

Eq. 21

$$BIC = -2\max\log L \times \log(n)k \,,$$

with, the maximum log-likelihood

Eq. 22

$$\max\log L = -\frac{n}{2}(1+\log(2\pi)) - \frac{n}{2}\log\left(\frac{RSS}{n}\right),$$

the residual sum of squares

Eq. 23

$$RSS = \sum_{i=1}^{n}(y_i - \bar{y})^2 \,,$$

n the sample size, and *k* the number of parameter in the model.

Step 4): The two best models of both subsets are compared in using four performance criteria: The BIC criterion, the Spearman's rank correlation coefficient (ϱ), describing how much of the variability the model can explain, Root mean square error (RMSE) and Nash Sutcliff efficiency index (NSE).

Step 5): As the observation period is dominated by dry weather conditions, only few larger events are observed. As a result, the sample size of rainfall runoff events is too small and the distribution much too skewed to allow a split sampling for model validation. Therefore jack-knifing is used as cross-validation technique. The performance of the model within jack-knifing is evaluated by means of the RMSE, the mean absolute error (MAR) and the Nash Sutcliff efficiency.

4.2.2 The hydrological model WaSiM ETH

The hydrological watershed model WaSiM ETH (Schulla, 1997; Niehof et al., 2001) is used to address objectives 2 and 3. The model conceptualises interception based on a storage approach, Evapotranspiration based on the Penman-Monteith equation, and infiltration based on the Green and Ampt approach (Peschke, 1987). Flow in the vadose zone is determined from the saturation deficit based on the TOPMODEL principles and the topographic wetness index (Beven and Kirby, 1979). This is deemed to fit well to the dominating runoff mechanism which is due the

findings in Chapter 3 vertical preferential flow, subsurface stormflow and fast mobilisation of ground water. Water storage in the unsaturated zone is described in a simplified manner by distinguishing three different subsurface stores: a) field capacity unsaturated store, b) gravitational store with free water above field capacity and c) the saturated store. The field capacity unsaturated storage is vertically sub-divided into the root zone and the below-root zone. When infiltration into the soil occurs (which is calculated in a preceding step), water fills the field capacity unsaturated storage if free pore space is still available. Otherwise, the infiltration water enters the gravitational unsaturated zone. Figure 27 gives an overview of the different storages.

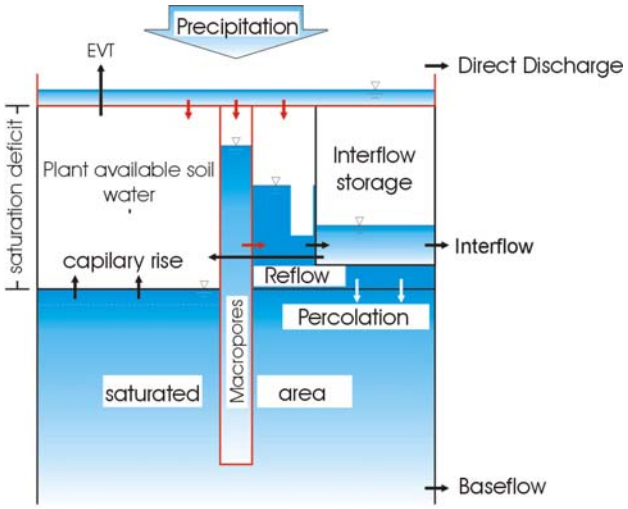

Figure 27: Sketch of the different storages used in WaSiM ETH, after Niehoff (2002) modified.

The gravitational unsaturated zone store controls interflow generation (which exfiltrates into the river system) and percolation into the saturated zone store. Exfiltration from the saturated zone store forms baseflow. Total runoff is composed from surface runoff, interflow and baseflow. Surface runoff and interflow, as well as the unsaturated zone storage, are conceptualised by means of linear stores for each grid cell while baseflow is calculated as a linear store for the entire sub-basins. The actual moisture conditions of the whole catchment are calculated continuously by the overall saturation deficit (*SD*) representing the catchment-wide difference between full catchment saturation and the actual moisture state. The spatial mean of the *SD* is calculated for each time step. The local *SD* distribution within the catchment (i.e. the local saturation deficit at each grid cell) is estimated indirectly from the spatial mean and the spatial distribution of topographic index (Beven and Kirkby, 1979; Krause and Bronstert, 2007). Therefore, not all soil water fluxes are simulated explicitly for each grid cell which results in a fast performance and allows the meso-scale usage. The kinematic wave concept is used for the routing of stream flow. For more details on WaSiM ETH please refer to Schulla (1997), and Schulla and Jasper (2007).

4.2.2.1 Calibration of WaSiM ETH

The model is setup at a regular grid size of 100 m and operated at an hourly time step. The Dynamically Dimensioned Search (DDS) optimization algorithm (Tolson and Shoemaker, 2007, Francke, 2010) is used for automatic calibration within the R environment (R-Team

Development Core, 2009) to estimate an adequate parameter set for the calibration period. DDS may be characterised as a parsimonious algorithm with quick convergence compared to other methods, especially for high-dimensional optimization problems. However, the procedure needs a sufficiently high number of evaluation steps to avoid convergence to a local minimum (Tolson and Shoemaker, 2008).

A set of 15 parameters was calibrated using the ranges (cf. Appendix Table 7) suggested by Reusser et al. (2009) for the two catchments of Ammelsdorf and Rehefeld according to three different versions during snow free conditions as explained below. Plant parameters were adjusted based on the findings of Chapter 3 for forest, for all other landuse values by Breuer et al. (2003) were used. Soil physical parameters were taken from Maidment (1993).

Version A): The model was calibrated for the period 2000-2006 and validated in the period of 2007-2010 based on the runoff time series and a baseflow time series produced by smoothed minima technique (Nathan and McMahon, 1990) of the runoff time series. A weighted sum of the Nash-Sutcliff efficiency index (NSE) and relative mean error (RME) as objective function (Eq. 24) and introduced a penalty (PB) for large errors during baseflow dominated periods (Tolson and Shoemaker, 2008) was used.

Version B): The model is calibrated for the complete time series 2000-2010 based on the Nash Sutcliff efficiency as objective function.

Version C): The model is calibrated for the complete time series 2000-2010 with the same objective function as in version A.

Eq. 24

$$OF = NSE - \max\left(0, \left|RME - 0.3\right|\right) - \max\left(0, \max\left(0, PB\right) - 0.3\right)$$

with,

Eq. 25

$$NSE = 1 - \frac{\sum_{i=1}^{n}\left(Q_{obs} - Q_{sim}\right)^2}{\sum_{i=1}^{n}\left(Q_{obs} - \overline{Q}_{obs}\right)^2},$$

Eq. 26

$$RME = \sqrt{\frac{\sum_{i=1}^{n}\left(Q_{obs} - Q_{sim}\right)^2}{n}}$$

and

Eq. 27

$$PB = \frac{1}{2}\overline{Q}_{GWobs} - \frac{\overline{Q}_{GWsim}}{\frac{1}{2}\overline{Q}_{GWobs}}.$$

Where Q_{sim} is the simulated runoff, Q_{obs} the observed, $\overline{Q}_{GWsim}$ simulated mean groundwater, $\overline{Q}_{GWobs}$, the observed mean groundwater, and n the sample size.

4.2.3 Data driven models to predict runoff coefficients

The obtained GLMs (Table 17) allow a good estimation of the C_r and are significantly better than the null model. It is worth to note the best models always rely on both measures for catchment wetness and measures for the either the total rainfall amount and, in case of the q_0 subset also for rainfall duration. For all three sub-basins P is the predictor with the most explanatory power followed by DP and WC_0 and q_0. Other predictors had, as could be expected from the scatter plots in Figure 24 and 25, a negligible explanatory power.

Table 17: Coefficients, error values and P-values of the best models for the three catchments and two subsets. The P-value is the estimate of the probability that the coefficient is significant. Herby are low values an indicator for significance. The standard error (Std. Error) describes the uncertainty of the coefficient.

Catchment	Subset	Predictor variable	Coefficient	Std. Error	P-Value
Ammelsdorf	WC_0	Intercept	-7.58	0.89	< 0.0001
		WC_0	13.29	2.82	< 0.0001
		P	0.03	0.01	< 0.0001
	q_0	Intercept	-3.99	0.28	< 0.0001
		q_0	0.03	0.01	< 0.0001
		P	0.03	0.01	< 0.0001
Rehefeld	WC_0	Intercept	-7.78	0.63	< 0.0001
		WC_0	14.08	1.98	< 0.0001
		P	0.04	0.01	< 0.0001
	Q_0	Intercept	-3.77	0.17	< 0.0001
		q_0	0.02	0.00	< 0.0001
		P	0.03	0.01	< 0.0001
Becherbach	WC_0	Intercept	-15.44	1.48	< 0.0001
		WC_0	35.25	4.79	< 0.0001
		DP	0.40	0.07	< 0.0001
		P	0.02	0.01	0.037
	Q_0	Intercept	-5.10	0.21	< 0.0001
		q_0	0.07	0.01	< 0.0001
		DP	0.67	0.04	< 0.0001

The equations of the best models for the three catchments are presented in Table 17 with P-values and standard error of the coefficients. The P-value is a measure of creditability of the null hypnotise (Crawley, 2007). Large P-values means that there is no compelling evidence to reject

the null hypnotise and that the predictor has low explaining power to describe the target variable. Low values are an indicator for rejecting it and therefore the predictor has a significant explaining power for target but in dependency of sample size and the number of predictors. By the standard error low values compared to the absolute value of the coefficient are aspired.

Table 18 presents the goodness of fit criteria for the best GLMs both for the entire dataset and for the cross validation. The Nash-Sutcliffe efficiencies for the best models at gauge Ammelsdorf are 0.61 for the q_0 subset and 0.68 for the WC_0, and 0.48 and 0.56, during cross validation respectively. Please note that although the catchment area is five orders of magnitude larger than the total extent of the soil moisture cluster, the WC_0 based GLM outperforms the GLM based on pre-event discharge. At Rehefeld is the same situation: the WC_0 based model outperforms the q_0 model for all sub-basins. The performance criteria NSE and RMSE for the Becherbach are in the calibration for both predictor variables similar. But ϱ is lower for WC_0 compared to q_0. In the cross validation NSE of WC_0 shows a better performance. The reason therefore is the high variation in q_0 compared to WC_0 under wet conditions (see 3.5.6).

Table 18: Comparison of the simple and best models for the nested catchments with performance criteria calculated from observed and modelled C_s: Spearman's rank correlation (ϱ), root mean square error (RMSE), degrees of freedom (DF), jackknifing results of the best models of the three catchments with performance criteria: Nash Sutcliff efficiency index (NSE), and root mean square error (RMSQ).

						After jackknifed	
	Sample size	DF	ρ	NSE	RMSE	NSE	RMSE
Ammelsdorf WC_0	59	56	0.79	0.68	0.028	0.56	0.033
Ammelsdorf q_0	59	55	0.72	0.61	0.031	0.48	0.036
Rehefeld WC_0	76	72	0.81	0.68	0.034	0.64	0.036
Rehefeld q_0	76	71	0.80	0.54	0.040	-0.20	0.065
BecherbachWC_0	54	50	0.57	0.98	0.018	0.69	0.065
Becherbach q_0	54	51	0.76	0.95	0.025	0.58	0.075

4.2.4 Quasi process based model WaSiM

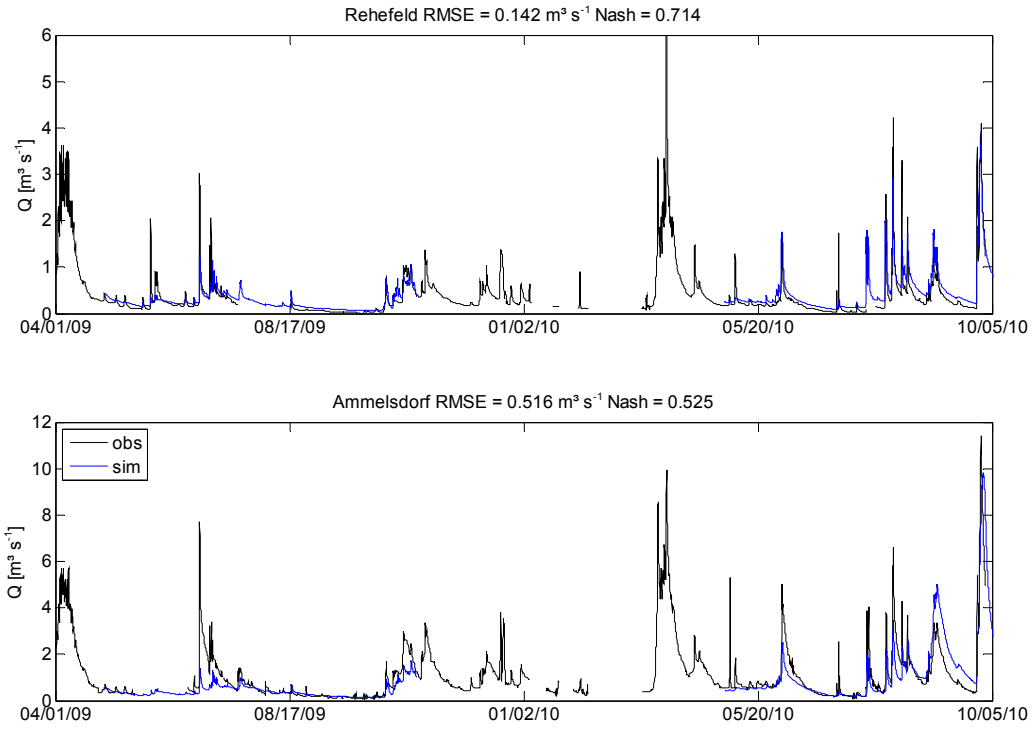

Figure 28: Simulated (with the NSE calibration scheme B) and observed runoff of the two catchments Rehefeld and Ammelsdorf exemplarily shown for the period 2009-2010. Only the simulated runoff for the snow free period is presented. Axes are cut at 6 m³s-1 (Rehefeld) and 12 m³s-1 (Ammelsdorf) for better readability. The maximum peaks in Rehefeld are at 7 m³s-1 for the shown period. In the header are NSE and RMSE for the complete simulation period.

Calibration with scheme A (see section 3.5) yielded a NSE of 0.60 at gauge Rehefeld and 0.32 at gauge Ammelsdorf. During the validation period, the model performed much worse with a NSE of -0.37 and -3.66 for these gauges, respectively. The best results were obtained with calibration scheme B when calibrating the model to the entire period based on the NSE as objective function. A NSE of 0.7 at gauge Rehefeld was optained and 0.53 at gauge Ammelsdorf. The simulated runoff for the winter period is not shown, because the focus of the work was on the snow free period (and the parameters of the snow model were not calibrated). Simulated discharge based on calibration scheme C matched observed values with a NSE of 0.6 at gauge Rehefeld and 0.4 at gauge Ammelsdorf. Whereas the baseflow is better represented with scheme C several events are not identifiable. Further analysis was carried out exclusively for the best model setup version B. Modelled and observed time series are shown in Figure 28.

Figure 29 shows observed C_r plotted versus predicted C_r after jackknifing and the best WaSiM ETH simulation for all three catchments. C_r values estimated with the GLM < 0.1 are overestimated for the two larger catchments and underestimated in the Becherbach. The absolute error in the two larger catchments increases with increasing C_r.

Runoff coefficients at gauge Ammelsdorf with WaSiM ETH are strongly underestimated, which may be explained with the relatively low model efficiency of 0.53. The accordance between simulated and observed C_r is clearly better at gauge Rehefeld, but still worse than for the predictions by the GLM. Please note that Figure 29 presents the runoff coefficients from the cross validation procedure of the GLM while runoff coefficients from WaSiM ETH are from a pure calibration procedure, i.e. without cross validation.

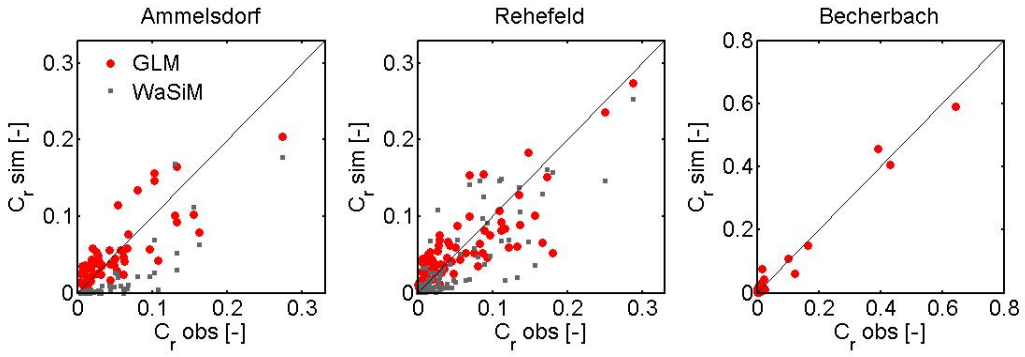

Figure 29: Simulated Cr from the jackknifing based on the best GLM (red circles) and from the best calibration with WaSIM ETH (grey squares) plotted against the observed Cr.

The temporal occurrence of the observed, fitted and predicted C_r are shown in Figure 30. Larger events with $C_r > 0.1$ normally occur in spring and autumn for all three catchments, except for June 2010 where severel convective precipitation events causes high runoff coefficients. The dry year 2008 can be well identified by $C_r < 0.05$ in the period June-September. Here the GLMs and GLMs of the jackknifed values overestimate the observed values, while WaSiM ETH underestimates for Rehefeld and Ammelsdorf. For the Becherbach the values are underestimated for that period.

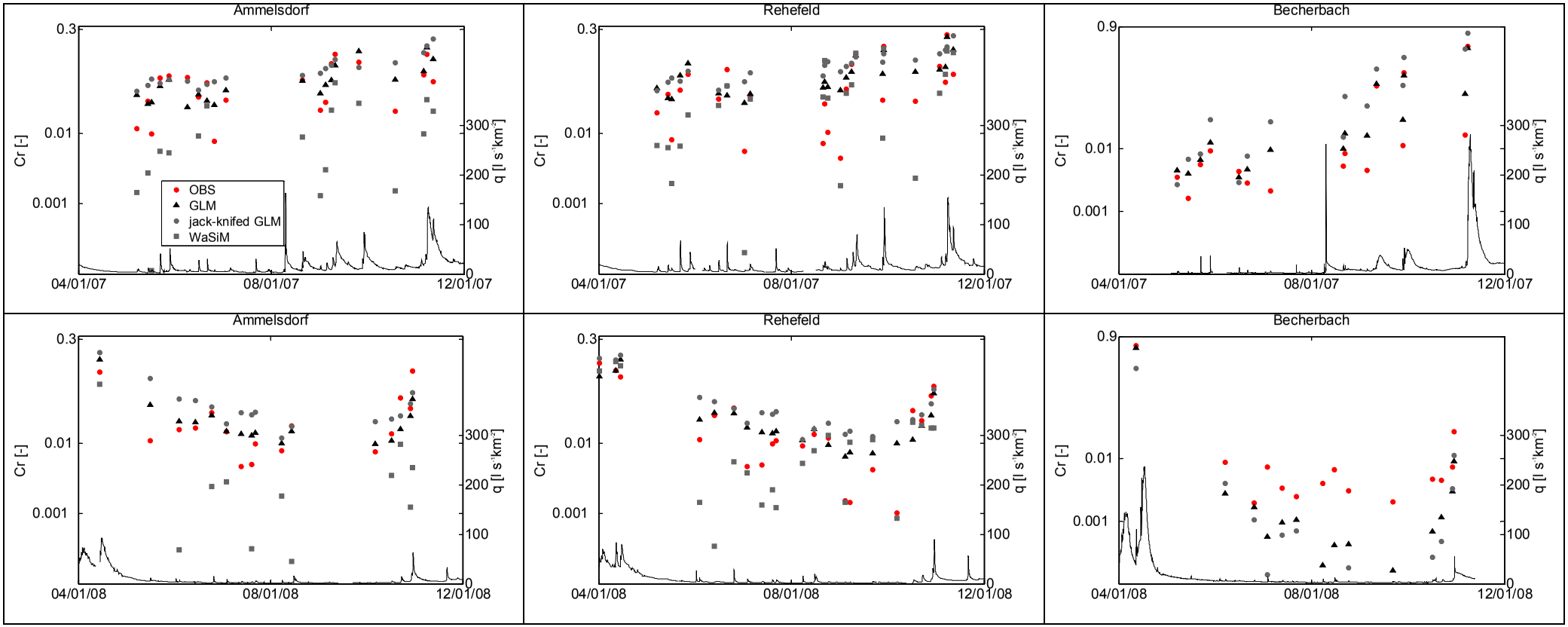

Figure 30:Temporal occurrence of the runoff events, their observed runoff coefficients (red circles), simulated C_r with GLM (black triangles) and cross validated with jackknifing (grey dots) and C_r simulated with the best calibration of WaSiM ETH (grey squares) and the specific runoff for the two snow free periods of 2007 and 2008.

4.3 Discussion, Outlook and Recommendations

4.3.1 Simulated saturation deficits and observed soil moisture data

Figure 31 presents the simulated saturation deficit *SD* of the grid cells that correspond to the locations of the TDR clusters for the summer periods 2007-2010. Even though there is a general trend for C2 that *SD* decreases with increasing observed average soil moisture *WC* the relation is highly variable and hysteretic. For the grassland site C1 no relationship is observable. The highest uncertainty occurs at an observed relative average soil moisture of approximately 0.3 where the corresponding saturation deficit ranges from 220 to 330 mm at C1 and 240 to 340 mm at C2.

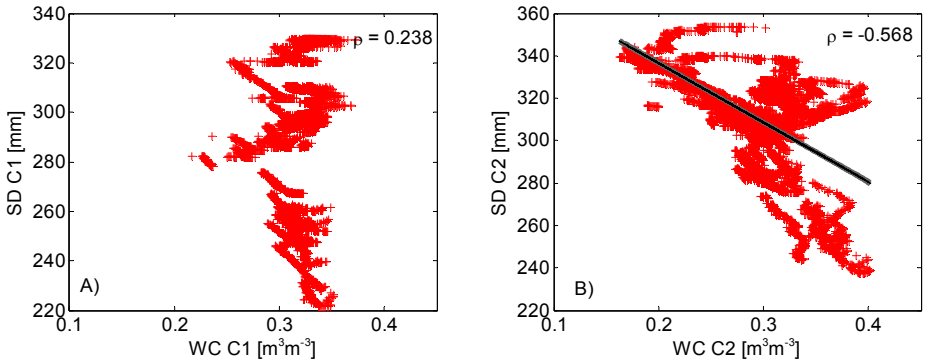

Figure 31: Saturation deficit simulated with WaSiM ETH (model calibrated to the Ammelsdorf gauge using scheme B) at the TDR locations C1 grassland (A) and C2 forest (B) plotted against the observed average soil moisture at these locations for the of the summer periods 2007-2010. The Spearman correlation coefficient ϱ is given above the plots.

By comparing the antecedent soil moisture prior to the observed events to a) the simulated antecedent saturation deficit at the corresponding grid cell and b) the catchment average antecedent saturation deficit, the correlation shows better results (Figure 32). The Spearman rank correlations are -0.65/-0.70 for the model calibrated at Rehefeld and -0.47/-0.59 for the model calibrated at Ammelsdorf for case a) and b) respectively.

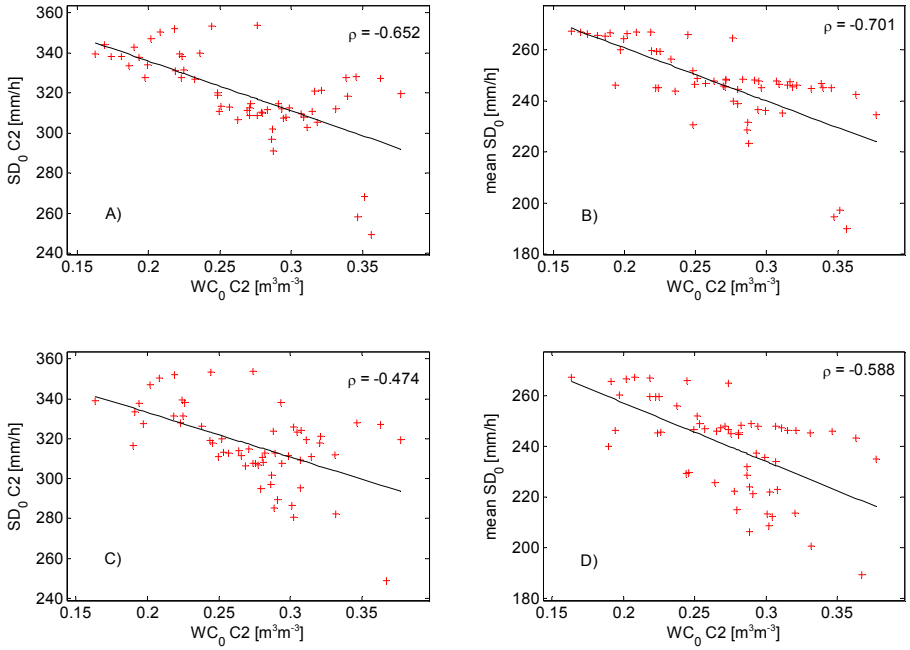

Figure 32: Comparison between the pre-event saturation deficit (*SD₀*) at position C2 and the mean *SD₀* for the entire catchment of the calibration scheme B) to the *WC₀* at C2 for the events of Rehefeld (A and B) and Ammelsdorf (C and D). The Spearman correlation coefficient ϱ is given above the plots.

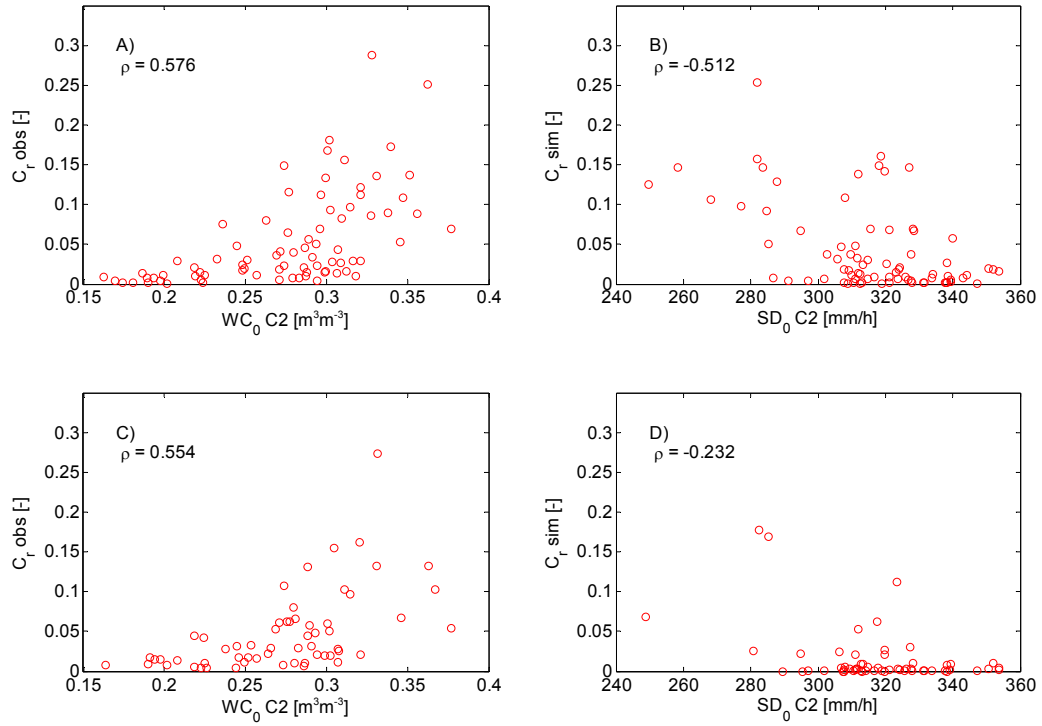

Figure 33: Observed *Cr* at Rehefeld (A) and Ammelsdorf (C) plotted against the observed average soil moisture *WC₀* at the forest cluster (C1) as well as *Cr* from WaSiM ETH simulation at Rehefeld (B) and Ammelsdorf (D) plotted against the simulated saturation deficit *SD₀*. Please note that the wettest state of *SD* is to the left and the driest to the right.

The relation between observed runoff coefficients and observed average soil moisture at the forested site as well as the corresponding relation of runoff coefficients from the modelled time series and the simulated saturation deficit at the forested site WaSiM ETH is shown in Figure 33. While a strong relationship was found for the observed data there is almost a lower relation between saturation deficit in the model and the runoff coefficients from the simulated flood events especially for Ammelsdorf. For the catchment Rehefeld the value of ϱ = -0.51 between the simulated SD_0 and C_r is comparable to the observed result of WC_0 to C_r (ϱ = 0.59). The negative correlation is because of opposite reaction of *SD* and *WC*. The drawback of the WaSiM simulations is that C_r is always underestimated.

4.4 Conclusions

4.4.1 Soil moisture at representative site outperforms large scale average wetness

In this study, it was found that the GLMs based on average soil moisture observed at the forested cluster outperformed the GLM based on pre-event discharge with respect to explaining and predicting runoff coefficients within the three nested catchments. This is remarkable as the total extent of the TDR cluster is four to five orders of magnitude smaller than the catchment area. Although predictive performance of the soil moisture based GLM decreases with increasing catchment size, it still represents still 56% of the variability of the observed runoff coefficients without a clear bias at gauge Ammelsdorf. NSE values during cross validation of the GLM data at gauges Becherbach and Rehefeld are remain high (> 0.64), while at Ammelsdorf at 0.56 is acceptable. Soil moisture data collected at a nearby grassland site were of less importance for explaining runoff coefficients. The most important meteorological predictor was the total rainfall amount.

It appears that the wetness state of the lower hillslope sector in the forested site is of greater importance for event runoff production than average catchment wetness represented by pre-event discharge. Thus it can be concluded that in the Rehefeld, Becherbach and parts of the Ammelsdorf catchment, forested sites likely contribute much more to event scale runoff production than grassland and that subsurface storm flow is the dominating process. It can be stated that spatiotemporally highly resolved sampling of representative soil moisture data in key landscape units can yield very valuable information for explaining and predicting runoff production. The forested site close to the Becherbach is obviously such a key site - not to determine the average catchment wetness as suggested by Grayson and Western (1998) or Brocca et al. (2007) - but maybe to indicate whether upslope forested areas are connected to the stream network and thus contributing to flood formation, as suggested by Spence et al. (2010).

It can be concluded furthermore that the derived GLMs might yield valuable data-based predictions of runoff coefficients and thus runoff volumes, which is of great importance for operating reservoirs. Installation of additional TDR clusters further downstream in the Ammelsdorf catchment and possibly of additional rain gauges could yield additional valuable predictors to improve the model performance at the Ammelsdorf gauge.

4.4.2 GLM performance versus performance of the distributed rainfall runoff model

An acceptable calibration of the distributed rainfall runoff model WaSIM ETH to the Rehefeld gauge with a NSE of 0.71, while for the Ammelsdorf gauge a NSE of 0.53 only is achieved. The calibrated model matched the water balance well, but runoff volumes and peak discharge are systematically underestimated. Runoff coefficients derived from the model calibration period are in less good accordance with the observed ones as runoff coefficients predicted within the cross validation test. It can be stated that the data driven GLM in the **cross validation** mode outperformed the rainfall runoff model in the calibration mode with respect to the prediction/explanation of observed runoff coefficients.

A clear relationship when comparing soil moisture observed at the two field sites was not found with the simulated saturation deficit from the corresponding grid cells, especially for the higher water contents. Thus, the locally observed relative soil moisture data is unlikely to be useful either for local corrections of the *SD* at these grid cells or as additional objective of the calibration efforts. Also the relation between antecedent soil moisture prior to the observed events to a) the simulated antecedent saturation deficit at the corresponding grid cell, and b) the catchment average antecedent saturation deficit were not strong for the largest catchment Ammelsdorf. Most importantly, it was found that there was almost no relation between saturation deficit in the model and the runoff coefficients derived from the simulated flood events for Ammelsdorf, while the relation in the real data was detectable. For Rehefeld, the correlation of saturation deficit and runoff coefficient was at an acceptable value, but most of the events were underestimated. Thus it can be concluded that a calibrated complex rainfall runoff model which matches rainfall-runoff behaviour of a catchment reasonable does not necessarily reproduce the interplay between average soil moisture of representative sites and runoff coefficients that has been observed in the target catchment. This has two important implications. The first one is that the here used conceptualisation of runoff production and runoff concentration is possibly not consistent with the functioning of this catchment, similar to the findings of Thapa (2009). The second one is that an update of the local saturation deficit using observed soil moisture data would not necessarily yield a better model performance.

The reason for the bad representation of runoff could be that the model structure, especially of the subsurface, is neither consistent with the real spatial architecture of the hydrological system nor with the topology of the subsurface flow paths. Runoff generation is conceptualised by means of linear reservoirs that all act in parallel and surface runoff that is once generated in the model cannot re-infiltrate even though this is quite likely in reality. This structural incompatibility of model structures and catchment architecture can be deemed as one major reason for predictive model uncertainty (Beven, 2006a, b). Obviously the catchments are still too small that errors due to the crucial simplification in WaSiM ETH I average out as Dooge (1986) has postulated.

CHAPTER 5 DISCUSSION, OUTLOOK AND RECOMMENDATIONS

5.1 Limited applicability of STDR in heterogeneous soils

The objective is to investigate the applicability of Spatial TDR (Becker, 2004; Schlaeger, 2005) in complex soils under field conditions. Spatial TDR is a combination of spatially distributed TDR probes with long wave guides and an inversion technique of the signal along the rods to get three-dimensional information of soil moisture at a fine resolution in time. Therefore the influence of rod deformations, the presence of objects in the sampling volume and the character of field soils were tested.

The different experiments showed that probe geometry has a massive effect on the shape of the reflected TDR signal, the reflectogram. This may lead to a complete misinterpretation of the soil moisture profile along the rods of the probe since the conceptual model of Schlaeger (2005) assumes constant width between the rods. A violation of this assumption will lead to misleading results.

The inversion method is ill-suited for complex soils with large amounts of gravel and high bulk density. These circumstances will not guarantee an accurate installation of 0.6 m rods, even by using templates and drilling with a 0.60 m long auger. The various tests under three different soil moisture conditions show, that because of the usage of coated rods the average soil moisture is almost unchanged which is consistent with results obtained by Ferré et al. (1998). Finally, it can be assumed that the mean values can be used even with geometrically complex rod deformation. Objects in the sampling volume have only little effect as long they are not electrical conductors (iron block). Finally, the algorithm was also tested, with accurate geometry as obtained within glass beads and with natural soils from the field site. In comparison with FDR probes, the profiles obtained are in good accordance. However, it must be noted that during infiltration or withdrawal, the accuracy of the inverted profile decreases. It is demonstrated furthermore that Spatial TDR is capable of monitoring fast infiltration and redistribution of irrigation water in soil. The Spatial TDR method is limited to applications in media with homogeneous conditions like disposal sites and dykes. For the later case, Scheuermann et al. (2009) obtained good results. Probes installed in a soil pit to guarantee exact probe geometry as a strongly invasive method can be an alternative to the use of inversion in the field.

The use of clustered TDR probes with long waveguides to observe a more representative soil volume is not affected by complex soils and is a promising alternative.

5.2 TDR clusters at a representative areas: key information in key landscape units

In this study it is clearly shown that the clustering of TDR probes gives important information about temporal and spatial distribution of soil moisture. Two clusters were installed, one at a

grassland site and one at a forest site. Both are located in the headwater catchments of the Wilde Weißeritz. Each cluster covers an area of 400 m² with 39 (grassland) and 32 probes (forest). A strong heterogeneity in the soils and their effect on the spatial development of patterns is shown in the study. The high spatial variability in soil moisture, with a range of 0.07 m^3m^{-3} (grassland) and 0.08 m^3m^{-3} (forest), is large compared to other studies (Bárdossy and Lehmann, 1998; Brocca et al., 2007; Blume et al., 2009) despite a smaller areal extent. From the findings of the temporal stability plots, it can be inferred that the use of single TDR measurements is not useful to assess a representative average soil moisture at that type of heterogeneous soil. This is different to results cited by Grayson and Western (1998), Brocca et al. (2007, 2009a, 2010) and Joshi et al. (2011) which report the existence of such a representative monitoring site. Also, a poor relationship between topographic factors and points close to the spatial mean were identified, contrary to Joshi et al. (2011).

Furthermore, clear evidence is found that clustering of TDR probes in combination with long-term monitoring allows identification of average spatial covariance structures at the small field scale at different wetness states. Compared to other studies (Brocca et al., 2007), the short range of covariance can be explained by the heterogeneity of soils. Small-scale heterogeneity of soil properties at the forested site is similar to that found at the grassland site. But the soil moisture patterns are different. Therefore it can be concluded that the correlation structure at the forested site is dominated by the pattern controlled by vegetation (throughfall and interception) and at the grassland site the soil moisture is dominated by small-scale variability of soil properties.

5.3 CATFLOW –soil and vegetation control on soil moisture at the hillslope scale

To understand the dynamics of the interaction of vegetation on the soil for both cluster sites, the hillslope model CATFLOW was used to estimate the specific phenological parameters. A combination of observed k_s and porosity values with van Genuchten parameters estimated from the pedo transfer function of Carsel and Parrish (1998) gives sufficient results of simulated soil moisture for both study sites. At the forest site, a best model set up can be presented (soil profile A, LAI = 13.5, plant cover = 0.85) with a correlation coefficient of 0.89 and a RMSE of 4.7×10^{-4} which is a good representation of the key areas in the headwater catchment of the Wilde Weißeritz. It can be concluded that the extent of the modelling grid used is large enough to asses the dynamics of average spatial soil moisture in an almost unbiased fashion. Simulated averaged soil moisture is within the confidence interval of the observed spatial average soil moisture for almost the whole period. At the grassland site, this shows that the vegetation is not sufficiently well represented (correlation coefficient of 0.753 and RMSE of 6.9×10^{-4}) and further work on surveying the annual vegetation cycle of plant morphological parameters must be resolved.

Outlook maybe stress that it would be interested to run similar simulations for heterogeneous hillslopes. Soil moisture distributions could be estimated based on available variograms. Most interesting part is whether best plant parameters allow still a good reproduction of both average soil moisture dynamics and dynamics spatial soil moisture variability.

5.4 Understanding flow and runoff processes with irrigation experiment

To understand the dominating hydrological processes, an irrigation experiment was carried out. Vertical preferential flow was identified as the main process, with overland flow and shallow lateral flow playing minor roles.
Fast responses to a depth of 2.7 m in less than 1.5 hours were observed. Deep lateral fluxes were observed with a lag of 6 hours. This led to the assumption that water and solute transport can reach velocities of approximately 10^{-4} m s^{-1}. The different response under changed initial conditions is similar to the observation of bimodal events in the Becherbach which only can be observed above 0.33 m^3m^{-3}. Above the threshold mobilisation of groundwater leads to much higher runoff coefficients.

5.5 Soil moisture controls on runoff

Statistical analysis between different predictor variables describing the catchment state shows that soil moisture at the forest site is an important factor of estimated runoff coefficients. The Spearman rank correlation between runoff coefficients and pre-event soil moisture is high for all three subcatchments (Becherbach = 0.63, Rehefeld = 0.67 and Ammelsdorf = 0.54). Duration of rainfall and precipitation sum have similar values. $API^{30}_{0.95}$, AP^{60}, CV and rainfall intensity have lower correlation values.

Pre-event runoff also shows high correlation to average soil moisture at both sites. It can be concluded that subsurface storm flow or fast groundwater flow is the dominating runoff generating process, at least in the snow-free period. Saturation excess overland flow plays a key role due to the high permeability of the top soil (more than 10^{-4}m s^{-1}), while the large amount of gravel has a minor role, which is consistent with the findings of the irrigation experiment and time series analysis. Subsurface storm flow is reported to be the dominant runoff process in many other studies in forested areas (Blume et al., 2008a, b; Tromp-van Meerveld et al., 2006a; Uhlenbrook et al., 2002). The wetness state of the lower hillslope sector in forested sites seems to be of greater importance for event runoff generation than average catchment wetness represented by pre-event runoff. It thus can be concluded that in the Ammelsdorf and Rehefeld catchments forested sites are likely to contribute more strongly to event scale runoff production than does grassland. Spatiotemporal highly resolved sampling of representative soil moisture data in key landscape units resolution yields very valuable information for explaining and predicting runoff production. The forested site close to the Becherbach can be identified as such a key site - not to determine the average catchment wetness (Brocca et al., 2007; Grayson and Western, 1998) but to determine the average wetness of landscape areas that contribute to flood formation.

In the Becherbach catchment a threshold process can be observed. Before a certain soil moisture is reached, runoff coefficients of the small tributary Becherbach are below 0.05. By exceeding 0.33 m^3m^{-3} as absolute values, runoff coefficients above 0.10 are observed. A closer look reveals complete different runoff response for dry and wet conditions, even if the catchment received the same amount of precipitation. A hysteretic relation between the average spatial soil moisture

and runoff was observed which switches from clockwise to anticlockwise response. This means that under dry conditions the soil storage has a longer recession time compared to the runoff and in the wet case it is reversed. Soil moisture returns to the starting value whereas runoff still increases.

The relation to groundwater to runoff is in both cases clockwise. However, while during dry conditions there is virtually no response observed in groundwater during the event, during wet conditions a fast response is observed which may last up to 4 to 5 days. This hysteretic behaviour of streamflow/subsurface flow and water content was found by several other authors (Graham et al. 2010, Hrnčíř et al. 2010, Penna et al. 2010). Spence et al. (2009) also found hysteretic patterns between discharge and storage. However, discovering hysteretic behaviour between storage and discharge is an indicator of system controls and time-variant dominant processes. Under dry conditions the unsaturated zone dominates the runoff response and groundwater has a minor effect. If the catchment wetness reaches a threshold value of WC_0, the upslope areas are connected to the main catchment which results in a fast response in groundwater level whereas the *WC* decreases to the starting level. This hypothesis should be validated through additional instrumentation and/or tracer techniques.

5.6 C_r and WaSiM ETH simulations

Statistical generalised linear models and the dynamical distributed hydrological model WasiM ETH I are tested to see how accurately they can predict the runoff coefficients of three headwater catchments of the Wilde Weißeritz. Statistical analysis of runoff coefficients with different *a priori* catchment states describing variables and meteorological variables is conducted to get a better understanding of which are the forcing predictor variables in flood events. Here, the mean pre-event soil moisture of the forest site important predictor of significant explanatory power compared to other catchment state variables such as pre-event runoff, antecedent precipitation index, antecedent precipitation, coefficient of variation.

The simulations with the hydrological model WaSiM ETH have shown that the model can represent the discharge adequately (NSE for the best setup B of 0.74 for Rehefeld and 0.53 for Ammelsdorf) but it was unable to predict the runoff coefficients accurately. It can be stated that the data driven GLM in the **cross validation** mode outperformed the rainfall runoff model in the calibration mode with respect to the prediction/explanation of observed runoff coefficients. A comparison of observed soil moisture and simulated saturation revealed a clear limitation of to represent the local state at the observed grid cell. At an observed average soil moisture of approximately 0.33 m^3m^{-3}, the range of the corresponding saturation deficit is between 240 to 340 mm at the forest site and the relationship is strongly hysteretic. The simulated soil storage at the grassland site was unable to reproduce the observed dynamics.
The relationships between antecedent soil moisture prior to the observed events to the simulated antecedent saturation deficit at the corresponding grid cell and to the average in the catchment are therefore better. For Ammelsdorf, there was almost no relation between saturation deficit in

the model and the runoff coefficients derived from the simulated flood events, although in the relation in the real data was detectable. A strategy for updating that storage with observed values will not be promising with unrealistically responding storage.
For Rehelfeld the correlation of saturation deficit and runoff coefficient is at an acceptable value and for the events the relation between soil storage and soil moisture is high, but most of the events are underestimated. Here an updating could be promising.

Finally, the operational use TDR clusters in head water catchments can be seen as a useful method to observe the catchment state and to predict the volumes of flood events. This issue is important for the management of the three storage reservoirs in the Weißeritz catchment and also for adjacent catchments in the Ore Mountains.

5.7 Overall conclusion

The determination of soil moisture with clustered probes is a promising method to assess important information about the spatial and temporal variability of soil moisture. A single soil moisture probe is not sufficient to estimate the spatial and temporal mean soil moisture since soil moisture variability is not dominated by topographic effects but reflects heterogeneity of the pore space.
The idia to get a nearly 3D image of soil moisture patterns will be in the study area not realisable. The use of the inversion of soil moisture profiles along the rods of a probe has the disadvantage that it requires parallel rod distance. This is not achievable in a non-invasive installation application. Thus the usage is strongly limited.

It is interesting and important to note that the soil moisture time series at the individual sampling locations do not intersect and the ranks of soil moisture in a cluster remain temporally stable. These findings suggest that the spatial variability in soil moisture measurements reflects spatial heterogeneity of stationary soil properties as well as of the micro topography rather than small scale variability of the matrix potential. Soil moisture time series within each cluster are furthermore highly correlated (0.90). It can be stated that a single probe at both clusters is a good estimator for the average soil moisture dynamics at the observed sites. This is good news as matrix potential – which is the driver for soil moisture dynamics – is much less variable in space than soil moisture. A distributed sensor network (Bogena et al., 2009) of soil moisture probes and tensiometers can thus yield representative data for soil moisture dynamics and matrix potential at headwater catchments and be used in flood forecasting (Anctil et al. 2008). These points look towards new, less expensive strategies to collect information about soil state variables at the head water scale.

The clustering of TDRs at relevant functional units in a catchment is a useful tool for understanding the important runoff processes. The heterogeneous study area would be not sufficiently observed by the use of only one probe as a representative sample. With the help of the hydrological Model CATFLOW, the *ET* parameters of forest sites can be estimated which is

important for further investigations of the long term water balance and to represent the typical landscape units in larger scale models.

The importance of pre-event soil moisture on the runoff formation is clearly shown for all three catchments. Small scale measured soil moisture is able to predict medium scale runoff coefficients. The observed small scale soil moisture can explain runoff formation even in 4-5 magnitudes larger Ammelsdorf catchment. A clear threshold process can be observed in the small catchment of the Becherbach. The degree of saturation of the soil moisture plays here an important part in the runoff generation. The comparison between GLM and the complex hydrological model WaSiM ETH I shows that the GLM can deliver much better results and the hydrological model always underestimates the observed runoff volumes, despite the Good performance measure values.
The forecast of runoff coefficients are a relevant issue for the management of storage reservoirs. The importance of the prediction of runoff coefficients with soil moisture from a representative land surface unit is shown. The study sites of the head catchments of the Weißeritz demonstrate that groundwater is an important part of the runoff generation, as the threshold response of runoff coefficients and the hysteretic response of dry and wet events have shown.
The study area is located in the headwater catchment of the Wilde Weißeritz catchment upstream of two reservoirs (Lehnmühle and Klingenberg). They were built to store fresh water and for prevention of flood events. This work can help to establish a new pre-warning system, by the estimation of runoff coefficients through meteorological forecasts and observed pre-event soil moisture. A possible combination with a flood forecasting system for the prediction of peak runoff (Kneis et al., 2010) is conceivable.
Other techniques to estimate soil moisture as discussed in Chapter 1 can be of interest: in particular, how well they can represent the catchment state and especially the pre-event soil moisture. Sensor networks with low cost probes should be of great importance. Remote sensing methods and cosmic ray techniques are not useful because of the large amount of forest coverage, which do not allow penetration of electromagnetic waves through it to the surface. Gravity applications have to be well sited to observe a representative area and have the drawback of high costs. Geophysical methods have the drawback of being bound to airborne campaigns and the need for complex analysis. Further works should take into account the dynamics of groundwater.

References:

Albergel, C., Rüdiger, C., Carrer, D., Calvet, J.C., Fritz, N., Naeimi, V., Bartails, Z., Hasenauer, S., An evaluation of ASCAT surface soil moisture products with in-situ observations in Southwestern France, Hydrol. Earth Syst. Sci., 13, 115-124, 2009.

Albertson, J.D. and Montaldo, N., Temporal dynamics of soil moisture variability: 1. Theoretical basis, Water Resour. Res., 39(10), W01274, 2003.

Alharthi, A. and Lange, J., Soil water saturation - dielectric determination, Water Resour. Res., 23(4), 591-594, 1987.

Ali, G.A. and Roy, A.G., A case study on the use of appropriate surrogates for antecedent moisture conditions, Hydr. Earth Syst. Sci., 14, 1843-1861, 2010.

Amoozegar, A., A compact constant-head permeameter for measuring saturated hydraulic conductivity of the vadose zone, Soil Sci. Soc. Am. J., 53, 1356-1361, 1989a.

Amoozegar, A., Comparison of the Glover solution with the simultaneous-equations approach for measuring hydraulic conductivity, Soil Sci. Soc. Am. J., 53, 1361-1367, 1989b.

Ambroise, B. Variable 'active' versus 'contributing' areas or periods: a necessary distinction, Hydrol. Proc., 18, 1149-1155, 2003.

Anctil, F., Lauzon, L., Filion, M., Added gains of soil moisture content observations for streamflow predictions using neural networks, J. Hydrol., 359(3-4), 225-234, 2008.

Anderson, A.E., Weiler, M., Alia, Y., Hudson, R.O., Dye staining and excavation of a lateral preferential flow network, Hydrol. Earth Syst. Sci., 13(6), 935-944, 2009.

Arnold, J.G., Srinivasan, R., Muttiah, R.S., Williams, J.R., Large area hydrologic modeling and assessment. Part I: Model development, J. Am. Water Res. Assoc., 341, 73-88, 1998.

Arya, P.S., Introduction to Micrometeorology, 2nd Ed. Academic Press, London. 410pp.

Aubert, D., Loumagne, C., Oudin, L., Sequential assimilation of soil moisture and streamflow data in a conceptual rainfall-runoff model, J. Hydrol., 280, 145-161, 2003.

Baker, T.H.W., Davis, J.L., Hayhhoe, H.N., Topp, G.C., Locating the frozen-unfrozen interface in soils using time-domain reflectometry, Can. Geotech. J., 19, 511-517, 1982.

Bänninger, D., Wunderil, H., Nussberger, M., Flühler, H., Inversion of TDR signals - revisited, Journal of Plant Nutrition and Soil Science-Zeitschrift für Pflanzenernährung und Bodenkunde, 171, 137-145, 2008.

Bárdossy, A., and Lehmann, W., Spatial distribution of soil moisture in a small catchment. Part 1: Geostatistical analysis, J. Hydrol., 206, 1-15, 1998.

Bárdossy, A., Calibration of hydrological model parameters for ungauged catchments, Hydr. Earth Syst. Sci., 11(2), 703-710, 2007.

Baroni, G., Facchi, A., Gandolfi, C., Ortuani, B., Horeschi, D., van Dam, J.C., Uncertainty in the determination of soil hydraulic parameters and its influence on the performance of two hydrological models of different complexity, Hydrol. Earth Syst. Sci., 14, 251-270, 2010.

Bartels, H., Malitz, G., Asmus, S., Albrecht, F.M., Dietzer, B., Günther, T., Ertel, H., Deutscher Wetterdienst KOSTRA Starkniederschlag für Deutschland, Offenbach am Main, Selbstverlag des Deutschen Wetterdienstes, in German, 1997.

Baumhardt, R.L., Lascano, R.J., Evett, S.R., Soil Material, Temperature, and Salinity Effects on Calibration of Multisensor Capacitance Probes, Soil Sci. Soc. Am. J., 64, 1940-1946, 2000.

Becker, R., Spatial Time Domain Reflectometry for Monitoring Transient Soil Moisture Profiles, Ph.D. thesis, Mitteilungen des Institutes für Wasser und Gewässerentwicklung - Bereich Wasserwirtschaft und Kulturtechnik mit "Theodor-Rehbock-Wasserbaulaboratorium", Heft 228, University of Karlsruhe, 2004.
Berthet, L., Andréassiana; V., Perrina; C., Loumagne, C., How crucial is it to account for the antecedent moisture conditions in flood forecasting? Comparison of event-based and continuous approaches on 178 catchments, Hydr. Earth Syst. Sci., 13, 819-831, 2009.
Beven, K.J. and Kirby, M., A physically based variable contributing area model of basin hydrology, Hydrological Sciences Bulletin, 24, 43-69, 1979.
Beven, K.J. and Germann, P., Macropores and Water-Flow In Soils, Water Resour. Res., 18(5), 1311-1325, 1982.
Beven, K.J. and Binley, A., The future of distributed models: model calibration and uncertainty prediction, Hydrol. Proc., 6(3), 265-277, 1992.
Beven, K.J., Rainfall-runoff modelling, John Wiley & sons, LTD, Chichister,360 pp., 2002.
Beven, K.J., A manifesto for the equifinality thesis, J. Hydrol., 320 (1-2), 18-36, 2006a.
Beven, K.J., Searching for the Holy Grail of scientific hydrology: Qt=(S, R, Δt) A as closure, Hydr. Earth Syst. Sci., 10, 609-618, 2006b.
Binley, A., Beven K.J., Elgy, J., A Physically Based Model of Heterogeneous Hillslopes .2. Effective Hydraulic Conductivities, Water Resour. Res., 25(6), 1227-1233, 1989.
Binley, A., Cassiani, G., Middleton, R., Winship, P., Vadose zone flow model parameterisation using cross-borehole radar and resistivity imaging, J. Hydrol., 267, 147-159, 2002.
Blöschl, G. and Sivapaln, M., Scale issues in hydrological modelling: a review, Hydrol. Proc., 9, 251-290, 1995.
Blöschl, G. and Zehe, E., On hydrological predictability, Hydrol Proc., 19, 3923-3929, 2005.
Blume T., Zehe, E., Iroume A., Bronstert A., Rainfall runoff response and baseflow separation, Hydrological Science Journal, 52(5), 843-862, 2007.
Blume, T., Zehe, E., Reusser D., Iroumé A., Bronstert, A., Investigation of runoff generation in a pristine, poorly gauged catchment in the Chilean Andes I: A multi-method experimental study. Hydrol Proc., 22(18), 3661-3675, 2008a.
Blume, T., Zehe, E., Bronstert, A., Investigation of runoff generation in a pristine, poorly gauged catchment in the Chilean Andes II: Use of Tracers, Hydrol Proc., 22(18), 3676-3688, 2008b.
Blume, T., Zehe, E., Bronstert, A., Use of soil moisture dynamics and patterns at different spatio-temporal scales for the investigation of subsurface flow processes, Hydrol. Earth Syst. Sci., 13, 1215-1234, 2009.
Blume, T., Hydrological processes in volcanic ash soils: measuring, modelling and understanding runoff generation in an undisturbed catchment, PhD Thesis, University of Potsdam, 153 p., 2008.
Bogena, H.R., Huisman, J.A., Oberdorster, C., Vereecken, H., Evaluation of a low-cost soil water content sensor for wireless network applications, J. Hydrol., 344(1-2), 32-42, 2007.
Bogena, H.R., Huisman, J.A., Meier, H., Rosenbaum, U., Weuthen, A., Hybrid Wireless Underground Sensor Networks: Quantification of Signal Attenuation in Soil, Vadose Zone J., 8(3), 755-761, 2009.
Boike, J. and Roth, K., Time Domain Reflectometry as a Field Method for Measuring Water Content and Soil Water Electrical Conductivity at a Continuous Permafrost Site, Permafr. Periglac. Process., 8(4), 359-370, 1997.

Borga, M, Boscolo, P., Zanon, f., Sangati, M. Hydrometeorological Analysis of the 29 August 2003 Flash Flood in the Eastern Italian Alps, J Hydrometeorology, 8, 1049-1067, 2007.
Borga, M., Gaume, E., Creutin, J.D., Marchi, L., Surveying flash floods: gauging the ungauged extremes, Hydrol. Proc., 22(18), 3883-3885, 2008.
Bormann, H., Breuer, L, Graeff, T., Huismann, J.A., Analysing the effects of soil properties changes associated with land use changes on the simulated water balance: A comparison of three hydrological catchment models for scenario analysis, Ecol. Model., 209(1), 29-40, 2008.
Bremicker, M., Aufbau eines Wasserhaushaltsmodells für das Weser- und das Ostsee-Einzugsgebiet als Baustein eines Atmosphären-Hydrologie-Modells, PhD Thesis, University of Freiburg, in German, 1998.
Brevik, E.C., Fenton T.E., Lazari, A., Soil electrical conductivity as a function of soil water content and implications for soil mapping, Precision Agriculture, 7, 1385-2256, 2006.
Breuer L., Eckhardt K., Frede H.G., Plant parameter values for models in temperate climates, Ecol. Model., 169, 237-293, 2003.
Brocca, L., Morbidelli, R., Melone, F., Moramarco, T., Soil moisture spatial variability in experimental areas of central Italy, J. Hydrol., 333(2-4), 356-373, 2007.
Brocca, L., Melone F., Moramarco, T, On the estimation of antecedent wetness conditions in rainfall–runoff modelling, Hydrol. Proc., 22, 629-642, 2008.
Brocca, L., Melone, F., Morbidelli, R., Moramarco, T., Soil moisture temporal stability over experimental areas in Central Italy, Geoderma 148, 364-374, 2009a.
Brocca, L., Melone, F., Moramarco, T., Morbidelli, R. Antecedent wetness conditions based on ERS scatterometer data, J. Hydrol., 364(1-2), 73-87, 2009b.
Brocca, L., Melone F., Moramarco, T., Singh, V.P., Assimilation of Observed Soil Moisture Data in Storm Rainfall-Runoff Modelling, Journal of Hydrologic Engineering, 14(2), 153-165, 2009c.
Brocca, L., Melone, F., Moramarco, T., Morbidelli, R., Spatial-temporal variability of soil moisture and its estimation across scales, Water Resour. Res., 46, W02516, DOI: 10.1029/2009wr008016, 2010a.
Brocca, L., Melone, F., Moramarco, T., Morbidelli, R., Wagner W., Naeimi, V., Bartalils, Z., Hasenauer, S., Improving runoff prediction through the assimilation of the ASCAT soil moisture product, Hydrol. Earth Syst. Sci., 14, 1881-1893, 2010b.
Bronstert, A. and Plate, E. J., Modelling of runoff generation and soil moisture dynamics for hillslopes and micro-catchments, J. Hydrol., 198(1-4), 177-195, 1997.
Bronstert, A. and Bárdossy, A., The role of spatial variability of soil moisture for modelling surface runoff generation at the small catchment scale, Hydrol. Earth Syst. Sci., 3, 505–516, 1999.
Bronstert, A., Creutzfeldt, B., Graeff, T., Hajnsek, I., Heistrmann, M., Itzerott, S., Jagdhuber, T., Kneis, D., Lück, E., Reusser, D., Zehe, E, Potentials and constraints of different type of soil moisture observations for flood simulations in headwater catchments, Natural Hazards, DOI: 10.1007/s11069-011-9874-9, 2011.
Bronstert, A., Capabilities and limitations of detailed hillslope hydrological modeling, Hydrol. Process., 13, 21-48, 1998.
Burt, T.P. and Butcher, D.P, Topographic controls of soil-moisture distributions, Soil Science, 36(3), 469-486, 1985.

Butler, D.K., Near-surface geophysics, Society of Exploration Geophysicists, in Friedman, S.P., Soil properties influencing apparent electrical conductivity: A review, Computers and Electronics in Agriculture 46, 45-70, 2005.
Butler, D. K., Near-surface geophysics, Society of Exploration Geophysicists, 2005.
Buytaert, W., and Beven, K.J., Regionalization as alearning process, Water Resour. Res., 45, W11419, 2009.
Carsel R.F. and Parrish, R.S., Development of joint probability distribution of soil water retention characteristics, Water Resour. Res., 24, 755-769, 1988.
Carminati, A., Moradi A.B., Vetterlein, D., Vontobel P., Lehmann, E., Weller, U., Vogel, H.J., Oswald, S.E., Dynamics of soil water content in the rhizosphere, Plant Soil, 332, 163-176, 2010.
Cassiani, G., Binley, A., Ferré, T.P.A., Unsaturated zone processes, in: Verrecken, H., Binley, A., Cassiani, G. Revil, A., Titov, C., Applied Gydrogeophysics, NATO Science Series, IV. Eart and Environmental Sciences Vol. 71, Springer, Dordrecht, 2006.
Cassiani, G., Godio, A., Stocco, S., Villa, A., Deiana, R., Frattini, P., Rossi, M., Monitoring the hydrologic behaviour of a mountain slope via time-lapse electrical resistivity tomography, Near Surface Geophysics, 7(5-6), 475-486, 2009.
Celia, M.A., Bouloutas E.T.B., Zarba, R.L., A general mass- conservative numerical solution for the unsaturated flow equation, Water Resour. Res., 26 (7), 1483-1496, 1990.
Collier, C.G., Flash flood forecasting: What are the limits of predictability? Quart. J. Roy. Meteorol. Soc., 133(622), 3-23, 2007.
Crawley, M.J., Statistical Computing: An Introduction to Data Analysis using S-Plus, John Wiley and Sons, West Sussex, 2002.
Crawley, M.J., The R-book, John Wiley and Sons, West Sussex, 2007.
Creutzfeldt B, Güntner A, Vorogushyn S, Merz, B., The benefits of gravimeter observations for modelling water storage changes at the field scale, Hydrol. Earth Syst. Sci., 14(9), 1715-1730, 2010a.
Creutzfeldt, B., Güntner, A., Thoss, H., Merz, B., Wziontek,H., Measuring the effect of local water storage changes on in-situ gravity observations: Case study of the Geodetic Observatory Wettzell, Germany, Water Resour. Res., 46, W08531, DOI: 10.1029/2009WR008359, 2010b.
Croke, B.F.W. and Jakeman, A.J., A catchment moisture deficit module for the IHACRES rainfall–runoff model, Environ. Modell Softw., 19, 1-5, 2004.
Crow, W. T., Bindlish, R., Jackson, T. J., The added value of spaceborne passive microwave soil moisture retrievals for forecasting rainfall-runoff ratio partitioning, Geophys. Res. Lett., 32, L18401, 2005.
Crow, W.T. and Ryu, D., A new data assimilation approach for improving runoff prediction using remotely-sensed soil moisture retrievals, Hydr. Earth Sys. Sci., 13(1), 1-16, 2009.
Chaves, J., Neill, C., Germer, S., Neto, S.G., Krusche, A., Elsenbeer, H., Land management impacts on runoff sources in small Amazon watersheds, Hydrol Proc., 22, 1766-1775, 2008.
Chen, R., Drnevich, V.P., Yu, X., Nowack, R., Chen, Y., Time Domain Reflectometry Surface Reflections for Dielectric Constant in Highly Conductive Soils, Journal of Geotechnical and Geoenvironmental Engineering, 133(12), 1579-1608, 2007.
Chirico, G.B., Grayson, R.B., Western, A.W., A downward approach to identifying the structure and parameters of a process-based model for a small experimental catchment, Hydrol Proc., 17(11), 2239-2258, 2003.

Christiansen, J. S., Thorsen, M., Clausen, T., Hansen, S., Refsgaard, J.C., Modelling of macropore flow and transport processes at catchment scale, J. Hydrol., 299(1-2), 136-158, 2004.
Costa, A., Bronstert, A., Kneis, D., Probabilistic flood forecasting for a mountainous headwater catchment (49 km²) using a nonparametric stochastic dynamic approach, Hydrological Science Journal, accepted 2011.
Dalton, F.N. and Van Genuchten, M.,T., The time-domain reflectometry method for measuring soil water content and salinity, Geoderma, 38, 237-250, 1986.
Deeks, L.K., Bengough, A.G., Low, D., Billett, M.F., Zhang, X., Crawford, J.W., Chessell, J.M., Young, I.M., Spatial variation of effective porosity and its implications for discharge in an upland headwater catchment in Scotland, J. Hydrol., 290, 217-228, 2004.
Dekker, L.W., Oostindie, K., Ritsema, C.J., Exponential increase of publications related to water repellency, Aust. J. Soil Res., 43, 403-441, 2005.
De Rooij, G.H., Averaging hydraulic head, pressure head, and gravitational head in subsurface hydrology, and implications for averaged fluxes, and hydraulic conductivity, Hydr. Earth Sys. Sci., 13 (7), 1123-1132, 2009.
Descroix, L., Nouvelot, J.F., Vauclin, M., Evaluation of an antecedent index to model runoff yield in the western Sierra Madre (north-west Mexico), J. Hydrol., 263, 114-130, 2002.
Detty, J.M. and McGuire, K.J., Threshold changes in storm runoff generation at a till-mantled headwater catchment, Water Resour. Res., 46, W07525, 2010.
De Vos, N.J. and Rientjes, T.H.M., Multiobjective training of artificial neural networks for rainfall-runoff modelling, Water Resour. Res., 44, W08434, DOI: 10.1029/2007WR006734, 2008.
Dingman, S.L.: Physical Hydrology, 575 pp., McMillan, New York, 1994.
Dixon, B. and Candade, N., Multispectral landuse classification using neural networks and support vector machines: one or the other, or both? International Journal of Remote Sensing 29(4), 1185-1206, 2008.
Dooge, J. C. I., Looking for hydrological laws, Water Resour. Res., 22(9), 46S-58S, 1986.
Dormann, C.F., Elith, J., Bacher, S., Buchmann, C., Carl, G., Carré, G., García Marquéz, J.R., Gruber, B., Lafourcade, B., Leitão, P.J., Münkemüller, T., McClean, C., Osborne, P.E., Reineking, B., Schröder, B., Skidmore, A.K., Zurell, D., Lautenbach, S., Collinearity: a review of methods to deal with it and a simulation study evaluating their performance, submitted Ecology, 2011.
Dunne T., Moore T.R., Taylor C.H., Recognition and prediction of runoff producing zones in humid regions. Hydrological Sciences Bulletin, 20(3), 305-327, 1975.
Ehret, U., Götzinger, J. Bárdossy, A., Pegram, G.G.S., Radar-based flood forecasting in small catchments, exemplified by the Goldersbach catchment, Germany, International Journal of River Basin Management, 6(4), 323-329, 2008.
Evett, SR.., Tolk, JA.., Howell, T.Q., Soil profile water content determination: Sensor accuracy, axial response, calibration, temperature dependence, and precision, Vadose Zone J., 5, 894-907, 2006.
Famiglietti, J. S., Ryu, D., Berg, A.A., Rodell, M., Jackson, T.J., Field observations of soil moisture variability across scales, Water Resour. Res., 44(1), W01423, 10.1029/2006wr005804, 2008.
Fedora, M.A. and Beschta, R.L., Storm runoff simulation using an antecedent precipitation index (API) model, J. Hydrol., 112(1-2), 121-133, 1989.
Feng, W., Lin, C.P., Deschamps, R.J. Drnevic, V.P., Theoretical model of a multisection time domain reflectometry measurement system, Water Resour. Res., 35(8), 2321-2331, 1999.
Fernandez-Galvez, J., Errors in soil moisture content estimates induced by uncertainties in the effective soil dielectric constant, International Journal of Remote Sensing, 29(11), 3317-3323, 2008.

Ferré, T.P.A., Rudolph, D.L., Kachanoski, R.G., Spatial averaging of water content by time domain reflectometry: Implications for twin rod probes with and without dielectric coatings, Water Resour. Res., 32, 271-279, 1996.
Ferré, T.P.A., Knight, J.H., Rudolph, D.L., Kachanoski, R.G., The sample areas of conventional and alternative time domain reflectometry probes, Water Resour. Res., 34, 2971-2979, 1998.
Fox, J., An R and S-PLUS companion to applied regression, Sage, Thousand Oaks, California, 2002.
Francke, T., López-Tarazón, J.A., Schröder, B., Estimation of suspended sediment concentration and yield using linear models, random forests and quantile regression forests, Hydrol. Proc., 22(25), 4892-4904, 2008.
Francke, T., Particle Swarm Optimization and Dynamically Dimensioned Search, optionally using parallel computing based on Rmpi. http://rforge.net/ppso/, 2010.
Francois, C., Quesney, A., Ottle, C., Sequential assimilation of ERS-1 SAR data into a coupled land surface-hydrological model using an extended Kalman filter, J. Hydrometeorol., 4(2), 473-487, 2003.
Friedman, S.P., Statistical mixing model for the apparent dielectric constant of unsaturated porous media, Soil Sci. Soc. Am., J61(3), 742-745, 1997.
Frisbee, M.D., Allan, C.J., Thomasson, M. J., Mackereth, R., Hillslope hydrology and wetland response of two small zero-order boreal catchments on the Precambrian Shield, Hydrol. Process., 21, 2979-2997, 2007.
Galagedara, L.W., Redman, J.D., Parkin, G.W., Annan, A.P., Endres, A.L., Numerical Modeling of GPR to Determine the Direct Ground Wave Sampling Depth, Vadose Zone J., 4, 1096-1106, 2005.
Gaskin, G.J. and Miller, J.D., Measurement of soil water content using a simplified impedance measuring technique, J. of Agricultural Engineering Research, 63(2), 153-159, 1996.
Germann, P. and Beven, K.J., Kinematic wave approximation to infiltration into soils with sorbing macropores, Water Resour. Res., 21(7), 1990-1996, 1985.
Gerten, D., Schaphoff, S., Lucht, W., Potential future changes in water limitations of the terrestrial biosphere, Climatic Change, 80, 277-299, 2007.
Goodrich, D. C., Schmugge, T. J., Jackson, T. J., Unkrich, C. L., Keefer, T. O., Parry, R., Bach, L. B., Amer, S. A., Runoff simulation sensitivity to remotely-sensed initial soil water content, Water Resour. Res., 30(5), 1393-1405, 1994.
Greco, R., Soil water content inverse profiling from single TDR waveforms, J. Hydrol., 317, 325-339, 2006.
Greco, R. and Guida, A., Field measurements of topsoil moisture profiles by vertical TDR probes, J. Hydrol., 348, 442-451, 2008.
Graeff, T., Zehe, E., Reusser, D., Lück, E., Schröder, B., Bronstert, A., Process identification through model rejection in a mid mountainous rural catchment I: observations of rainfall-runoff response and geophysical conditions, Hydrol. Proc., 23(5), 702-718, 2009.
Graeff, T., Zehe, E., Schlaeger, S., Morgner, M., Bauer, A., Becker, R., Creutzfeld, B., Bronstert, A., Assessment of plot and field scale soil moisture dynamics by means of Spatial-TDR I: A quality assessment of retrieved soil moisture profiles in homogenous and strongly heterogeneous media, Hydr. Earth Syst. Sci., 14(6), 1007-1020, 2010.

Grayson, R.B., Western, A.W., Chiew, F.H.S, Blöschl, G., Preferred states in spatial soil moisture patterns: Local and nonlocal controls, Water Resour. Res., 33, 2897-2908, 1997.
Grayson, R.B., Western, A.W., Towards areal estimation of soil water content from point measurements: time and space stability of mean response, J. Hydrol. 207(1-2), 68-82, DOI: 10.1016/S0022-1694(98)00096-1, 1998.
Green, R., Sampling design and statistical methods for environmental biologists, John Wiley and Sons, New York, 1979.
Gurtz, J., Baltensweiler, A., Lang H., Spatially distributed hydrotope-based modelling of evapotranspiration and runoff in mountainous basins, Hydrol Proc., 13(17), 2751-2768, 1999.
Guse, B., Thieken, A.G., Merz, B., Effects of intersite dependence of nested catchment structures on probabilistic regional envelope curves, Hydrol. Earth Syst. Sci., 13, 1699-1712, 2009.
Gutknecht, D., Reszler, C., Blöschl, G., Das Katastrophenhochwasser vom 7. August 2002 am Kamp – eine erste Einschätzung (The August 7, 2002 – flood of the Kamp – a first assessment). Elektrotechnik und Informationstechnik, 119(12), 411-413, 2002.
GWR: iGravTM SG, Simplified superconducting gravimeter for portable operation, GWR Instruments, Inc., San Diego, USA, 2009.
Hajnsek, I., Jagdhuber, T., Schön, H., Papathanassiou, K.P., Potential of Estimating Soil Moisture under Vegetation Cover by means of PolSAR, IEEE Trans. Geosci. Remote Sensing, 47(2), 442-454, 2009.
Hakansson, G., Reconstruction of soil moisture profiles, Master's thesis, Royal Institute of Technology, Department of Electromagnetic Theory, Stockholm, 1997.
Harrell, F.E., Jr., Regression modeling strategies: with applications to linear models, logistic regression, and survival analysis, Springer, New York, 2001.
Hausbrock, S.N., Chabrillat, S., Kuhnert, M., Hostert, P., Kaufmann, H., Surface soil moisture quantification and validation based on hyperspectral data and field measurements, J. Applied Remote Sensing, 2, 023552, 2008.
Heggen, R.J., Normalized antecedent precipitation index. Journal of Hydrologic Engineering, 6(5), 377-381, 2001.
Heilmann, H. and Symmangk R., Böden. In: Pälchen, W., Walter, H.: Geologie von Sachsen. E. Schweizerbart'sche Verlagsbuchhandlung (Nägele u. Obermiller), Stuttgart, in German, 2008.
Heimovaara, T.J., Huisman, J.A., Vrugt, J.A., Bouten W., Obtaining the spatial distribution of water content along a TDR probe using the SCEM-UA Bayesian inverse modelling scheme, Vadose Zone J., 3, 1128-1145, 2004.
Heikkinen, R.K., Luoto, M. Kuussaari, M., Pöyry, J., New insights into butterfly-environment relationships using partitioning methods, Proc. R. Soc. B, 272, 2203-2210, 2005.
Herkelrath, W.N., Hamburg, S.P., Murphy, F., Automatic Real-Time Monitoring of Soil Moisture in a Remote Field Area with Time Domain Reflectometry, Water Resour. Res., 27(5), 857-864, 1991.
Hoeg, S., Uhlenbrook, S., Leibundgut, C., Hydrograph separation in a mountainous catchment-combining hydrochemical and isotopic tracers, Hydrol. Proc., 14(7), 1199-1216, 2000.
Holsten, A., Vetter, T., Vohland, K., Krysanova, V., Impact of climate change on soil moisture dynamics in Brandenburg with a focus on nature conservation areas, Ecol. Model., 220(17), 2076-2087, 2009.

Hrnčíř, M., Šanda, M., Kulasová, A., Cáslerová, M., Runoff formation in a small catchment at hillslope and catchment scales, Hydrol. Proc., 24, 2248-2256, 2010.
Holliger, K., Tronicke, J., Paasche, H., Dafflon, B., Quantitative Integration of hydrogeophysical data: Geostatistical approaches. In: Darnault, C. (Ed.), Overexploitation and Contamination of Shared Groundwater Resources, Springer, New York, 67-82, 2008.
Huebner, C., Schlaeger, S., Becker, R., Scheuermann, A., Brandelik, A., Schädel, W., Schuhmann R., Advanced measurement methods in time domain reflectometry for soil moisture determination, in Electromagnetic Aquametry, edited by K. Kupfer, pp. 317-347, Springer, Berlin, 2005.
Huisman, J.A., Hubbard, S., Redman, J.D., Annan, A.P., Measuring Soil Water Content with Ground Penetrating Radar: A Review, Vadose Zone J., 2(4), 476-491, 2003.
Huisman, J.A., Lin, C.P., Weihermüller, L., Vereecken, H., Accuracy of Bulk Electrical Conducvity Measurements with Time Domain Reflectometry, Vadose Zone J., 7(2), 426-433, 2008.
Hundecha, Y. and Bárdossy, A., Modelling of the effect of land use changes on the runoff generation of a river basin through parameter regionalization of a watershed model, J.Hydrol., 292(1-4), 281-295, 2004.
Jacob, T., Bayer, R., Chery, J., Jourde, H., Moigne, N. L., Boy, J.-P., Hinderer, J., Luck, B., Brunet, P., Absolute gravity monitoring of water storage variation in a karst aquifer on the larzac plateau (Southern France), J. Hydrol., 359, 105-117, 2008.
Jacob, T., Chery, J., Bayer, R., Moigne, N. L., Boy, J.-P., Vernant, P., and Boudin, F., Time-lapse surface to depth gravity measurements on a karst system reveal the dominant role of the epikarst as a water storage entity, Geophys, J. Int., 17, 347-360, 2009.
Jacobs, J.M., Meyers, D.A., Whitfield, B.M., Improved rainfall/runoff estimates using remotely-sensed soil moisture, J. Am. Water Resour. Assoc., 39(2), 313–324, 2003.
James, A. L. and Roulet, N. T., Investigating Hydrologic Connectivity and Its Association With Threshold Change in Runoff Response in a Temperate Forested Watershed, Hydrol. Proc., 21, 3391-3408, 2007.
Jayawardena, A.W. and Zhou, M.C., A modified spatial soil moisture storage capacity distribution curve for the Xinanjiang model, J. Hydrol., 227(1-4), 93-113, 2000.
Jones, S.B., and Or, D., Frequency domain analysis for extending time domain reflectometry water content measurement in highly saline soils, Soil Sci. Soc. Am. J.68, 1568-1577, 2004.
Joshi, C., Mohanty, B.P., Jacobs, J.M., Ines, V.M., Spatiotemporal analysis of soil moisture from point to footprint scale in two different hydroclimatic regions, Water Resour. Res., 47, W01508, DOI: 10.1029/2009WR009002, 2011.
Katra, I., Blumberg, D.G., Lavee, H., Sarah, P., A method for estimating the spatial distribution of soil moisture of arid microenvironments by close range thermal infrared imaging, International Journal of Remote Sensing, 27(12), 2599-2611, 2006.
Katra, I., Blumberg, D.G., Lavee, H., Sarah, P., Topsoil moisture patterns on arid hillsides - Micro-scale mapping by thermal infrared images, J. Hydrol., 334(3-4), 359-367, 2007.
Kemna, A., Vanderborght, J., Kulessa, B., Vereecken, H., Imaging and characterisation of subsurface solute transport using electrical resistivity tomography (ERT) and equivalent transport models, J. Hydrol., 267, 125-146, 2002.

Kim, J.G., Lee, G.H., Lee, J.S., Chon, C.M., Kim, T.H., Ha, K., Infiltration pattern in a regolith-fractured bedrock profile: field observation of a dye stain pattern, Hydrol Proc., 20(2), 241-250, 2005.
Kirsch, R., Groundwater Geophysics: A Tool for Hydrogeology, Springer, 2007.
Klaus, J. and Zehe, E., Modelling rapid flow response of a tile-drained field site using a 2D physically based model: assessment of 'equifinal' model setups, Hydrol Proc., 24(12), 1595-1609, 2010.
Kneis, D. and Heistermann, M., Quality assessment of radar-based precipitation estimates with the example of a small catchment. Hydrologie und Wasserbewirtschaftung, 53(3), 160-171, 2009.
Kneis, D., Bürger, G., Bronstert, A., Evaluation of medium-range runoff forecasts for a 50 km² watershed. J. Hydrol., submitted 2010.
Knight, J.H., Ferré, T.P.A., Rudolph, D.L., Kachanoski, R.G., A numerical analysis of the effects of coatings and gaps upon relative dielectric permittivity measurement with time domain reflectometry, Water Resour. Res., 33, 1455-1460, 1997.
Koehler, B., Zehe, E., Corre, M.D., Veldkamp, E., An inverse analysis reveals limitations of the soil-CO2 profile method to calculate CO2 production and efflux for well-structured soils, Biogeosciences, 7(8), 2311-2325, 2010.
Koster, R., Dirmeyer, P.A., Guo, Z., Bonan, G., Chan, E., Cox, P., Gordon, C.T., Kanae, S., Kowalczyk, E., Lawrence, D., Liu, P., Lu, C.H., Malyshev, S., McAvaney, B., Mitchell, K., Mocko, D., Oki, T., Oleson, K., Pitman, A., Vasic, R., Xue, Y., Yamanda, T., Regions of strong coupling between soil moisture and precipitation, Science, 305, 1138-1140, 2004.
Koyama, C., Korres, W., Fiener, P., Schneider, K., Variability of Surface Soil Moisture Observed from Multitemporal C-Band Synthetic Aperture Radar and Field Data, Vadose Zone J., 9, 1014-1024, 2010.
Krause, S. and Bronstert, A., The impact of groundwater-surface water interactions on the water balance of a mesoscale lowland river catchment in northeastern Germany, Hydrol. Proc., 21(2), 169-184, 2007.
Krysanova, V., Müller-Wohlfeil, D.I., Becker, A., Development and test of a spatially distributed hydrological water quality model for mesoscale watersheds, Ecol. Model., 106(1-3), 261-289, 1998.
Kume, T., Komatsu, H., Kuraji, K., Suzuki, M., Less than 20-min time lags between transpiration and stem sap flow in emergent trees in a Bornean tropical rainforest, Agricultural and Forest Meteorology, 148 (6-7), 1181-1189, 2008.
Kume, T., Takizawa,H., Yoshifuji, N., Tanaka, K., Tantasirin, C., Tanaka, N., Suzuki, M., Impact of soil drought on sap flow and water status of evergreen trees in a tropical monsoon forest in northern Thailand, Forest Ecology and Management, 238(1-3), 220-230, 2007.
Kupfer, K., Trinks, E., Wagner, N., Huebner, C., TDR measurements and simulations in high loosy bentonite materials, Measurement Science & Technology, 18, 1118-1136, 2007.
Kustas, W. P., Zhan, X., Schmugge, T.J., Combining optical and microwave remote sensing for mapping energy fluxes in a semiarid watershed, Remote Sensing of Environment, 64(2), 116-131, 1998.
Ladouche, B., Probst, A., Viville, D., Idir, S., Baque, D., Loubet, M., Probst, J.L., Bariac, T., Hydrograph separation using isotopic, chemical and hydrological approaches (Strengbach catchment, France), J. Hydrol., 242(3-4), 255-274, 2001.

Lakshmi, V., The role of satellite remote sensing in the Prediction of Ungauged Basins, Hydrol. Proc., 18(5), 1029-1034, 2004.
Landesamt für Umwelt und Geologie, Bodenkonzeptkarte 25 des Freistaates Sachsen, Blatt 5248, Altenberg, in German, 2006.
Larson, K.M., Small, E.E. Gutmann, E., Bilich, A.L., Braun, J.J., Zavorotny, V.U., Use of GPS receivers as a soil moisture network for water cycle studies, Geophysical Research Letters, 35(24), 2008.
Larson, K.M., Braun, J.J., Small, E.E., Zavorotny, V.U., Gutmann, E., Bilich, A.L., GPS Multipath and Its Relation to Near-Surface Soil Moisture Content, IEEE JOURNAL OF SELECTED TOPICS IN APPLIED EARTH OBSERVATIONS AND REMOTE SENSING, 3(1), 91-99, 2010.
Latron, J., and Gallart, F., Runoff generation processes in a small Mediterranean research catchment (Vallcebre, Eastern Pyrenees), J. Hydrol., 358, 206-220, 2008.
Laurent, J.P., Ruelle, P., Delage, L., Zairi, A., Nouna, B.B., Adjmi, T., Monitoring Soil Water Content Profiles with a Commercial TDR System: Comparative Field Tests and Laboratory Calibration, Vadose Zone J., 4, 1030-1036, 2005.
Lehmann, P., Hinz, C., McGrath, G., Tromp-van Meerveld, H.J., McDonnell, J.J., Rainfall threshold for hillslope outflow: an emergent property of flow pathway connectivity, Hydr. Earth Syst. Sci., 11, 1047-1063, 2007.
Lesmes, D.P., Friedman, S.P., Relationship between the electrical and hydrogeological properties of rocks and soil, in: Robin, Y. and Hubbard, S.S., Hydrogeophysics, Water Science and Technology Library, Volume 50, Springer, Dordrecht, 2005.
Lin, C.P., Chung, C.C., Huisman, J.A., Tang, S.H., Clarification and Calibration of Reflection Coefficient for Electrical Conductivity Measurement by Time Domain Reflectometry, Soil Sci. Soc. Am. J., 72(4), 1033-1040, 2007.
Lin, M.W., Thaduri, J., Abatan, A.O., Development of an electrical time domain reflectometry (ETDR) distributed strain sensor, Measurement Science & Technology, 16, 1495-1505, 2005.
Lin, H., Temporal Stability of Soil Moisture Spatial Pattern and Subsurface Preferential Flow Pathways in the Shale Hills Catchment, Vadose Zone J., 5, 317-340, 2006.
Lindenmaier, F., Zehe, E., Dittfurth, A., Ihringer, J., Process Identification at a slow-moving Landslide in the Vorarlberg Alps, Hydrol Proc., 19(8), 1635-1651, 2005.
Longobardi A, Villani, P., Grayson, R.B., Western, A.W., On the relationship between runoff coefficient and catchment initial conditions, In Proceedings of MODSIM 2003; 867-872, 2003.
MacNally, R., Hierarchical partitioning as an interpretative tool in multivariate inference, Aust. J. Ecol., 21, 224-228, 1996.
Maidment, DR (Ed.), Handbook of Hydrology, McGraw-Hill, Inc., 1993.
Malicki, M.A., Plagge, R., Roth, C.H., Improving the calibration of dielectric TDR soil moisture determination taking into account the solid soil, European J. of Soil Science, 47, 357-366, 1996.
Maurer, T., Physikalisch begründete, zeitkontinuierliche Modellierung des Wassertransports in kleinen ländlichen Einzugsgebieten. Universität Karlsruhe, Mitteilungen des Instituts für Hydrologie und Wasserwirtschaft. Vol. 61, in German, 1997.
McGlynn, B.L., McDonnell, J.J., Shanley, J.B., Kendall, C., Riparian zone flowpath dynamics during snowmelt in a small headwater catchment, J. Hydrol., 222(1-4), 72-92, 1999.

McGlynn, B.L., McDonnell, J.J., Seibert, J., Kendall, C., Scale effects on headwater catchment runoff timing, flow sources, and groundwater-streamflow relations, Water Resour. Res., 41, W05002, DOI: 10.1029/2004WR003657, 2005.
McIntyre, N., Al-Qurashi, A., Wheater, H., Regression analysis of rainfall-runoff data from an arid catchment in Oman, HYDROLOGICAL SCIENCE JOURNAL, 52(6), 1103-1118, 2007.
McLeod, A.I. and Xu, C., http://cran.r-project.org/web/packages/bestglm/, 2010.
McNamara, J.P., Chandler, D., Seyfried, M., Achet, S., Soil moisture states, lateral flow, and streamflow generation in a semi-arid, snowmelt-driven catchment, Hydrol Proc., 19, 4023-4038, 2005.
McPherson J.M. and Jets, W., Effects of species' ecology on the accuracy of distribution models. Ecography, 30, 135-151, 2007.
Merz, B., and Bárdossy, A., Effects of spatial variability on the rainfall runoff process in a small loess catchment, J. Hydrol., 213(1-4), 304-317, 1998.
Merz, B., Bárdossy, A., Schiffler, G.R., Different methods for modelling the areal infiltration of a grass field under heavy precipitation, Hydrol Proc., 16, 1383-1402, 2002.
Merz, B. and Plate, E.J., An analysis of the effects of spatial variability of soil and soil moisture on runoff, Water Resour. Res., 33(12), 2909-2922, 1997.
Merz, R. and Blöschl, G., A process typology of regional floods, Water Resour. Res., 39(12), 1340, DOI: 10.1029/2002WR001952, 2003.
Meyles, E., Williams, A., Ternan, L., Dowd, J., Runoff generation in relation to soil moisture patterns in a small Dartmoor catchment, Southwest England, Hydrol Proc., 17, 251-264, 2003.
Montgomery, D.R, Dietrich, W.E., Torres, R., Anderson, S.P., Heffner, J.T., Loauge, K. , Hydrologic response of a steep, unchanneled valley to natural and applied rainfall, Water Resour. Res., 33(1), 91-109, 1997.
Montgomery, D.R, and Dietrich, W.E., Runoff generation in a steep, soil-mantled landscape, Water Resour. Res., 38(9), WR000822, 2002.
Moret, D., Arrúe, J.L., López, M.V., Gracia. R., A new TDR waveform analysis approach for soil moisture profiling using a single probe, J. Hydrol. 321, 163-172, 2006.
Moret-Fernández, D.; Lera, F., Arrúe, J.L., López, M.V., Measurement of soil bulk electrical conducctvity using partially coated TDR probes, Vadose Zone J., 8, 594-600, 2009.
Morgan J.A. and Tatar J.F., Calculation of the Residual Sum of Squares for all Possible Regressions, Technometrics, 14, 317-325, 1972.
Mosley, M.P. and McKerchar, A.L., Streamflow, In: Maidment, D.R. (Ed.): Handbook of Hydrology, McGraw-Hill, Inc, 1993.
Mualem, Y., Extension of the Similarity Hypothesis Used for Modeling the Soil Water Characteristics, Water Resour. Res., 13(4), 773-780, 1977.
Nathan, R.J. and McMahon, T.A., Evaluation of Automated Techniques for Base Flow and Recession Analyses, Water Resour. Res., 26(7), 1465-14, 1990.
Nichol, C., Beckie, R., Smith, L., Evaluation of uncoated and coated time domain reflectometry probes for high electrical conductivity systems, Soil Sci. Soc. Am. J., 66, 1454-1465, 2002.
Olea, P.P., Mateo-Tomás, P., de Frutos, Á., Estimating and Modelling Bias of the Hierarchical Partitioning Public-Domain Software: Implications in Environmental Management and Conservation, Plos One, 5(7), e11698, DOI: 10.1371/journal.pone.0011698, 2010.

Oswald, B., Full wave solution of inverse electromagnetic problems, Ph.D. thesis Swiss Federal Institute of Technology, Zürich, 2000.
Niehoff, D., Fritsch, U., Bronstert, A., Land-use impacts on storm-runoff generation: scenarios of land-use change and simulation of hydrological response in a meso-scale catchment in SW-Germany, J. Hydrol., 267(1-2), 80-93, 2001.
Niehoff, D., Modellierung des Einflusses der Landnutzung auf die Hochwasserentstehung in der Mesoskala, Brandenburg. Umweltberichte, Potsdam, Heft 11, in German, 2002.
Noribiato, D., Borga, M., Merz, R., Blöschl, G., Carton, A., Controls on event runoff coefficients in the eastern Italian Alps, J. Hydrol., 375, 312-325, 2009.
Noto, L.V., Ivanov, V.Y., Bras, R.L., Vivoni E.R., Effects of initialization on response of a fully-distributed hydrologic model, J. Hydrol., 352(1-2), 107-125, 2008.
Oswald, B., Benedickter, H.R., Bächtold, W., Flühler, H., Spatially resolved water content profiles from inverted time domain reflectometry signals, Water Resour. Res., 39(12), 1357, 2003.
Paasche, H., Tronicke, J., Holliger, K., Green, A. G., Maurer, H., Integration of diversephysical-property models: Subsurface zonation and petrophysical parameter estimation based on fuzzy c-means cluster analyses, Geophysics, 71, H33-H44, 2006.
Parajka, J., Naemi, V., Blöschl, G., Wagner, W., Merz, R., Scipal, K., Assimilating scatterometer soil moisture data into conceptual hydrologic models at coarse scales, Hydr. Earth Syst. Sci., 10, 353-368, 2006.
Penna, D., Borga, M., Norbiato, D., Fontana, G.D., Hillslope scale soil moisture variability in a steep alpine terrain, J. Hydrol., 364, 311-327, 2009.
Penna, D., Tromp-van Meerveld, H.J., Gobbi, A., Borga, M., Dalla Fontana, G., The influence of soil moisture on threshold runoff generation processes in an alpine headwater catchment, Hydr. Earth Syst. Sci., 15, 689-702, 2011.
Peschke, G., Soil moisture and runoff components from a physically founded approach, Acta Hydrophys. 31, 191-205, 1987.
Peters, N.E., Freere, J., Auenbach, B.T., Hydrological Dynamics of the Panola Mountain Research Watershed, Georgia, Ground water, 41(7), 973-988, 2003.
Pfister, L., Iffly, J.F., Hoffmann, L., Use of regionalized stormflow coefficients with a view to hydroclimatological hazard mapping, Hydrological Science Journal, 47(3), 479-491, 2003.
Pfister, L., Drogue, A., Humbert, J., Iffly, J.F., Matgen, P., Hoffmann, L., Predicting peak discharge through empirical relationships between rainfall, groundwater level and basin humidity in the Alzette River basin (Grand-Duchy of Luxembourg), Journal of Hydrology and Hydromechanics, 51(3), 210-220, 2003.
Pilgrim, D.H. and Cordery, I., Flood runoff. In: Maidment, D.R. (Ed.): Handbook of Hydrology, McGraw-Hill, Inc., 1993.
Pöhler, H.L., Anpassung von WaSiM-ETH und die Erstellung und Berechnung von Landnutzungsund Klimaszenarien f¨ur die Niederschlag-Abfluss-Modellierung am Beispiel des Osterzgebirges, Freiberg, Disertation, in German, 2006.
Porporato, A., Daly, E., Rodriguez-Iturbe, I., Soil water balance and ecosystem response to climate change, American Naturalist, 164(5), 625-632, 2004.
Prange, N., Personal comments about bimodal peaks in the Weißeritz catchment, TU Dresden, Germany, 2010.

R-Team Development Core, R: A Language and Environment for Statistical Computing. R Foundation for Statistical Computing, Vienna, Austria. ISBN 3-900051-07-0. http://cran.r-project.org/, 2009.
Refsgaard, J.C., Storm, B., MIKE SHE, in Singh, V.P., Computer models of watershed hydrology, Water Resources Publication, Highlands Ranch, Colorado, 1995.
Refsgaard, J.C., Validation and intercomparison of different updating procedures for real-time forecasting, Nordic Hydrol., 28, 65-84, 1997.
Reineking B., Schröder B., Constrain to perform: Regularization of habitat models, Ecol. Model., 193(3-4), 675-690, 2006.
Rejiba, F., Cosenza, P., Camerlynck, C., Tabbagh, A., Three-dimensional transient electro-magnetic modeling for investigating the spatial sensitivity of time domain reflectometry measurements, Water Resour. Res., 41, W09411, DOI: 10.1029/2004WR003505, 2005.
Reusser, D.E., Blume, T., Schaefli, B., Zehe, E., Analysing the temporal dynamics of model performance for hydrological models, Hydr. Earth Syst. Sci., 13(7), 999-1018, 2009.
Rivera Villarreyes, C.A., Baroni, G., Oswald, S.E., Integral quantification of seasonal soil moisture changes in farmland by cosmic-ray neutrons, Hydrol. Earth Syst. Sci. Discuss., 8, 6867-6906, DOI: 10.5194/hessd-8-6867-2011, 2011.
Robinson, D.A., Bell, J.P., Batchelor, C.H., Influence of iron minerals on the determination of soil water content using dielectric techniques, J. Hydrol., 161, 169-180, 1994.
Robinson, D.A., Jones, S.B., Wraith, J.M., Or, D., Friedman, S.P., A Review of Advances in Dielectric and Electrical Conductivity Measurement in Soils, Vadose Zone J., 2, 444-475, 2003.
Sheets, C.H., Malicki, M.A., Plagge, R., Empirical evaluation of the relationship between soil dielectric constant and volumetric water content and the basis for calibrating soil moisture measurements by TDR, J. of Soil Science, 43, 1-13, 1992.
Roth, K.U., Wollschlager, U., Cheng, Z.H., Zhang, J.B., Exploring Soil Layers and Water Tables with Ground-Penetrating Radar, Pedosphere, 14, 273-282, 2004.
Rubin, Y. and Hubbard, S.S., Hydrogeophysics, Springer, Dordrecht, 2005.
Sayde, C., Gregory, C., Gill-Rodriguez, M., Tufillaro, N., Tyler, S., van de Giesen, N., English, M., Cuenca, R., Selker, J.S., Feasibility of soil moisture monitoring with heated fiber optics, Water Resour. Res., 46, W06201, DOI: 10.1029/2009WR007846, 2010.
Schädel, W., Schritte zur Verbesserung der Hochwasserwarnung mittels Online-Bodenfeuchtemessungen, Ph.D. thesis, Institute of Water and River Basin Management, Univ. of Karlsruhe, in German, 2006.
Scheuermann, A., Huebner, C., Schlaeger, S., Wagner, N., Becker, R., Bieberstein, A., Spatial-Time Domain Reflectometry and its application for the measurement of water content distributions along flat ribbon cables in a full scale levee model, Water Resour. Res., 45, W00D24, DOI: 10.1029/2008WR007073, 2009.
Schlaeger, S., A fast TDR-inversion technique for the reconstruction of spatial soil moisture content, Hydrol. Earth Syst. Sci., 9, 481-492, 2005.
Schmitz, G.H., Cullmann, J., PAI-OFF: A new proposal for online flood forecasting in flash flood prone catchments, J. Hydrol., 360(1-4), 1-14, 2008.
Schneeberger, K., Schwank, M., Stamm, C., De Rosnay, P., Matzler, C., Flühler, H., Topsoil structure influencing soil water retrieval by microwave radiometry, Vadose Zone J., 3(4), 1169-1179, 2004.

Schön, J.H., Physical properties of rocks: Fundamentals and principles of Petrophysics, Pergamon, 1998.
Schulla, J., Hydrologische Modellierung von Flussgebieten zur Abschätzung der Folgen von Klimaänderungen. Dissertation, ETH- Zürich, in German, 1997.
Schulla, J. and Jasper, K., Modell descrition WaSiM-ETH, 2007.
Schulze, E.D., Beck, E., Müller-Hohenstein, K., Lawlor, D. Plant ecology, Springer, 2005.
Sheets, K.R., and Hendrickx, J.M.H. (1995): Non-invasive soil water content measurement using electromagnetic induction, Water Resour. Res., 31, 2401-2409, 1995.
Singh, V.P., Computer models of watershed hydrology, Water Resources Publication, Highlands Ranch, Colorado, 1995.
Sivapalan, M., Process complexity at hillslope scale, process simplicity at the watershed scale: is there a connection? Hydrol. Proc., 17(5), 1037-1041, 2003.
Šimunek, J., Šejna, M., Van Genuchten, M. T., Hydrus 2-D software package for simulating the two-dimensional movement of water, heat, and multiple solutes in variably saturated media. Riverside, U.S. Salinity Laboratory, Agricultural Research Service ARS, U.S. Department of Agriculture USDA, 1999.
Spittlehouse, D.L., Using time domain reflectometry in stony forest soil, Canadian Journal of Soil Science, 80(1), 3-11, 2000.
Spence, C., Guan, X.J., Phillips, R., Hedstrom, N., Granger, R., Reid, B., Storage dynamics and streamflow in a catchment with a variable contributing area, Hydrol. Proc., 24, 2209-2221, 2009.
Stamm, C., Sermet R., Leuenberger, J., Wunderli, H., Wydler, H., Flühler, H., Gehre, M., Multiple tracing of fast solute transport in a drained grassland soil, Geoderma, 109, 245-268, 2002.
Starr, J. L. and Timlin, D. J., Using high-resolution soil moisture data to assess soil water dynamics in the vadose zone, Vadose Zone J., 3, 926-935, 2004.
Steele-Dunne, S.C., Rutten, M.M., Krzeminska, D.M., Hausner, M., Tyler, S.W., Selker, J., Bogaard, T.A., van de Giesen, N.C., Feasibility of soil moisture estimation using passive distributed temperature sensing, Water Resour. Res., 46, W03534, DOI: 10.1029/2009WR008272, 2010.
Steinbrech, A. and Weiler, M., Ausweisung der für die Hochwasserentstehung wichtigen Abflussbildungsprozesse für Baden-Württemberg, In: Caspar, M., and Gronz, O., Forum für Hydrologie und Wasserbewirtschaftung Hydrologische Wissenschaften; Fachgemeinschaft in der DWA, 171-185, 2010.
Tang, Q., Durand, M., Lettenmaier, D.P., Hong, Y., Satellite-based observations of hydrological processes, International Journal of Remote Sensing, 31(14), 3661-3667, 2010.
Tani, M., Runoff generation processes estimated from hydrological observations on a steep forested hillslope with a thin soil layer, J. Hydrol., 200(1-4), 84-109, 1997.
Teuling, A. J., Uijlenhoet, R., Hupet, F., Van Loon, E.E., Troch P.A. Estimating spatial mean root-zone soil moisture from point-scale observations, Hydrol. Earth Syst. Sci., 10(5), 755-767, 2006.
Thapa, P., Physically-based spatially distributed rainfall runoff modelling for soil erosion estimation. PhD-Thesis, Institute of Hydraulic Engineering, University of Stuttgart, 160pp., 2009.
Timmermans, W. J., Su, J., Olioso, A., Footprint issues in scintillometry over heterogeneous landscapes, Hydrol. Earth Syst. Sci., 13(11), 2179-2190, 2009.

Tolson, B.A. and Shoemaker, C.A., Dynamically dimensioned search algorithm for computationally efficient watershed model calibration, Water Resour. Res., 43(1), W01413, DOI: 10.1029/2005WR004723, 2007.
Tolson, B.A. and Shoemaker, C.A., Reply to comment on "Dynamically dimensioned search algorithm for computationally efficient watershed model calibration" by Ali Behrangi et al. Water Resour. Res., 44, W012604, DOI: 10.1029/2008WR006862, 2008.
Topp, G.C., Davis, J.L., Annan, A.P., Electromagnetic determination of soil water content: measurement in coaxial transmission lines, Water Resour. Res., 16, 574-582, 1980.
Topp, G.C., and Davis, J.L., Electromagnetic determination of soil water content using TDR: Applications to wetting fronts and steep gradients, Soil Sci. Soc. Am. J., 46, 672-678, 1982.
Tromp-van Meerveld, H. J. and McDonnell, J.J.: Threshold relations in subsurface stormflow 1. A storm analysis of the Panola hillslope, Water Resour. Res., 42, W02410, DOI: 10.1029/2004WR003778., 2006a.
Tromp-van Meerveld, H. J., McDonnell, J.J., Threshold relations in subsurface stormflow: 2. The fill and spill hypothesis, Water Resour. Res., 42, W02411, DOI: 10.1029/2004WR003800, 2006b.
Tromp-van Meerveld, H.J., and Weiler, M., Hillslope dynamics modeled with increasing complexity, J. Hydrol., 361, 24-40, 2008.
Trubilowicz, J., Cai, K., Weiler, M., Viability of motes for hydrological measurement, Water Resour. Res., 45, W00d22, 10.1029/2008wr007046, 2009.
Uhlenbrook, S., Frey, M., Leibundgut, C., Maloszewski, P., Hydrograph separations in a mesoscale mountainous basin at event and seasonal timescales, Water Resour. Res., 38(6), 1096, 2002.
Uhlenbrook, S. and Leibundgut, C., Process-oriented catchment modeling and multiple-response validation, Hydrol. Proc., 16, 423-440, 2002.
Uhlemann, S., Thieken, A.H., Merz, B., A consistent set of trans-basin floods in Germany between 1952-2002, Hydrol. Earth Syst. Sci., 14, 1277-1295, 2010.
Van Dam, R.L., Schlager, W., Dekkers, M.J., Huisman, J.A., Iron oxides as a cause of GPR reflections, Geophysics, 67(2), 536-545, 2002.
VanderKwaak, J. E. and Loague, K., Hydrologic-response simulations for the R-5 catchment with a comprehensive physics-based model, Water Resour. Res., 37(4), 999-1013, 2001.
Van Genuchten, M.T., A closed form equation forpredictingthe hydraulic conductivity of unsaturated soils, Soil Sci. Soc. Am. J., 44, 992-998, 1980.
Van Schaik, N.L.M.B., Hendriks, R.F.A., van Dam, J.C., Parameterization of Macropore Flow Using Dye-Tracer Infiltration Paterns in the SWAP Model, Vadose Zone J., 9, 95-106, 2010.
Vereecken, H., Binley, A., Cassiani, G., Revil, A., Titov, K., Applied Hydrogeophysics, Springer, Dordrecht, 2006.
Vivoni, E.R., Entekapi, D., Bras, R.L., Ivanov, V.Y., Controls on runoff generation and scale-dependence in a distributed hydrologic model, Hydrol. Earth Syst. Sci., 11, 1683-1701, 2007.
Vogel, H.J. and Roth, K., Moving through scales of flow and transport in soil, J. Hydrol., 272, 95-106, 2003.
Vogel, H.J., Hoffmann, H., Roth, K., Studies of crack dynamics in clay soil - I. Experimental methods, results, and morphological quantification, Geoderma, 125(3-4), 203-211, 2005a.
Vogel, H.J., Hoffmann, H., Leopold, A., Roth K., Studies of crack dynamics in clay soil - II. A physically based model for crack formation. Geoderma, 125(3-4), 213-223, 2005b.

Vogel, H.J. and Ippisch, O., Estimation of a critical spatial discretization limit for solving Richards' equation at large scales, Vadose Zone J., 7(1), 112-114, 2008.
Wagener, T. and Gupta, H.V., Model identification for hydrological forecasting under uncertainty, Stochastic Environmental Research and Risk Assessment, 19(6), 378-387, 2005.
Wagner, W., Blöschl, G., Pampaloni, P., Calvet, J.C., Bizzarri, B., Wigneron, J.P., Kerr, Y., Operational readiness of microwave remote sensing of soil moisture for hydrologic applications, Nordic Hydrology, 38(1), 1-20, 2007a.
Wagner, W., Naeimi, V., Scipal, K., de Jeu, R., Martínez-Fernández, J., Soil moisture from operational meteorological satellites, Hydrogeology Journal, 15, 121-131, 2007b.
Walsh, C. and Mac Nally, R., The hier.part package. Hierarchical Partitioning. R project for statistical computing. URL: http://cran.r-project.org/, 2003.
Weiler, M. and Flühler, H., Inferring flow types from dye patterns in macroporous soils, Geoderma, 120(1-2), 137-153, 2004.
Weiler, M. and McDonnell, J.J., Virtual experiments: a new approach for improving process conceptualization in hillslope hydrology, J. Hydrol., 285, 3-18, 2004.
Weiler, M. and McDonnell, J.J., Conceptualizing lateral preferential flow and flow networks and simulating the effects on gauged and ungauged hillslopes, Water Resour. Res., 43(3), W03403, 2007.
Wenninger, J., Uhlenbrook, S., Lorentz, S., Leibundgut, C., Identification of runoff generation processes using combined hydrometric, tracer and geophysical methods in a headwater catchment in South Africa, Hydrological Science Journal, 53(1), 65-80, 2008.
Western, A.W., Blöschl, G., Grayson, R.B., Geostatistical characterisation of soil moisture patterns in the Tarrawarra a catchment, J. Hydrol., 205, 20-37, 1998.
Western, A.W., Zhou, S.L., Grayson, R.B., McMahon, T.A., Blöschl, G., Wilson, D.J., Spatial correlation of soil moisture in small catchments and its relationship to dominant spatial hydrolgical processes, J. Hydrol., 286, 113-134, 2004.
Wienhoefer, J., Germer, K., Lindenmaier, F., Färber, A., Zehe, E., Applied tracers for the observation of subsurface stormflow at the hillslope scale, Hydrol. Earth Syst. Sci., 13, 1145-1161, 2009.
Wigmosta, M.S. and Vail, L.W., Lettenmaier ,D.P., A distributed hydrology vegetation model for complex terrain, Water Resour Res., 306, 1665-1679, 1994.
Wilker, H., Drusch, M., Seuffert, G., Simmer, C., Effects of the near-surface soil moisture profile on the assimilation of L-band microwave brightness temperature, J. Hydrometeorology, 7(3), 433-442, 2006.
Williams, C.J., McNamara, J.P., Chandler, D.G., Controls on the temporal and spatial variability of soil moisture in a mountainous landscape: the signature of snow and complex terrain, Hydr. Earth Syst. Sci., 13, 1325-1336, 2009.
Wilson, D.J., Western, A.W., Grayson, R.B., Identifying and quantifying sources of variability in temporal and spatial soil moisture observations, Water Resour. Res., 40(2), W2507, 2004.
Wollny, K., Die Natur der Bodenwelle des Georadar und ihr Einsatz zur Feuchtebestimmung. Herbert Utz Verlag, Wiss., München, 1999.
Xia, J., O'Connor, K.M., Kachroo, RK.., Liang, G.C., A non-linear perturbation model considering catchment wetness and its application in river flow forecasting. J. Hydrol., 200(1-4), 164-178. DOI: 10.1016/S0022-1694(97)00013-9, 1997.

Zappa, M., Objective quantitative spatial verification of distributed snow cover simulations—an experiment for the whole of Switzerland, Hydrological Science Journal, 53, 179-191, 2008.
Zehe, E., and Flühler, H., Slope scale variation of flow patterns in soil profiles, J. Hydrol., 247, 116-132, 2001a.
Zehe, E. and Flühler, H., Preferential transport of isoproturon at a plot scale and a field scale tile drained site, J. Hydrol., 247(1-2), 100-115, 2001b.
Zehe, E., Maurer, T., Ihringer, J., Plate, E., Modeling water flow and mass transport in a Loess catchment, Physics and Chemistry of the Earth Part B-Hydrology Oceans and Atmosphere, 26(7-8), 487-507, 2001.
Zehe, E., and Blöschl, G., Predictability of hydrologic response at the plot and catchment scales – the role of initial conditions, Water Resour. Res., 40, W10202, 2004.
Zehe, E., Becker, R., Bárdossy, A., Plate, E., Uncertainty of simulated catchment sale runoff response in the presence of threshold processes: role of initial soil moisture and precipitation, J. Hydrol., 315(1-4), 183-202, 2005.
Zehe, E, Lee, H, Sivapalan, M., Dynamical process upscaling for deriving catchment scale state variables and constitutive relations for meso-scale process models, Hydrol. Earth Syst. Sci., 10(6): 981-996, 2006.
Zehe, E., Elsenbeer, H., Lindenmaier, F., Schulz, K., Blöschl, G., Patterns of predictability in hydrological threshold systems, Water Resour. Res., 43, W07434, 2007.
Zehe, E. and Sivapalan, M., Threshold behavior in Hydrological Systems as (human) Geo-Ecosystems: Manifestations, Controls and Implications, Hydrol. Earth Syst. Sci., 13, 1273-1297, 2009.
Zehe, E., Graeff , T., Morgner, M., Bauer, A., Bronstert, A., Plot and field scale soil moisture dynamics and subsurface wetness control on runoff generation in head water in the Ore Mountains, Hydrol. Earth Syst. Sci., 14, 873-889, 2010.
Zeppel, M., Macinnis-Ng, C.M.O., ford, C.R., Eamus, D., The response of sap flow to pulses of rain in a temperate Australian woodland, Plant and Soil, 305(1-2), 121-130, 2008.
Zillgens, B., Merz, B., Kirnbauer, R., Tilch, N., Analysis of the runoff response of an alpine catchment at different scales, Hydrol. Earth Syst. Sci., 14, 1441-1454, 2007.
Zimmermann, B, Zehe, E., Hartmann, N.K., Elsenbeer, H., Analyzing spatial data: An assessment of assumptions, new methods, and uncertainty using soil hydraulic data, Water Resour. Res., 44, W10408, 2008.
Zreda, M., Desilets, D., Ferré, T.P.A., Scott, R.L., Measuring soil moisture content noninvasively at intermediate spatial scale using cosmic-ray neutrons, Geophysical Research Letters, 35(21), L21402, 10.1029/2008gl035655, 2008.

List of Figures

List of Tables

Acknowledgements:

First of all I would like to thank my supervisors Erwin Zehe from the Chair for Hydrology at the Karlsruhe Institute of Technology KIT and Axel Bronstert from the Institute of Earth and Environmental Science at University of Potsdam. It was Erwin who gave me a lot of input and understanding in fruitful discussions about the influence of the small scale. Axel supported me by the application and installation of new sensors and always has time for a discussion.

I would like to thank Ilja Tromp Van Meerveld from Vrije Universiteit, Amsterdam, the Netherlands for taking the time to work through my thesis.

Great thanks go to Theresa Blume for long nights and days of discussing which the ongoing processes are and what tool can be used to understand it.

I would like to thank Andreas Bauer and Markus Morgner for their formidable determination in installing and testing the equipment.

Furthermore, I would like to thank Dominik Reusser, Andre Terwei, Silja Hund, Erik Sommerer, Enrico Grams, Heiko Thoss, Niko Bornemann, Bettina Schaefli Maik Heistermann, David Kneis, Thomas Jagdhuber, Peter Biro, Katharina Appel and Peter Eckard, for their help during the field season and laboratory work, and again Dominik Reusser, Till Francke, Boris Schröder, Jan Wienhöfer, Stephan Jakobi, Christian Mohr, Benjamin Creutzfeldt, Conrad Jackisch, Julian Klaus, Alexandre Cunha Costa, Celia Kirkby, Damaris Zurell, Loes van Schaik, Julia Reinhard, Sibylle Itzerott and Tobias Vetter for their valuable comments.

I would like to thank Peter Senft for permanent observation of the measurement equipment. and Uwe Höhne and the Landeshochwasserzentrum Sachsen LfULG and Ulf Winkler the Landestalsperrenverwaltung and for the good cooperation. I furthermore thank Dr. Sven Irrgang from Sachsenforst department Bärenfels for supporting field measurements with Spatial TDR.

Special thanks are going to my family with Cathrin, Helena and Frieda leading the way, for their patience with my never ending work and the high labour costs.

This study was partly funded by the German Ministry of Education and Research (BMBF) as part of RIMAX (Risikomanagement extremer Hochwasserereignisse), by the University of Potsdam, the Potsdam Graduate School, and by the Technische Universität München. It is part of the OPAQUE (operational discharge and flooding predictions in head catchments) project that aims at improving operational flood forecasting in mountainous headwaters (FKZ number 0330713D).

Appendix:

Table 1: Event data set of the Becherbach, with accumulated event precipitation (P), 2 hours sum precipitation (*P2h*), duration of precipitation (*DP*), mean intensity of rainfall (I), antecedent precipitation index of the past 30 days with an *a* of 0.95 ($API^{30}_{0.95}$), antecedent precipitation of the past 60 days (AP^{60}), runoff coefficient (C_r), pre-event soil moisture at the two clusters (WC_0), pre-event runoff (q_0), and coefficient of variation of soil moisture at cluster C2 (*CV*).

Date	*P* [mm]	*P2h* [mm]	*DP* [h]	*I* [mm/h]	$API^{30}_{0.95}$ [mm]	AP^{60} [mm]	C_r [-]	WC_0 C1 [m^3m^{-3}]	WC_0 C2 [m^3m^{-3}]	q_0 [$l\ s^{-1}km^{-2}$]	*CV* [-]
05.05.2007 01:00	29.88	0.26	1.38	6.65	0.03	45.28	0.00	0.23	0.25	1.15	0.24
14.05.2007 21:00	11.55	1.15	0.54	6.65	0.46	79.35	0.00	0.26	0.28	1.11	0.25
22.05.2007 17:00	30.97	9.40	0.58	9.25	0.02	84.79	0.01	0.26	0.30	0.96	0.24
28.05.2007 18:00	21.05	1.10	0.75	9.74	7.52	113.36	0.01	0.31	0.31	1.39	0.26
16.06.2007 01:00	28.70	0.01	0.67	10.64	1.21	161.13	0.00	0.29	0.25	1.45	0.22
21.06.2007 09:00	16.55	8.90	0.54	8.89	0.25	195.29	0.00	0.30	0.27	1.45	0.22
05.07.2007 23:00	9.30	0.19	0.71	3.33	5.39	252.36	0.00	0.32	0.29	1.88	0.28
21.08.2007 02:00	26.64	0.27	0.88	4.99	0.63	216.09	0.01	0.31	0.28	4.66	0.27
22.08.2007 03:00	12.24	5.41	0.58	3.49	10.22	240.49	0.01	0.33	0.31	5.61	0.27
05.09.2007 00:00	14.13	1.10	0.88	2.37	2.22	233.22	0.00	0.33	0.30	4.33	0.27
11.09.2007 01:00	27.12	2.39	3.00	2.11	3.25	255.88	0.10	0.34	0.33	8.15	0.26
27.09.2007 15:00	17.91	0.74	0.96	3.68	1.08	241.39	0.01	-	0.32	5.58	0.25
28.09.2007 11:00	30.08	0.00	2.92	4.32	9.50	248.70	0.16	0.34	0.34	6.20	0.25
06.11.2007 04:00	15.51	0.41	1.04	2.09	1.14	165.70	0.02	-	0.35	9.01	0.25
07.11.2007 21:00	58.17	1.96	3.00	4.87	6.67	177.32	0.43	-	0.36	38.81	0.25
11.04.2008 22:00	56.43	0.03	6.33	4.25	1.72	176.95	0.64	-	0.35	27.41	0.27
07.06.2008 08:00	5.23	4.13	0.75	3.27	0.24	120.75	0.01	-	0.26	4.01	0.25
25.06.2008 12:00	21.10	0.83	0.75	5.00	0.00	72.84	0.00	-	0.23	3.19	0.25
04.07.2008 02:00	23.90	3.19	0.88	3.02	0.00	86.99	0.01	-	0.20	2.59	0.26
13.07.2008 06:00	10.60	0.07	0.75	8.19	1.66	125.65	0.00	-	0.22	2.84	0.27
22.07.2008 06:00	10.56	0.15	0.71	5.05	1.49	143.72	0.00	0.30	0.23	2.72	0.26
07.08.2008 22:00	26.04	5.51	0.92	2.40	0.09	140.29	0.00	0.25	0.16	1.80	0.28
15.08.2008 06:00	26.11	1.98	0.96	2.52	0.62	163.94	0.01	0.30	0.19	2.31	0.30
24.08.2008 05:00	8.48	1.17	0.71	10.60	1.31	200.64	0.00	0.31	0.20	2.41	0.28
21.09.2008 06:00	12.47	0.60	0.71	3.31	0.14	135.46	0.00	0.32	0.17	1.86	0.22
16.10.2008 08:00	12.30	1.00	1.08	2.69	0.29	101.10	0.00	0.32	0.21	2.62	0.27
22.10.2008 03:00	17.65	0.27	1.21	6.67	0.07	109.92	0.00	0.33	0.22	2.95	0.27
29.10.2008 05:00	13.42	0.10	0.79	2.68	3.78	124.13	0.01	0.34	0.25	4.17	0.28
30.10.2008 04:00	25.77	0.67	1.04	2.45	9.58	136.71	0.03	0.35	0.28	6.88	0.28
29.04.2009 18:00	12.70	0.33	0.71	1.42	0.05	145.67	0.01	-	0.29	7.37	0.25
22.05.2009 10:00	14.03	11.71	0.67	1.40	4.80	117.46	0.01	0.32	0.28	4.66	0.25
26.05.2009 21:00	38.48	13.26	0.92	1.92	0.11	94.95	0.01	-	0.27	4.01	0.25
16.06.2009 13:00	11.47	2.00	0.92	4.89	8.26	199.79	0.01	-	0.30	7.88	0.25
21.06.2009 14:00	18.70	17.13	0.71	8.58	0.23	204.62	0.00	-	0.30	5.99	0.25
17.07.2009 16:00	21.32	5.75	1.38	13.17	0.34	290.02	0.02	0.32	0.27	6.42	0.25
23.07.2009 16:00	8.76	8.61	0.63	8.04	0.12	297.27	0.01	0.33	0.29	7.68	0.26
02.08.2009 16:00	15.53	0.25	1.00	8.62	0.00	238.79	0.01	0.30	0.27	5.38	0.25
17.08.2009 16:00	20.95	2.45	0.71	5.12	0.19	234.69	0.00	0.31	0.25	3.87	0.24
04.09.2009 19:00	9.04	3.22	0.63	5.95	0.03	158.29	0.01	0.29	0.22	2.95	0.26
29.09.2009 11:00	13.32	0.30	0.96	15.13	0.04	94.73	0.00	-	0.19	3.19	0.27
02.11.2009 12:00	19.03	0.36	0.83	3.92	0.03	179.30	0.02	-	0.30	13.21	0.23
02.05.2010 07:00	10.63	0.07	0.88	1.92	2.20	94.24	0.00	-	0.30	5.78	0.26
06.05.2010 06:00	19.23	1.19	0.79	2.22	1.24	112.25	0.00	-	0.30	5.99	0.22

24.05.2010 04:00	12.29	1.40	1.04	0.11	0.23	142.59	0.00	-	0.31	3.70	0.22
28.05.2010 13:00	7.55	0.81	0.58	4.48	0.78	138.77	0.00	-	0.31	3.84	0.26
02.06.2010 19:00	23.13	0.07	2.25	2.57	2.01	155.13	0.12	-	0.32	7.21	0.25
17.07.2010 07:00	14.11	3.00	0.67	2.89	0.31	139.45	0.00	-	0.19	1.05	0.26
12.08.2010 14:00	22.90	22.50	1.21	6.34	1.13	262.94	0.01	-	0.30	6.01	0.29
15.08.2010 23:00	15.70	0.70	0.54	18.50	1.60	290.74	0.00	-	0.30	2.29	0.26
27.08.2010 01:00	12.90	1.50	0.92	8.90	0.51	321.53	0.00	-	0.28	1.69	0.27
28.08.2010 02:00	15.60	0.30	0.67	8.10	5.52	334.40	0.00	-	0.29	1.94	0.26
02.09.2010 08:00	7.60	3.20	1.42	16.00	7.00	391.85	0.02	-	0.33	6.69	0.26
27.09.2010 04:00	64.60	1.20	6.08	6.30	21.97	241.80	0.39	-	0.33	6.14	0.22

Table 2: Event data set of Rehefeld (abbreviations cf. Table 1).

Date	P [mm]	$P2h$ [mm]	DP [h]	I [mm/h]	$API^{30}_{0.95}$ [mm]	AP^{60} [mm]	C_r [-]	WC_0 C1 [m^3m^{-3}]	WC_0 C2 [m^3m^{-3}]	q_0 [$l\ s^{-1}km^{-2}$]	CV [-]
08.05.2007 00:00	30.32	0.04	1.54	6.06	0.01	44.88	0.02	0.23	0.25	3.58	0.26
14.05.2007 18:00	14.59	3.82	1.08	5.15	0.53	79.74	0.04	0.27	0.27	3.58	0.24
17.05.2007 02:00	9.86	0.15	0.58	2.54	2.56	95.99	0.01	0.28	0.28	6.99	0.24
22.05.2007 15:00	33.76	21.77	0.67	21.18	0.02	87.69	0.04	0.27	0.27	4.33	0.25
27.05.2007 16:00	35.97	2.11	2.50	7.99	1.70	105.79	0.07	0.29	0.30	5.14	0.24
15.06.2007 23:00	25.27	0.02	1.04	8.93	1.10	171.47	0.03	0.29	0.25	5.14	0.22
21.06.2007 07:00	19.23	2.44	0.96	8.65	0.30	202.70	0.08	0.30	0.26	5.14	0.22
02.07.2007 11:00	9.70	0.00	0.63	2.55	0.19	238.15	0.01	0.30	0.27	5.14	0.28
05.07.2007 21:00	10.17	0.16	1.00	3.85	6.39	259.06	0.03	0.32	0.29	8.43	0.28
21.08.2007 00:00	18.74	0.03	0.75	6.27	0.21	221.11	0.01	0.31	0.28	6.99	0.27
22.08.2007 03:00	14.70	2.56	1.21	4.24	8.53	239.88	0.03	0.33	0.31	13.58	0.27
23.08.2007 22:00	6.85	0.23	0.67	3.40	4.75	253.94	0.01	0.33	0.32	9.99	0.27
31.08.2007 23:00	12.36	0.05	0.58	3.44	0.97	244.23	0.00	0.31	0.29	6.99	0.27
04.09.2007 14:00	18.97	0.11	1.33	3.68	1.32	232.57	0.04	0.33	0.31	6.99	0.27
08.09.2007 04:00	21.44	0.00	1.92	2.83	0.94	247.17	0.10	0.33	0.31	8.43	0.26
10.09.2007 15:00	30.46	1.27	1.67	3.17	3.07	264.17	0.14	0.34	0.33	15.66	0.26
27.09.2007 14:00	18.74	0.59	0.92	4.17	0.64	254.53	0.03	-	0.32	8.43	0.25
28.09.2007 10:00	32.57	0.00	1.46	5.25	10.37	261.85	0.17	0.34	0.34	17.79	0.26
18.10.2007 11:00	18.99	0.60	1.67	1.30	0.03	205.70	0.03	0.33	0.32	8.43	0.22
02.11.2007 19:00	15.11	0.87	2.13	1.20	0.98	189.92	0.09	-	0.34	11.73	0.22
06.11.2007 09:00	14.60	0.34	0.96	2.30	1.13	184.73	0.05	-	0.35	17.79	0.26
07.11.2007 13:00	38.23	0.18	1.67	4.39	6.78	196.41	0.25	-	0.36	25.30	0.25
11.11.2007 10:00	19.72	0.28	0.96	5.34	5.95	205.74	0.07	-	0.38	48.47	0.26
01.04.2008 11:00	12.93	2.26	1.83	2.47	0.04	147.31	0.14	-	0.35	34.26	0.25
11.04.2008 21:00	19.80	0.01	1.17	4.51	1.90	173.88	0.11	-	0.35	34.26	0.27
14.04.2008 20:00	27.23	0.02	1.33	5.10	1.08	193.88	0.09	-	0.36	34.26	0.27
03.06.2008 22:00	9.14	7.59	0.50	5.78	0.32	115.21	0.01	-	0.26	5.14	0.24
13.06.2008 03:00	18.12	5.03	2.88	3.77	0.18	93.81	0.02	-	0.25	2.31	0.25
25.06.2008 14:00	23.38	0.84	0.83	7.07	0.00	71.82	0.03	-	0.23	2.31	0.25
04.07.2008 02:00	23.71	3.09	0.63	5.59	0.00	84.96	0.00	-	0.20	2.31	0.26
13.07.2008 10:00	10.65	0.06	0.63	2.45	1.36	123.86	0.00	-	0.22	2.31	0.27
19.07.2008 21:00	10.90	0.22	0.63	5.62	1.48	130.95	0.01	0.28	0.22	2.31	0.26
22.07.2008 05:00	10.80	0.18	0.75	2.48	1.54	142.67	0.01	0.30	0.23	2.31	0.26
08.08.2008 02:00	25.40	5.61	0.63	9.75	0.07	141.39	0.01	0.26	0.16	1.33	0.28
15.08.2008 10:00	26.31	2.07	0.71	3.41	0.48	163.36	0.01	0.30	0.19	2.31	0.30
24.08.2008 09:00	8.17	1.11	0.88	2.48	1.06	200.06	0.01	0.31	0.20	2.31	0.23
04.09.2008 01:00	7.40	2.00	0.42	3.65	0.15	164.34	0.00	0.29	0.17	2.31	0.27
07.09.2008 04:00	8.59	1.15	0.46	2.98	1.02	173.28	0.00	0.31	0.18	2.31	0.29
21.09.2008 07:00	11.90	0.60	0.67	6.50	0.15	133.88	0.00	0.32	0.17	1.33	0.22
06.10.2008 16:00	8.90	1.24	0.54	1.10	0.30	162.68	0.00	0.33	0.20	2.31	0.27
16.10.2008 17:00	9.44	1.18	1.21	2.72	2.26	102.52	0.03	0.33	0.21	0.58	0.27
22.10.2008 13:00	17.36	1.22	1.00	2.42	0.26	104.60	0.02	0.33	0.22	3.58	0.27
28.10.2008 08:00	17.13	0.06	1.54	1.96	2.20	117.49	0.05	0.34	0.24	5.14	0.28
30.10.2008 04:00	25.15	0.95	0.92	6.27	9.67	135.56	0.06	0.35	0.28	22.65	0.28
29.04.2009 18:00	12.58	0.34	0.54	5.14	0.07	146.06	0.01	-	0.29	15.66	0.25
06.05.2009 07:00	15.20	1.05	1.00	1.51	0.47	146.77	0.02	0.31	0.29	13.58	0.26
11.05.2009 09:00	15.50	0.26	1.13	4.82	0.15	142.24	0.05	0.32	0.29	8.43	0.25
21.05.2009 21:00	20.33	5.87	1.79	8.73	0.20	113.58	0.04	0.30	0.28	5.14	0.25
26.05.2009 19:00	38.06	13.04	1.54	8.46	0.12	94.92	0.12	-	0.28	5.14	0.25
29.05.2009 09:00	31.00	2.97	2.54	3.35	4.97	132.15	0.16	-	0.31	13.58	0.25
15.06.2009 18:00	22.30	0.88	1.63	6.13	0.52	188.23	0.05	-	0.29	8.43	0.25

21.06.2009 13:00	16.43	14.98	0.67	11.34	0.23	204.07	0.02	-	0.30	8.43	0.25
17.08.2009 18:00	20.52	2.37	0.71	14.85	0.19	233.12	0.02	0.31	0.25	5.14	0.25
29.09.2009 17:00	15.27	0.30	1.04	1.88	0.03	94.74	0.01	-	0.19	0.58	0.27
01.10.2009 20:00	6.65	3.02	0.42	2.95	2.88	111.39	0.00	-	0.22	2.31	0.26
06.10.2009 04:00	15.00	1.18	1.42	2.62	0.33	104.70	0.01	-	0.22	1.33	0.26
11.10.2009 07:00	39.56	2.10	2.46	3.49	1.16	106.49	0.08	-	0.24	2.31	0.26
16.10.2009 18:00	9.16	0.50	0.63	1.43	5.80	155.33	0.02	-	0.29	9.99	0.26
02.11.2009 14:00	19.87	0.54	0.79	2.18	0.03	181.06	0.03	-	0.30	20.16	0.23
04.11.2009 16:00	13.01	0.74	1.00	2.02	6.98	200.03	0.12	-	0.32	25.30	0.22
10.04.2010 19:00	30.15	2.09	2.50	1.93	0.10	91.34	0.11	-	0.30	20.16	0.23
02.05.2010 19:00	14.95	1.02	0.67	2.75	1.32	104.37	0.02	-	0.29	9.99	0.22
06.05.2010 02:00	21.20	1.22	1.50	4.24	1.38	121.25	0.13	-	0.30	11.73	0.22
14.05.2010 13:00	12.87	0.14	0.96	1.08	0.13	136.06	0.02	-	0.30	9.99	0.22
24.05.2010 04:00	13.49	4.44	1.08	4.14	0.26	144.48	0.01	-	0.31	8.43	0.22
30.05.2010 12:00	12.58	1.31	1.17	3.67	1.02	145.89	0.02	-	0.31	9.99	0.25
02.06.2010 12:00	24.74	0.25	1.38	3.72	3.46	163.66	0.11	-	0.32	15.66	0.26
17.07.2010 06:00	14.14	10.31	0.50	6.97	0.44	152.75	0.01	-	0.19	2.31	0.26
12.08.2010 15:00	22.90	22.50	1.04	16.00	1.08	171.92	0.17	-	0.30	22.65	0.29
15.08.2010 23:00	16.10	0.70	0.96	9.80	1.60	171.45	0.18	-	0.30	25.30	0.26
27.08.2010 03:00	11.20	0.40	0.63	6.30	1.75	170.07	0.02	-	0.27	11.73	0.26
28.08.2010 06:00	15.70	0.20	0.88	3.40	4.74	170.03	0.06	-	0.29	15.66	0.26
30.08.2010 01:00	12.70	0.80	1.08	2.20	5.18	170.02	0.09	-	0.30	15.66	0.25
31.08.2010 06:00	18.80	0.50	1.08	2.60	7.64	169.06	0.08	-	0.31	34.26	0.25
02.09.2010 07:00	6.60	0.10	0.71	2.70	2.90	168.92	0.09	-	0.33	41.02	0.25
25.09.2010 16:00	61.80	1.20	1.25	8.40	0.00	6.80	0.15	-	0.27	6.99	0.22
27.09.2010 04:00	55.60	1.20	1.83	3.40	0.00	4.40	0.29	-	0.33	65.28	0.22

Table 3: Event data set of Ammelsdorf (abbreviations cf. Table 1).

Date	P [mm]	$P2h$ [mm]	DP [h]	I [mm/h]	$API^{30}_{0.95}$ [mm]	AP^{60} [mm]	C_r [-]	WC_0 C1 [m^3m^{-3}]	WC_0 C2 [m^3m^{-3}]	q_0 [$l\ s^{-1}km^{-2}$]	CV [-]
08.05.2007 00:00	29.95	0.07	1.46	6.16	0.02	45.19	0.01	0.23	0.25	3.26	0.26
14.05.2007 23:00	13.54	1.92	1.17	5.98	0.44	79.01	0.03	0.26	0.27	1.62	0.25
17.05.2007 04:00	9.12	0.17	0.79	2.58	2.24	93.15	0.01	0.28	0.28	4.41	0.24
22.05.2007 16:00	30.74	11.33	1.33	11.04	0.02	83.46	0.06	0.26	0.27	1.25	0.25
28.05.2007 02:00	33.36	2.93	2.08	8.43	4.09	105.23	0.07	0.29	0.28	4.41	0.25
08.06.2007 19:00	6.36	0.47	2.25	3.13	0.61	149.77	0.06	0.29	0.28	3.55	0.22
15.06.2007 23:00	28.85	0.03	1.50	11.28	1.50	164.49	0.03	0.29	0.25	4.41	0.22
21.06.2007 10:00	16.14	4.35	1.17	6.03	0.24	198.72	0.05	0.30	0.27	4.41	0.22
26.06.2007 02:00	9.34	0.40	0.71	2.25	0.30	217.79	0.01	0.30	0.27	4.41	0.28
03.07.2007 10:00	21.11	0.04	3.29	2.84	4.92	242.41	0.03	0.31	0.28	3.55	0.28
20.08.2007 15:00	28.37	0.03	1.29	4.70	0.65	221.19	0.06	0.31	0.29	7.10	0.27
01.09.2007 00:00	13.27	0.12	1.04	2.94	0.78	234.01	0.02	0.31	0.29	8.64	0.27
04.09.2007 13:00	16.63	0.13	1.25	2.63	1.51	228.39	0.03	0.33	0.31	7.10	0.27
08.09.2007 05:00	18.52	0.00	2.13	1.74	0.88	241.51	0.10	0.33	0.31	8.64	0.26
10.09.2007 13:00	28.18	1.35	1.92	2.11	2.96	255.04	0.13	0.34	0.33	17.09	0.26
25.09.2007 07:00	52.81	0.31	4.33	4.49	0.04	247.01	0.10	0.32	0.31	9.07	0.22
18.10.2007 13:00	16.66	2.18	1.50	1.23	1.03	205.83	0.02	0.33	0.32	8.64	0.22
05.11.2007 11:00	15.24	0.03	1.88	1.91	2.77	172.92	0.07	-	0.35	17.64	0.25
07.11.2007 10:00	35.44	0.02	1.29	4.32	7.41	185.73	0.13	-	0.36	29.01	0.25
11.11.2007 09:00	16.52	0.23	0.71	3.87	8.90	204.44	0.05	-	0.38	69.29	0.26
14.04.2008 11:00	31.81	0.03	1.88	3.60	1.75	196.89	0.10	-	0.37	43.77	0.26
16.05.2008 17:00	5.90	0.21	0.46	5.58	0.14	173.77	0.01	-	0.31	5.70	0.24
04.06.2008 00:00	9.72	7.71	1.00	5.87	0.30	119.32	0.02	-	0.26	3.26	0.24
14.06.2008 07:00	10.36	3.05	2.00	2.97	2.89	93.13	0.02	-	0.25	2.52	0.21
24.06.2008 11:00	23.46	0.85	2.54	7.19	0.02	78.95	0.03	-	0.24	1.40	0.25
04.07.2008 03:00	23.82	3.08	1.29	5.52	0.00	85.03	0.01	-	0.20	0.74	0.26
13.07.2008 10:00	10.63	0.06	0.71	2.44	1.39	124.05	0.00	-	0.22	2.26	0.27
19.07.2008 23:00	10.86	0.21	0.75	5.59	1.39	131.00	0.01	0.28	0.22	2.26	0.26
22.07.2008 06:00	10.78	0.17	0.92	2.48	1.46	142.69	0.01	0.30	0.23	2.26	0.26
08.08.2008 04:00	25.55	5.60	0.96	9.87	0.06	141.14	0.01	0.26	0.16	1.40	0.28
14.08.2008 07:00	26.29	2.05	1.88	3.39	1.94	170.70	0.02	0.30	0.19	1.07	0.30
06.10.2008 13:00	8.96	1.23	0.92	1.09	0.30	162.84	0.01	0.33	0.20	1.40	0.27
16.10.2008 20:00	9.42	1.18	1.17	2.71	2.14	102.54	0.01	0.33	0.21	2.26	0.27
22.10.2008 14:00	17.39	0.59	1.83	2.43	0.28	104.60	0.04	0.33	0.22	2.26	0.27
28.10.2008 15:00	20.02	0.89	1.63	1.96	1.84	117.57	0.03	0.34	0.24	4.41	0.28
30.10.2008 03:00	26.01	1.19	2.17	6.27	9.55	134.95	0.11	0.35	0.27	16.02	0.28
28.04.2009 06:00	12.67	0.07	2.21	5.07	0.01	152.08	0.03	-	0.29	7.10	0.25
06.05.2009 09:00	14.80	1.05	0.79	1.51	0.47	146.24	0.01	0.31	0.29	7.10	0.26
11.05.2009 09:00	15.35	0.26	0.79	4.80	0.15	141.70	0.01	0.32	0.29	5.70	0.25
21.06.2009 17:00	16.65	15.19	0.71	11.53	0.19	203.73	0.02	-	0.30	7.10	0.25
17.07.2009 14:00	23.23	6.31	1.54	5.02	0.36	286.97	0.06	0.32	0.28	8.64	0.25
02.08.2009 17:00	11.49	0.23	0.71	6.30	0.00	237.09	0.02	0.30	0.26	4.47	0.25
10.08.2009 21:00	27.98	9.77	3.04	8.35	0.00	241.17	0.02	0.29	0.25	5.70	0.25
17.08.2009 23:00	20.61	2.36	0.46	14.87	0.15	232.97	0.00	0.31	0.24	6.18	0.24
29.09.2009 21:00	14.48	0.66	1.38	1.90	0.93	95.92	0.01	-	0.19	1.40	0.28
01.10.2009 09:00	7.70	0.50	0.83	2.94	3.85	110.40	0.00	-	0.23	2.26	0.26
05.10.2009 19:00	55.07	1.19	7.46	3.50	0.45	104.73	0.04	-	0.22	1.40	0.26
16.10.2009 16:00	12.21	0.37	1.25	1.41	7.18	153.85	0.05	-	0.29	10.32	0.26
02.11.2009 11:00	42.79	0.51	3.63	2.18	0.03	180.44	0.15	-	0.30	18.14	0.23
02.05.2010 20:00	15.22	0.04	1.04	2.27	1.09	97.29	0.04	-	0.29	10.32	0.22
06.05.2010 05:00	18.86	0.02	1.04	3.52	1.35	114.26	0.03	-	0.31	10.32	0.25

13.05.2010 19:00	12.89	0.04	1.67	1.10	0.19	132.55	0.02	-	0.30	9.48	0.22
02.06.2010 14:00	26.86	0.17	1.58	4.00	2.77	152.95	0.16	-	0.32	18.14	0.25
17.07.2010 08:00	12.94	4.91	0.63	4.32	0.28	141.64	0.01	-	0.19	1.83	0.26
12.08.2010 17:00	22.90	22.50	1.25	16.00	0.97	157.38	0.06	-	0.30	30.24	0.29
16.08.2010 01:00	15.40	0.50	0.58	9.80	1.88	157.03	0.05	-	0.30	27.12	0.26
28.08.2010 05:00	48.90	0.20	4.08	3.40	4.99	156.00	0.13	-	0.29	16.02	0.26
25.09.2010 03:00	62.60	1.20	1.83	8.40	0.00	6.80	0.08	-	0.28	6.75	0.25
27.09.2010 03:00	56.60	0.40	2.08	3.40	0.00	4.80	0.27	-	0.33	55.79	0.21

Table 4: Correlation matrix of predictors and response variable for the Becherbach (abbreviations cf. Table 1).

	P	$P2h$	DP	I	$API^{30}_{0.95}$	AP^{60}	C_r	WC_0 C1	WC_0 C2	q_0	CV
P	1.00	-0.01	0.46	0.19	-0.01	-0.03	0.36	-0.13	0.19	0.12	-0.16
$P2h$	-0.01	1.00	-0.18	0.49	-0.19	0.11	0.07	-0.12	-0.05	-0.01	-0.15
DP	0.46	-0.18	1.00	-0.48	0.18	0.12	0.56	0.33	0.29	0.50	0.11
I	0.19	0.49	-0.48	1.00	-0.29	0.01	-0.10	-0.47	-0.12	-0.24	-0.24
$API^{30}_{0.95}$	-0.01	-0.19	0.18	-0.29	1.00	0.38	0.26	0.58	0.54	0.30	0.26
AP^{60}	-0.03	0.11	0.12	0.01	0.38	1.00	0.25	0.41	0.40	0.35	0.15
C_r	0.36	0.07	0.56	-0.10	0.26	0.25	1.00	0.49	0.54	0.75	-0.08
WC_0 C1	-0.13	-0.12	0.33	-0.47	0.58	0.41	0.49	1.00	0.38	0.74	0.33
WC_0 C2	0.19	-0.05	0.29	-0.12	0.54	0.40	0.54	0.38	1.00	0.60	-0.21
q_0	0.12	-0.01	0.50	-0.24	0.30	0.35	0.75	0.74	0.60	1.00	-0.06
CV	-0.16	-0.15	0.11	-0.24	0.26	0.15	-0.08	0.33	-0.21	-0.06	1.00

Table 5: Correlation matrix of predictors and response variable for the Rehefeld (abbreviations cf. Table 1).

	P	$P2h$	DP	I	$API^{30}_{0.95}$	AP^{60}	C_r	WC_0 C1	WC_0 C2	q_0	CV
P	1.00	0.15	0.60	0.29	-0.18	-0.14	0.60	-0.10	0.23	0.20	-0.19
$P2h$	0.15	1.00	0.03	0.31	-0.30	-0.36	-0.01	-0.22	-0.27	-0.24	-0.21
DP	0.60	0.03	1.00	-0.25	0.05	-0.08	0.72	0.28	0.47	0.30	-0.26
I	0.29	0.31	-0.25	1.00	-0.19	-0.04	-0.05	-0.53	-0.21	-0.15	-0.05
$API^{30}_{0.95}$	-0.18	-0.30	0.05	-0.19	1.00	0.39	0.28	0.46	0.35	0.37	0.27
AP^{60}	-0.14	-0.36	-0.08	-0.04	0.39	1.00	0.09	0.47	0.46	0.38	0.24
C_r	0.60	-0.01	0.72	-0.05	0.28	0.09	1.00	0.30	0.67	0.67	-0.27
WC_0 C1	-0.10	-0.22	0.28	-0.53	0.46	0.47	0.30	1.00	0.34	0.45	0.28
WC_0 C2	0.23	-0.27	0.47	-0.21	0.35	0.46	0.67	0.34	1.00	0.88	-0.22
q_0	0.20	-0.24	0.30	-0.15	0.37	0.38	0.67	0.45	0.88	1.00	-0.16
CV	-0.19	-0.21	-0.26	-0.05	0.27	0.24	-0.27	0.28	-0.22	-0.16	1.00

Table 6: Correlation matrix of predictors and response variable for the Ammelsdorf (abbreviations cf. Table 1).

	P	$P2h$	DP	I	$API^{30}_{0.95}$	AP^{60}	C_r	WC_0 C1	WC_0 C2	q_0	CV
P	1.00	0.05	0.58	0.14	-0.11	0.06	0.63	-0.05	0.24	0.28	-0.04
$P2h$	0.05	1.00	-0.04	0.37	-0.29	-0.13	-0.16	-0.06	-0.42	-0.36	-0.03
DP	0.58	-0.04	1.00	-0.29	0.02	-0.02	0.63	0.26	0.16	0.12	-0.14
I	0.14	0.37	-0.29	1.00	-0.40	-0.04	-0.10	-0.65	-0.19	-0.14	-0.20
$API^{30}_{0.95}$	-0.11	-0.29	0.02	-0.40	1.00	0.12	0.18	0.32	0.21	0.26	0.35
AP^{60}	0.06	-0.13	-0.02	-0.04	0.12	1.00	0.18	0.39	0.41	0.43	0.10
C_r	0.63	-0.16	0.63	-0.10	0.18	0.18	1.00	0.30	0.63	0.62	-0.17
WC_0 C1	-0.05	-0.06	0.26	-0.65	0.32	0.39	0.30	1.00	0.30	0.51	0.33
WC_0 C2	0.24	-0.42	0.16	-0.19	0.21	0.41	0.63	0.30	1.00	0.88	-0.28
q_0	0.28	-0.36	0.12	-0.14	0.26	0.43	0.62	0.51	0.88	1.00	-0.16
CV	-0.04	-0.03	-0.14	-0.20	0.35	0.10	-0.17	0.33	-0.28	-0.16	1.00

Table 8: WaSiM ETH parameters calibrated with the Dynamically Dimensioned Search algorithm.

Parameter	Process / Module	Spatial Scope
Recession coefficient of saturation deficit	Soil	sub-basin
Correction factor of transmissivity	Soil	Sub-basin
Correction factor of hydrological conductivity	Soil	Sub-basin
Recession coefficient of direct runoff	Overland flow	Sub-basin
Capacity of interflow storage	Soil and Interflow	Sub-basin
Recession coefficient of interflow	Interflow	Sub-basin
Threshold value of activity of macroporosity	Soil	Sub-basin
Decreasing factor of capillary rising into plant available soil storage	Soil	Sub-basin
Surface/Canopy resistance factor	ET	Global
Effective Leave area index factor	Interception and ET	Global
Effective root depth factor	ET	Global
Soil water of usable field capacity factor	Infiltration	Global
Effective porosity factor	Infiltration	Global
Hydraulic conductivity factor	Infiltration and Soil	Global
Suction at the wetting front factor	Infiltration	Global

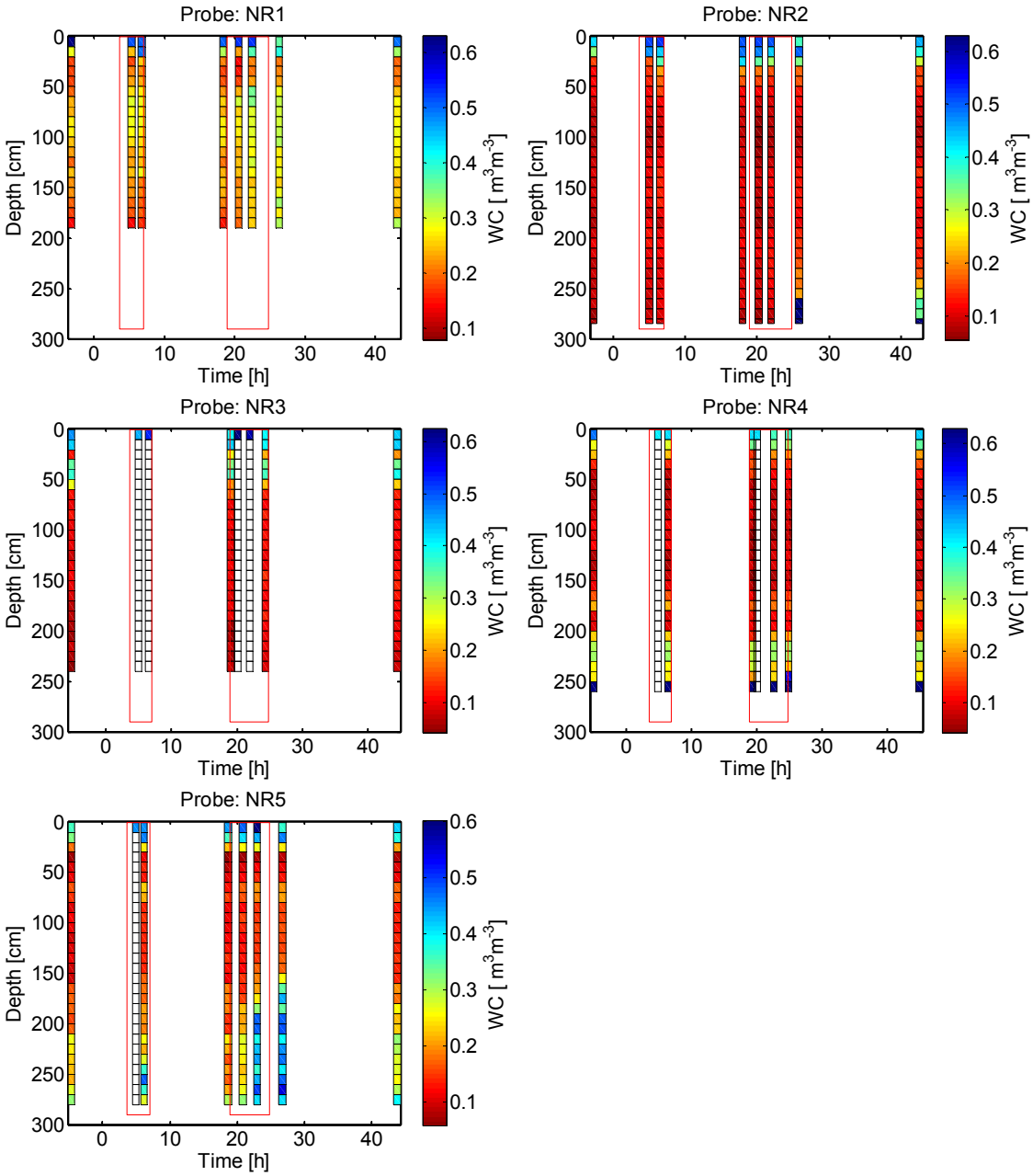

Figure 1: Absolute values soil moisture profiles measured with TRIME probe for the five access tubes. The red boxes mark the irrigation period.